INVESTIGATING THE ROLES OF REACTIVE OXYGEN AND NITROGEN SPECIES IN PLANT PROGRAMMED CELL DEATH, CYTOSKELETAL AND MITOCHONDRIAL DYNAMICS

A Thesis submitted to the College of

Graduate Studies and Research

in partial fulfillment of the requirements

for the degree of Master of Science

in the Department of Biology

University of Saskatchewan,

Saskatoon,

Saskatchewan, Canada

By

Dushantha Sanjaya Bandara Ekanayake

PERMISSION TO USE

In presenting this thesis in partial fulfillment of the requirements for a postgraduate degree from the University of Saskatchewan, I agree that the Libraries of this University may make it freely available for inspection. I further agree that permission for copying of this thesis in any manner, in whole or in part, for scholarly purposes may be granted by the professor or professors who supervised my thesis work or, in their absence, by the Head of the Department or the Dean of the College in which my thesis work was done. It is understood that any copying or publication or use of this thesis or parts thereof for financial gain shall not be allowed without my written permission. It is also understood that due recognition shall be given to me and to the University of Saskatchewan in any scholarly use which may be made of any material in my thesis.

Requests for permission to copy or to make other use of material in this thesis in whole or part should be addressed to:

Head of the Department of Biology

112 Science Place

University of Saskatchewan

Saskatoon, Saskatchewan

S7N 5E2

ABSTRACT

Mitochondria are usually considered simply as the "powerhouses of the cell", however in recent years it has become apparent that mitochondria are also of fundamental importance in programmed cell death (PCD), which refers to cell death resulting from a controlled, genetically defined pathway. In Arabidopsis, PCD induced by either heat shock or treatment with strong oxidants is found to be correlated with an early and irreversible change in mitochondrial morphology which manifests as an increase in the size of individual mitochondria. In addition, PCD causes a clustering of mitochondria and loss of motility. In this study, I have used two arginase negative mutant Arabidopsis lines (*argah1-1* and *argah2-1*) which have elevated cellular NO concentrations to examine the effect of nitrosative stress on mitochondria undergoing PCD. Another three different Arabidopsis lines (mito-GFP/mTalin-mCherry, mito-GFP/MAP4-mCherry, mito- mCherry/EB1b-GFP) were used to visualize cytoskeletal elements alongside mitochondria to examine the mechanisms responsible for the mitochondrial morphology transition, clustering and motility inhibition. Results indicate that the elevated concentration of NO found in arginase negative mutants is not sufficient to induce PCD. There was no significant mitochondrial morphology or dynamic change detected between arginase negative mutants and wild type plants, with or without a heat shock. Disruption of either actin or microtubule (MT) cytoskeletal elements leads to the formation of mitochondrial clusters, although they showed different cluster morphology and sizes. Mitochondrial clusters were observed to be moving along the remaining actin cables after a mild heat treatment or cytoskeletal depolymerizing drug treatment. Intact microtubules or MT plus ends visualized with EB1b did not show any interaction with mitochondria under normal conditions. However, after a mild heat stress, EB1b appeared to be associated with clusters of enlarged, possibly swollen mitochondria.

ACKNOWLEDGEMENTS

I'd like to take this opportunity to express my gratitude and thanks to the droves of people who supported me in the achievement of this degree. Foremost, Dr. David Logan, for taking me in as one of his students and allowing me to tackle such an interesting and challenging project that allowed me to develop proficiencies in a wide range of cellular-molecular, microscopy techniques and image analysis. My heartfelt thanks also extend to Dr. Christopher Todd, my co-supervisor. Without his assistance, guidance, and patient editing, this thesis would have been very different.

Thanks also extend to my external examiner Dr. Hong Wang for his insightful questions, and to my advisory committee; Dr. Yangdou Wei and Dr. Som Niyogi for their comments and suggestions that were instrumental to the completion of this degree. Thanks also extend to the Department of Biology for assisting me. Numerous colleagues in Biology Department are appreciated for their technical and moral support. This includes, but is not limited to, Dr. Guosheng Liu, Sourav Gangopadhyay, Adel Saeed Al and Amr El Zawily.

I wish to thank Mr. Dilshan Benaragama for his support in experimental design and statistical analysis. I also wish to thank and acknowledge the support and encouragement of my friends. Without them, this degree would have been impossible.

DEDICATION

This thesis is especially dedicated in loving memory of my late parents, ***Bandara Manike Alahakoon*** *and* ***Loku Banda Ekanayake****, both my sisters* ***Deepamala*** *and* ***Anoja Ekanayake****, for the love, sacrifices and encouragements they gave me throughout my academic career. So, this is for you …….*

TABLE OF CONTENTS

LIST OF TABLES

LIST OF FIGURES

LIST OF ABBREVIATTIONS

°C	Degree Celsius
35S	35S promoter from Cauliflower Mosaic virus
ABP	Actin binding protein
ADF	Actin depolymerizing factor
ADP	Adenosine diphosphate
ARP2/3	Actin related protein 2 and 3
ATP	Adenosine 5'-triphosphate
Bad	Bcl-2 antagonist of cell death
Bak	Bcl2-antagonist killer 1
Bax	Bcl2-associated X protein
Bcl-2	B-cell lymphoma 2 protein
Bcl-xL	Bcl-2 related protein, long isoform
BDM	2,3-butanedione monoxine
Bid	BH3-interacting domain death agonist
bp	Base pair
BSA	Bovine serum albumin
DIC	Differential interference contrast
DNA	Deoxyribonucleic acid
Drp1	Dynamin-related protein 1
EndoG	Endonuclease G
et al.	*et alterni* (Lat.) and others
EtOH	Ethanol
F1	First generation
F2	Second generation
F-actin	Filamentous actin (actin MFs)
FDA	Fluorescein diacetate
Fig.	Figure
Fis1	Fission 1 protein

g	Gram
G-actin	Globular actin (actin monomers)
GDP	Guanosine diphosphate
GFP	Green fluorescent protein
HS	Heat shock
IMS	Inter-membrane space
in vitro	Within glass, In an artificial environment
in vivo	Within a living organism
IPTG	isopropyl β-D-thiogalactoside
kDa	Kilo dalton
LatB	Latrunculin B
LB	Luria-Bertani medium
MAP	Microtubule associated protein
Mcl-1	Myeloid cell leukemia sequence 1
Mfn2	Mitofusin 2
mPTP	Mitochondrial permeability transition pore
MT	Microtubules
OMM	The outer mitochondrial membrane
PCD	Programmed cell death
RFP	Red fluorescent protein
SDS	Sodium dodecyl sulfate
sec	second
T1	First generation after transformation
WT	wild type
x *g*	(times) gravity
µ	micro

CHAPTER 1

1. GENERAL INTRODUCTION

Eukaryotic cells have specialized compartments called organelles to carry out specific tasks essential to their survival. Most of these organelles have lipid bilayer membranes to separate them from the cytoplasm and allow them to perform their specific biochemical reactions inside. Mitochondria are one such cytoplasmic organelle, believed to be evolved from an α-proteobacterium–like organism that was free living in ancient times (Dyall et al., 2004). Mitochondria are semi-autonomous organelles, possessing their own genome (mitochondrial DNA, mtDNA), and gene expression machinery to help perform their duty as "the powerhouse of the cell" (Takasugi et al., 2010).

1.1 Mitochondria

Mitochondria are vital to almost every eukaryotic organism because they provide cells with energy converting carbon compounds into ATP. The name mitochondria derives from two Greek words, *mitos* for "thread" and *chondros* for "grain", representing the two most frequent shapes of this morphologically distinct structure observed inside of cells by early cytologists (Scheffler, 2007; Scott and Logan, 2007). First descriptions of mitochondria emerged in pre-1900s with the observations of their "bacteria like movements" in cytoplasm. Although, there were some staining and high-contrast microscope techniques developed to visualize mitochondria, it was only in the 1950s with the development of the transmission electron microscope that researchers were able to take high resolution electron micrographs of mitochondria (~30 Å) showing the presence of an outer membrane and a highly-folded inner membrane (they named as *cristae mitochondriales*). These images defined two spaces inside the mitochondrion: the inter-membrane space and the mitochondrial matrix (Palade, 1953; Sjostrand, 1953). At the same period, based on scholarly work done by Albert Lehninger (who was the pioneer of bioenergetics) and Nobel Prize-winner Peter D. Mitchell (who introduced the chemiosmotic theory), it was discovered that mitochondria were the site of cellular respiration and oxidative phosphorylation (Scheffler, 2007). The discovery of DNA in mitochondria in 1960s paved the

way to start sequencing projects and the identification of mammalian mtDNA genes later in the 1980s; it took another 10 years to complete the plant mtDNA sequencing project. Then, the discovery of the role played by mitochondria in *apoptosis* and more generally in programmed cell death (PCD) revolutionized the field of cell biology in mid 1990s (Jacobson et al., 1993; Richter et al., 1995).

1.1.1 Structure of mitochondria

The basic structure of mitochondria was defined from early electron microscopic observations, which revealed the outer and inner membranes, the matrix completely surrounded by the inner membrane, and the inter-membrane space (IMS) between those two membranes (Palade, 1953; Sjostrand, 1953). However, there was a debate about inner mitochondrial membrane arrangement. Sjöstrand's model described it as outer double membranes joining with an inner membrane, making compartments by septa-like structures (Frey and Mannella, 2000). But according to Palade, they were like baffles directed towards to the matrix (see Fig.1.1 left image) (Frey and Mannella, 2000) (Palade, 1953). Until recently, Palade's model was widely accepted with a few modifications (Fig.1.1 right image). According to this modified (baffle) model, the inner membrane is a continuous membrane with infoldings into the matrix of mitochondria (Fig. 1-1).

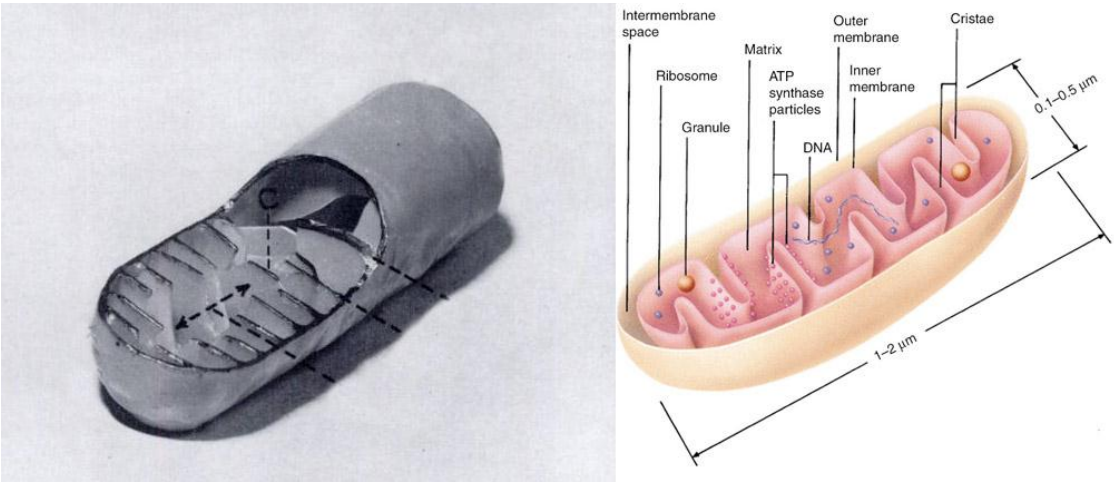

Figure 1-1 Mitochondrial models , left Palade's original model based on early EM data (Palade, 1953) , right: modified (baffle) model based on Palade's model, a typical textbook diagram (Frey and Mannella, 2000). Images reprinted with the permission from publishers.

In recent years, with the advancement of electron microscopic (EM) tomography and 3-D image analysis capabilities, a new model has been suggested. According to this new model (a model prepared by segmentation of the 3D tomogram of a mitochondrion in different animal tissues), cristae are not baffles as proposed by Palade (1953), but are pleomorphic in shape and have extensively tubular structures (see Fig 1.2 A) (Frey and Mannella, 2000). These sac-like highly tubular cristae are connected to the inner membrane (inner boundary membrane) and to each other. Structurally distinct cristae are connected to the inner membrane via cristae junctions to form a continuous membrane (showing in different colours) (see Fig.1.2 B and C). Image C shows the morphological variation among different cristae observed. The yellow cristae pattern is the most common observed in chick cerebellum (Frey and Mannella, 2000).

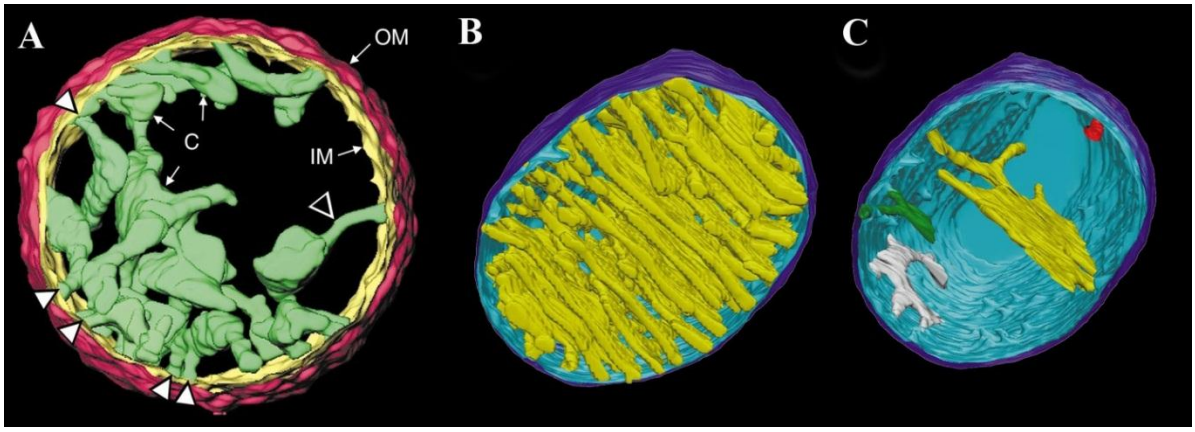

Figure 1-2 Recently proposed model for mitochondria. Image (A) Surface-rendered tomography 3-D image of an isolated rat-liver mitochondrion: C, cristae; IM, inner boundary membrane; OM, outer membrane. Arrowheads point to tubular regions of cristae that connect them to IM and to each other. Images (B) and (C) from mitochondrion in chick cerebellum. (B) The entire model shows all cristae in yellow, the inner boundary membrane in light blue, and the outer membrane in dark blue. (C) The outer membrane, inner boundary membrane and four representative cristae in different colours. Images reprinted with permission from Frey and Mannella (2000).

According to this new model, there are six different compartments in mitochondria (Fig. 1-2), namely: the outer membrane (OM or OMM), inter-membrane space (IMS), inner (boundary) membrane (IM), cristal membrane, inter-cristal space, and matrix (Logan, 2006). The outer membrane of mitochondria is permeable to any molecule less than 10 kDa in size via a channel protein called porin (Pical et al., 1993). Inner membrane however, is highly impermeable (even to protons). This inner membrane contains most of the respiratory chain proteins that are responsible for ATP production. The mitochondrial matrix is largely occupied with mtDNA and

ribosomes needed to make proteins inside the mitochondria. Mitochondria also have machinery to selectively import nuclear encoded mitochondrial proteins from the cytosol via outer and inner membranes. Actually, the vast majority (e.g. the ADP/ATP translocator and TIM 22 and 23 proteins) of proteins needed for mitochondria are transcribed from this nuclear derived pathway (Mackenzie and McIntosh, 1999). Although most animal and yeast cells contain a long tubular or reticular ramified chondriome (all the mitochondria of a cell collectively), the higher plant chondriome is composed of dynamic, pleomorphic, and physically discrete numerous organelles (0.5 to 1 μm in diameter), frequently in a spherical to sausage-shaped morphology (Fig. 1-3) (Scott and Logan, 2007).

1.1.2 Major functions of plant mitochondria

Cellular energy production of eukaryotes involves three interconnected pathways, namely glycolysis, the tricarboxylic acid cycle, and the electron transport chain. Soon after glucose breakdown by the process of glycolysis, the resulting pyruvate is transported into the mitochondria matrix (by pyruvate carrier protein in yeasts, the exact mechanism is still unknown in plants) (Picault et al., 2004). Pyruvate is then oxidized and decarboxylzed into CO_2, acetyl–CoA and NADH by Pyruvate dehydrogenase complex. This provides the substrate to function in the tricarboxylic acid (TCA) cycle (inside the mitochondrial matrix) to make reducing equivalents such as NADH and $FADH_2$ and CO_2 as the end product.

These resulting NADH and $FADH_2$ are then utilized by the electron transport chain (ETC), which is composed of four major complexes called: NADH-ubiquinone oxidoreductase (I), succinate dehydrogenase (II), cytochrome bc_1 complex (III), and cytochrome *c* oxidase (IV) which are embedded into the inner mitochondrial membrane. When electrons flow through these complexes, protons are pumped from the matrix to the IMS producing a proton gradient across the IMS. This gradient will then be used to power ATP synthesis from ADP and Pi, powering the eukaryotic cells.

Other than this vital function, plant mitochondria are involved with various other pathways, such as: photorespiration (alone with the peroxisomes and chloroplasts) (Douce and Neuburger, 1999), cysteine biosynthesis, one-carbon metabolism, and programmed cell death (PCD).

1.1.3 Plant mitochondrial dynamics and morphology

Unlike the classical textbook example of elongated and spherical shaped mitochondria, actual mitochondrial shape tends to change with various factors (Yaffe, 1999). They fuse and divide to make network like structures in most of eukaryotic organisms. Dorothea Smith (1931) was the first person to observe the mitochondrial network (in rat liver cells). However soon after that, there were significant number of observations recorded in different organisms (Bereiter-Hahn and Voth, 1994). With the advancement of bright field microscopy, chemical dyes, time-lapse imaging, and mitochondrial-targeted fluorescent proteins, morphological changes and cellular distribution of mitochondria were finally observed in real time (Lewis and Lewis, 1914; Bereiter-Hahn and Voth, 1994; Yaffe, 1999; Logan and Leaver, 2000). This process of maintaining the shape, size, number and the cellular distribution of mitochondria is called mitochondrial dynamics (Logan, 2010).

Mitochondrial dynamics varies by cell type and organism (Shaw and Nunnari, 2002). In animals, mitochondria are typically reticulo-tubular shaped, in yeast, mitochondria (usually 5-10 per cell) are in elongated tubular shape making extensive networks, while in higher-plants, hundreds of mitochondria are in spherical, tubular or vermiform shapes (Fig. 1.3) (Logan and Leaver, 2000; Frank et al., 2001; Arimura and Tsutsumi, 2006; Logan, 2010). Most of our current knowledge on mitochondrial morphology dynamics comes from research done with budding-yeast *Saccharomyces cerevisiae*, mainly after the identification of three mutants having altered mitochondrial distribution and morphology (*mdm*) (McConnell et al., 1990). By 1999, researchers using yeast found that, in order to maintain normal mitochondrial dynamics and morphology, the rate between fission and fusion of mitochondria (in yeast) is very important (Bleazard et al., 1999; Sesaki and Jensen, 1999). When there is a high rate of fusion relative to fission, mitochondria form a reticular network, while under the opposite conditions of a high rate of fission, relative to fusion, mitochondria become fragmented (Shaw and Nunnari, 2002).

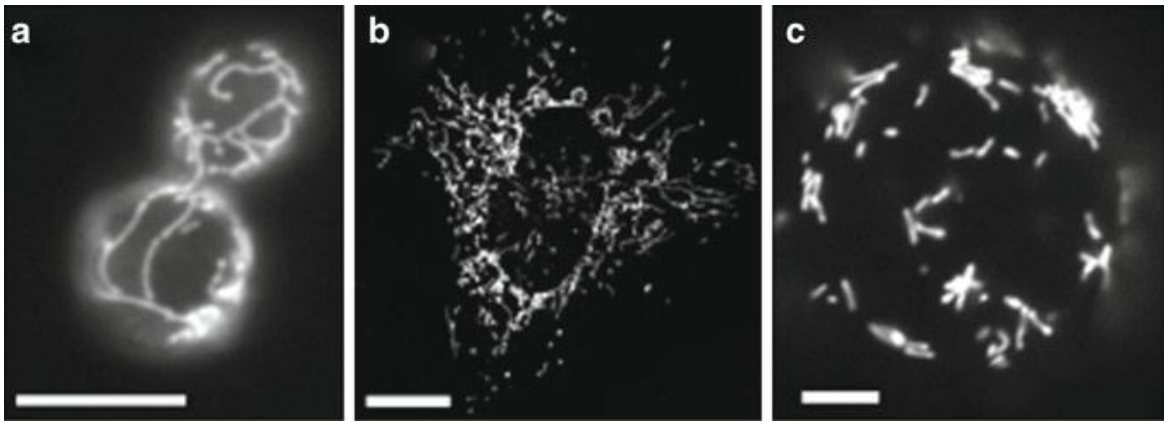

Figure 1-3 Typical mitochondrial structures in (a) yeast (Westermann and Neupert, 2000), (b) human - HeLa cell (image courtesy of Megan Cleland), (c) and plant (Arabidopsis). Scale bar in all images = 5 µm. Images reprinted with permission from Scott and Logan (2011).

The plant chondriome (all the mitochondria of a cell collectively) is composed of a population of dynamic physically discrete organelles, but acts as a "discontinuous whole" as a result of continuous inter-mitochondrial fusion and fission which allow mitochondria to exchange mtDNA and other materials (Logan, 2006). Apart from the mechanoproteins and regulatory factors involved in organelle fission and fusion, mitochondrial dynamics can be regulated by cell architecture, and cellular metabolism (Liesa et al., 2009) through direct and indirect interactions with the cytoskeleton (Anesti and Scorrano, 2006; Scott and Logan, 2007; Benard and Karbowski, 2009). Plant mitochondria are very dynamic organelles, which need to move or meet each other and have to be distributed in the cell for its proper function (Scott and Logan, 2007; Logan, 2010). As far as mitochondrial movements and distribution are concerned, the cytoskeleton (composed of microtubules, actin and intermediate filaments) plays a major role. It has been recorded that mitochondria can move through the cytosol up to 10 µm s^{-1} speed in growing Arabidopsis root hairs (Zheng et al., 2009).

1.2 Cytoskeleton

The cytoskeleton is a network of protein filaments which contributes to the coordination of cellular events in eukaryotes. Although as the name implies, the cytoskeleton works as a cellular scaffold to give structural support to the cell, it also plays a critical role in intercellular transport, motility, cell division, and cell signaling (Alberts, 2008). This diverse range of activities performed by the cytoskeleton depends on its three components; thin microfilaments (or actin

filaments), medium sized intermediate filaments, and thick microtubules (MT). Although they have different mechanical properties and dynamics, they are all self-assembled helical polymers of specific protein subunits that have an ability to assemble and disassemble according to the cellular demand (Mollinedo and Gajate, 2003). Microtubules and actin filaments account for most eukaryotic cellular movements. Microtubules are firm hollow rods designed to handle tension and compression of the cell, while actin filaments are more flexible and arranged into bundles to handle asymmetrical forces.

In Animals, microtubules believed to be playing major role of organelle transport including mitochondria (Heggeness et al., 1978) and Golgi apparatus (Thyberg and Moskalewski, 1999). Similar observations have been made in mitochondrial movement in fission yeast *Schizosaccharomyces pombe* (Yaffe et al., 1996). Whereas actin filaments found to be playing predominant role in mitochondria (Van Gestel et al., 2002) and chloroplast (Jouhet and Gray, 2009) movements in higher plants and mitochondrial movements in budding yeast *Saccharomyces cerevisiae* (Hermann and Shaw, 1998).

Similar to yeast and animals, in plants it has been found that MT and actin filaments are co-arranged (Fig. 1- 4) and have cooperative functions in many aspects (Sampathkumar et al., 2011).

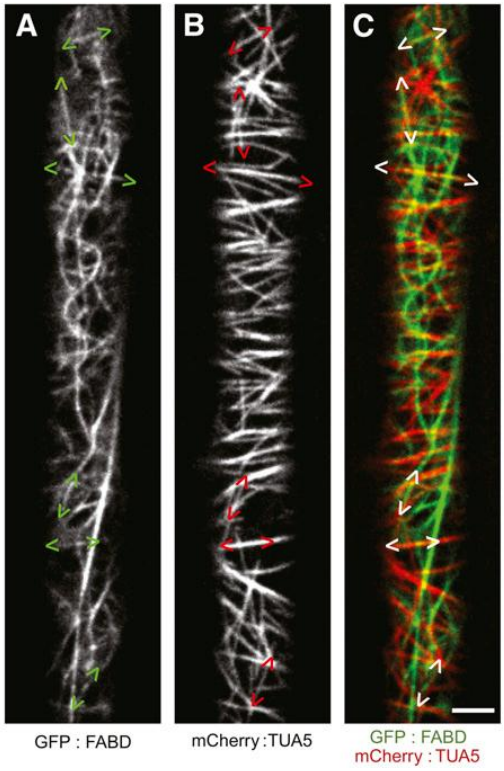

Figure 1-4 Co-alignment between Cortical actin filaments (AFs) and microtubules (MTs) in Arabidopsis Hypocotyl Cells, (A) Green fluorescent protein (GFP): F-actin binding domain of fimbrin 1 (FABD) showing cortical AF pattern that is duel labelled with (B) mCherry: α-tubulin 5 isoform (TUA5) to show cortical MT array. Co-aligned regions are showing in yellow colour in the composite image (C). Scale bar in all images = 5 µm. Images reprinted with permission from Sampathkumar et al.,(2011).

1.2.2 Plant microtubule dynamics

Microtubules are the thickest and most rigid component of the plant cytoskeleton (Schaap et al., 2006), a very dynamic filamentous network. Microtubules are composed of globular tubulin (protein) building blocks, which are made out of non-covalently linked α-tubulin and β-tubulin molecules (heterodimers). These α-tubulin and β-tubulin dimers then bind end to end to make protofilaments, and 13 of these protofilaments are positioned to form the walls of the overall rigid, hollow, and cylindrical MT structure, which is about 25 nm in diameter (Fosket and Morejohn, 1992; Mollinedo and Gajate, 2003). In tubulin heterodimers, GTP bound to β-tubulin can be hydrolyzed (and exchanged freely, E-site) but GTP bound to α-tubulin is never hydrolyzed and is non-exchangeable (non-exchangeable N site), which gives the stability (GTP cap) to the MT. In addition to α and β-tubulin, MTs are composed with a relatively little amount

of γ-tubulin, which helps in MT formation via stabilization or by nucleation (Dryková et al., 2003; Binarová et al., 2006).

Microtubules are polar filaments with two discrete ends, a fast growing plus end and a slowly growing minus end. Both ends of individual protofilaments are capable of adding more tubulin heterodimers, supporting MT elongation, however net MT growth happens at plus end direction while net shrinkage occurs in the minus end (Mollinedo and Gajate, 2003). Thus MTs are very dynamic in nature, undergoing cycles of growing, shrinking and pausing in between.

Plants can have several different MT arrays dependent on the developmental stage of the cell. The preprophase band which surrounds the nucleus in cells that are about to undergo cellular division, the phragmoplast that forms in late cytokinesis, and the cortical array which is positioned in the cytoplasm just below the plasma membrane and parallel to it (Van Damme et al., 2004; Ehrhardt and Shaw, 2006). These individual cortical array MTs can be as long as 10 µm in length and run parallel to each other (Fig 1- 4 B) with overlapping ends (Morrissette et al., 2004), however this MT arrangements can be varied depending on the cell type and the developmental stage (Ehrhardt and Shaw, 2006). In plants, MT growth and shrinkage velocities differ from their yeast and animal counterparts, which is around 2-19 µm/min and 3-32 µm/min for the growth rate and shrinkage in yeast and animal cells respectively, while it is only 3-4 µm/min in growth and 5-9 µm/min in shrinkage for plant cells (Vos et al., 2004).

The diverse array of functions carried out by MTs are achieved either by posttranslational modifications of the filament or by interacting with regulatory proteins, for instance microtubule associated proteins (MAPs). These MAPs are essential for all aspects of tubulin biochemistry, especially stabilizing MT polymerization and linking them together (Marc et al., 1998). Because of its high affinity for MTs, the microtubule binding domain (MBD) of MAP4 chimeric with fluorescent protein is frequently used to visualize mammalian and plant MT dynamics (Marc et al., 1998). MT plus end tracking proteins (+TIPs), also a group of proteins belonging to the MAP family, are used to visualize MTs *in vivo*. Because of their specific accumulation at plus ends and low affinity to the MT body, when chimeric with fluorescent proteins, they are specifically able to track the growing plus end of MT. End binding 1 (EB1) is one such +TIP protein group that has a highly conserved N-terminal domain (Hugdahl and Morejohn, 1993). There are 3 EB1-like genes in Arabidopsis, designated as AtEB1a, AtEB1b and AtEB1c (Chan et al., 2003), AtEB1a

and AtEB1b chimeric with fluorescent proteins are usually used as +TIP markers in MT dynamics studies (Young and Bisgrove, 2011).

Movements along MT in eukaryotes are largely dependent on two motor proteins, kinesin which moves towards the plus end and dynein, towards to the minus end. Other than these motor proteins, there are several MAPs identified to play a role in mitochondrial movements along MT (Scott and Logan, 2010). Milton and Miro are two such MAPs, which have been studied extensively. Milton was first found in Drosophila nerve cells and has a loose association with mitochondria. Its interactions with mitochondria depends on Miro, which is found (orthologues) in all eukaryotes including Arabidopsis (Scott and Logan, 2010). However, unlike their animal and yeast counterparts, plant mitochondrial movements do not directly depend on MT arrangements (Boldogh and Pon, 2007; Scott and Logan, 2010).

1.2.3 Plant actin dynamics

Actin plays a major role in mitochondrial moments in plants. Filamentous actin (F-actin/ actin microfilament) are made out of actin monomers (globular actin/G-actin) joined end to end to make a double standard F-actin helix which is around 7 nm in diameter (Staiger, 2000). As with MTs, actin filaments are polar having a "barbed" plus end and "pointed" minus end. Actin filaments grow faster at the plus end since it has a high affinity to G-actin monomers. At the minus (pointed) end, disassociation of G-actin monomers from actin filament occurs at a greater rate than that in plus end, resulting in shrinkage of filament length. This growth or shrinkage according to monomer addition or loss is called actin turnover. When the rate of addition is equal to loss, it's called threadmilling and actin appears to move in this stage (Zheng et al., 2009). For plant cells F-actin is more important than its free form G-actin (Staiger, 2000), and it plays a vital role in cytoplasmic streaming, cell shape formation, signaling, cell wall synthesis, response to pathogen attack in hypersensitive response (HR), and mitochondria (and other organelle) trafficking (Liu and Luan, 1998; Furuse et al., 1999; Staiger, 2000; Tominaga et al., 2000; Šamaj et al., 2004; Pollard and Cooper, 2009; Scott and Logan, 2010; Wightman and Turner, 2010). These actin filaments then make more complex structures like orthogonal networks and parallel bundles. Plants use these actin bundles as railway tracks to transport organelles such as mitochondria, for long distances. In animals, different sets of actin bundles are made according to the cellular demand and function, usually they vary by the participating actin-cross linking

proteins; in plants however less variation of actin bundles has been observed (Thomas et al., 2009). In Arabidopsis, most of the elongated cells (hypocotyl cells, leaf petiole cells) show thick longitudinal actin bundles (Fig. 1-4 A) while irregular shaped cells (epidermal pavement cells, mesophyll cells) show randomly oriented actin bundles. Root meristem cells show randomly organized actin filaments in cytoplasm and transverse bundles in the cortex, whereas root hairs show extensive longitudinal arrays of actin filaments arranged in fine and thick bundles (Hashimoto, 2011).

The actin cytoskeleton is a highly dynamic system, which is controlled by various actin-binding proteins (ABPs). Myosins are one such ABP superfamily acting as a motor protein for cellular cargo movements. A few of the Arabidopsis myosin gene family proteins (e.g. class XI, a close relative to fungal and mammalian class V) have been identified to be involved with mitochondrial movements (Scott and Logan, 2010). However, according to a recent study using a plant myosin inhibitory drug (BDM), it has been suggested that mitochondria are capable of moving along actin cables, with or without the help of myosin motor but using actin turnover (Zheng et al., 2009). To visualize actin filaments *in vivo*, several methods have been developed, such as the chimeric fluorescent construct of the actin binding domain of mouse talin fused to the C-terminus of GFP (GFP-mTalin) (Kost et al., 1998). Although there is some speculation about artifacts introduced into developing cells by GFP-mTalin and other fluorescent contracts, there was no difference observed in fully-grown Arabidopsis root cells (Ketelaar et al., 2004). According to a study by Sampathkumar et al., (2011) using actin and MT de-polymerizing drugs (Oryzalin and LatB), the arrangement of the cortical actin array depends on (or requires) the presence of a functioning cortical MT array in Arabidopsis (Fig 1-4).

1.2.4 Cytoskeletal interactions in plants

As described previously, actin and microtubules make two different cytoskeletal networks and act like a scaffold in eukaryotic cells. Until recently, it has been widely believed that these two different cytoskeletal elements function independently to facilitate the movements of two different sets of organelles. Although these two different networks function separately, new evidence based on pharmacological studies, cytoskeletal mutants and microscopic observations, suggests that these two elements work in a coordinated manner in plants.

In Arabidopsis under normal conditions, it has been observed that MT and actin filaments are co-aligned at the cell cortex (Fig. 1-4 A to C) (Staiger et al., 2009; Sampathkumar et al., 2011). However, there is a controversy among researchers on how microtubules behave when actin filaments are destroyed by long-term drug treatments (Latrunculin B and Cytochalasin B). For example, according to some research, MTs remain unaffected with these treatments (Collings et al., 2006), while there is at least one report of increased randomization of transverse microtubules after actin disruption (Ueda and Matsuyama, 2000). However, in most of the scenarios it has been identified that the re-arrangement of MT results from actin disruption (Kobayashi et al., 1988; Yoneda et al., 2004). On the other hand, when MT is destroyed actin filaments have been found to be hypersensitive to the actin disrupting drug Latrunculin B (Lat-B) (Collings et al., 2006). Moreover such conditions resulted in partial loss of the fine transversely oriented cortical actin filaments and actin filament re-establishment in Arabidopsis cells (Sampathkumar et al., 2011). Following observations of mitochondria in tobacco cells (*Nicotiana tabacum;* (Van Gestel et al., 2002), and mitochondrial *fmt* mutants (Logan et al., 2003; Logan, 2006), it has been suggested that although mitochondria move along the actin filaments, MTs may play a role in mitochondrial positioning in the cortical cytoplasm.

1.2.5 Cytoskeleton disrupting chemicals

There are several classes of chemicals available to disrupt MT polymerization. Oryzalin, a dinitroaniline herbicide, binds to α-tubulin in polymerized MT, as free monomers (Akhmanova and Steinmetz, 2010). When oryzalin binds with free α-tubulin, it prevents protofilaments from binding with each other and slows down MT formation. In the base of polymerized MTs oryzalin destabilizes the interaction between protofilaments and thus depolymerizes the MT (Marc et al., 1998; Akhmanova and Steinmetz, 2010). Other than Oryzalin, chemicals such as nocodazole vinca alkaloids, taxoids and colchicine also depolymerize the MT at high doses (Moisoi et al., 2002).

Latrunculin B (Lat-B) is a compound initially isolated from the red sea sponge *Latrunculia magnifica* that acts to depolymerize actin. It is capable of disrupting actin filament organization and actin polymerization by G-actin monomer sequestration (Gibbon et al., 1999). Similar to Latrunculin B, Cytochalasin B also disrupts actin filament arrangements in plants (Toyota et al., 2008).

1.3 Cell death

Cell death, in broad terms can be of two types of events; necrosis, which is a non-physiological event involving swelling, plasma membrane rupture, and the inflammatory leakage of cellular contents before death (Pennell and Lamb, 1997), and programmed cell death (PCD) which is a physiological process that has an active and genetically defined pathway to facilitate the selective removal of damaged, infected or unnecessary cells, usually with the help of mitochondria (Gadjev et al., 2008; Logan, 2010).

1.3.2 Programmed cell death

As described previously, it was a revolutionary discovery to find the relationship between programmed cell death and mitochondria. The term "programmed cell death" was first used by Lockshin and Williams,(1965) to describe a physiological event in insect metamorphosis. In multi-cellular organisms, PCD is essential for growth and development processes such as embryo formation in animals, root aerenchyma formation, differentiation of tracheary elements in xylem tissue, and phloem cell development in plants (Drew et al., 2000; Gadjev et al., 2008). Recently animal PCD has been subdivided into three groups, apoptosis (type I), autophagic cell death (Type II), and necrotic PCD (Type III) according to the morphological and biochemical features (Reape et al., 2008).

1.3.3 Apoptosis as a form of animal PCD

In early 1970s, John Kerr and colleagues first identified what they later described as "apoptosis" using electron micrographs of shrinkage necrosis in the adrenals of prednisolone-treated rats (Kerr, 2002). The word "apoptosis" comes from the idea of old leaves falling away from a tree, derived from the Greek roots, "*apo*", which means separation, and "*ptosis",* to give the meaning of "fall away from" (Bredesen et al., 2004). This pioneering work of studying physiological cell death opened the new field of study of cell biology. Cells that are undergoing apoptosis are exhibiting series of biochemical and morphological changes, which can be used as markers for apoptosis. These include cytoplasmic shrinkage, DNA fragmentation (visible as laddering), nuclear condensation, and the production of apoptotic bodies (Strasser et al., 2000; Lord and Gunawardena, 2012). Nuclear fragmentation can be easily identified by the terminal deoxynucleotidyl transferase mediated dUTP nick-end labelling (TUNEL) method, while DNA

laddering can be readily identified by simple gel-electrophoresis showing 180-200 bp DNA fragments (Richberg et al., 1998; Lord and Gunawardena, 2012).

Cell death is largely linked to the breakdown of protein compounds by a class of enzymes called proteases. There are several main families of proteases involved in this process, such as aspartate, serine, and cysteine proteases (Beers et al., 2004). Apoptotic cell death is initiated by activation of a class of cysteine proteases known as caspases. There are two major pathways leading to the activation of these caspases: the extrinsic pathway, involving death receptors in the cell surface, and the intrinsic pathway, controlled by mitochondria and followed by the release of cytochrome c and assembly of the apoptosome (Reape and McCabe, 2008). Caspases are highly conserved throughout evolution and can be found in nematodes, insects and humans (Budihardjo et al., 1999), however, no record of caspases (or homologous proteins) have been found in the Arabidopsis genome.

In addition to caspases, there is an another family of proteins called the BCL-2 family, which is also involved with apoptosis in an anti / pro-apoptotic fashion (Kelekar and Thompson, 1998). These BCL-2 proteins have an ability to manipulate the OMM in order to achieve their purpose, either by inducing OMM permeability which will leads to PCD (Bax, Bak, Bad and Bid) or by inhibiting the permeability of OMM (Bcl-2, Bcl-xL, Mcl-1) and therefore preventing PCD (Karbowski, 2010; Lord and Gunawardena, 2012). Such proteins in plants have yet to be identified. Most of the mitochondrial morphogenesis and remodeling proteins (e.g. Mfn2, Fis1 and Drp1) directly interact with the BCL-2 family proteins validating the notion of mitochondrial morphology change due to PCD (Karbowski, 2010). In mammals, the apoptotic process is known to be amplified by the factors (e.g. cytochrome c, apoptosis-inducing factor and endonuclease G) released from the mitochondrial inner membrane space, which may result from opening of the hypothetical mitochondrial permeability transition pore (mPTP) (Petronilli et al., 2001) or BCL-2 mediated pore formation (Kroemer et al., 2007). This is believed to cause a reduction in mitochondrial membrane potential and mitochondrial matrix swelling leading to rupturing of the OMM, which initiates a chain reaction of apoptosome formation, caspase activation, chromatin condensation, and DNA fragmentation (Lord and Gunawardena, 2012).

1.3.4 Programmed cell death in plants

Unlike the animal PCD classification system, no unified classification system exists in plants, although plant PCD can be broadly classified into several groups using various criteria. One such system uses the source of PCD induction as classification criterion, and according to this classification, plant PCD can be environmentally induced or developmentally regulated (Lord and Gunawardena, 2012). Examples of environmentally induced PCD are heat treatment, hypersensitive response (due to pathogen attacks) and aerenchyma formation (due to low oxygen content). On the other hand, leaf and flower senescence, leaf morphogenesis and xylem formation are examples of developmentally regulated PCD (Lord and Gunawardena, 2012).

A second classification system is based on the morphological changes taking place during PCD and subtypes of PCD within this category include autolytic and non-autolytic PCD (van Doorn, 2011). In the first type under this classification, which involves rapid clearance of the cytoplasm after tonoplast rupture, as well as chromatin condensation, and an increase in vacuolar volume (e.g. for this type of PCD are developmental PCD, heat, oxygen and drought stress). In the second type, cells undergoing non-autolytic PCD do not show rapid clearance of cytoplasm or volume increase in the vacuole, but show swelling of organelles (e.g. hypersensitive response) (van Doorn, 2011). However, overall, there is an overlap that exists between each of these modes in the plant PCD spectrum (Reape et al., 2008).

In animal apoptosis, apoptotic bodies (small globular cytoplasmic fragments, sometimes with fragments of nuclei) (Kerr et al., 1972) are produced in the final steps of apoptosis, then these apoptotic bodies are eventually subjected to engulf by surrounding phagocytes. In plants, although there is some evidence for apoptotic body formation (McCabe and Pennell, 1996), the vast majority of cases do not show any sign of apoptotic processes that are equivalent to the one in animal cells (Logan, 2008; Reape et al., 2008). Although, there have been no records of caspases (or homologous proteins) in plants, there are evidences to support the existence of caspase-like activities, particularly by metacaspases (MCPs) that are plant cysteine proteases found in various plant systems (Korthout et al., 2000; Lam and del Pozo, 2000; Watanabe and Lam, 2011). These metacaspases are found to be arginine-/lysine-specific and structurally related to caspases (in animal system) with emerging lines of evidence that they are playing a role in oxidative stress generating physical (UV and heat) and chemical (H_2O_2, methyl viologen)

treatment induced PCD (Vercammen et al., 2007; He et al., 2008). This is also true with Bcl-2 family proteins, where BCL-2-like proteins exist in plants (Chen and Dickman, 2004; Lam, 2004), especially BI-1 (yeast BAX inhibitor-1) homologues found in various plants, which induced the expression during pathogen interaction in Arabidopsis (Sanchez et al., 2000) and negatively correlate with the DNA fragmentation and PCD in Tobacco (Bolduc and Brisson, 2002). But there is no evidence to show the existence of actual Bcl-2 proteins (Lord and Gunawardena, 2012).

Even though plants doesn't have these crucial proteins which are playing major role in animal PCD, as an important similarity plants possess DNA fragmentation and laddering during their PCD process, which can be readily detected by using the TUNEL method (van Doorn and Woltering, 2005; Lord et al., 2011).

1.3.5 Plant PCD markers / indicators

In the late 90s, McCabe and colleagues tried to identify cellular morphology variations among carrot cells induced to undergo PCD by heat shock at different temperatures. Surprisingly, this resulted in a clear differentiation between PCD and necrotic cell death morphologies. Heat shock at, or below, 50^{o}C resulted in a specific type of morphology among corpses which was morphologically similar to plasmolysis, while cells subjected to more than 50^{o}C heat stress (at around 75^{o}C) died without plasmolysis (Reape et al., 2008). This condensed-cell morphology (plasmolysis) and fragmented DNA are now frequently used as markers for PCD in plants (McCabe and Leaver, 2000).

It was believed during early studies on animal apoptosis that there was no morphological change affecting mitochondria during PCD. However, with the invention of fluorescent protein tagging (e.g. GFP) systems to visualize mitochondria, it has been possible to observe morphological changes in the chondriome during apoptosis (Frank et al., 2001). This morphological change is found to be closely associated with the release of cytochrome-c and cell death (Karbowski and Youle, 2003). The prevention of mitochondrial morphology changes by anti-Drp1 antibodies reduced cell death significantly, indicating a strong connection between mitochondrial morphology change and apoptosis (Frank et al., 2001). However, there is an important morphological difference between animal PCD (particularly apoptosis) and plant PCD. The animal cell chondriome is typically a reticulo-tubular morphology, and during the induction

of apoptosis the chondriome fragments to produce a punctiform distribution of physically discrete organelles (known as the thread-grain transition) (Frank et al., 2001). In contrast, plant mitochondria are already punctiform, and do not show a size reduction or an increase in number during PCD (Scott and Logan, 2008). However, according to recent research conducted using Arabidopsis protoplasts, subjected to either chemical (which releases reactive oxygen species; ROS) or physical (a mild heat shock) stresses to induce cell death, mitochondria morphology changes do occur prior to cell death (Scott and Logan, 2008).

1.3.6 Mitochondria in plant programmed cell death

In animal cells, as described previously, mitochondria play a definitive role in PCD via cytochrome-c release activating caspases and the roles of BCL-2 proteins. And mitochondrial morphology changes with the induction of PCD. Similar to animal cells, PCD induction in plant cells leads to swelling of the mitochondrial matrix, as a result of changes in the permeability of the inner mitochondrial membrane by mitochondrial permeability transition (MPT) and membrane depolarization (Lord and Gunawardena, 2011, 2012). As a result of these actions, it has been found to be releasing large amount of cytochrome c from inter-membrane space in both animals and plant mitochondria (Vacca et al., 2006). Although in animal PCD, there is a direct link between cytochrome-c release and the initiation of caspase activity, and since plant cells does not have caspase, it is unclear the role cytochrome-c plays in plant PCD. However, recently it has been proposed that cytochrome-c release can amplify the reactive oxygen species levels in plant cells which eventually leads to PCD (Sweetlove and Foyer, 2004). Alternatively, cytochrome-c can activate a “caspase-like” protein cascade (or metacaspase) in plant cells that will also lead to PCD (Jones, 2000).

In plants, soon after the induction of PCD, mitochondrial morphology changes occur and plant mitochondria arrange in clusters or aggregates in the cell. Usually this occurs in the cytosol but it can occur in the vicinity of the nucleus, although the exact reason for this is yet unknown, it is believed to be incorporated with signaling the nucleus to initiate PCD (Logan, 2008; Lord and Gunawardena, 2012). According to some studies, in sites where clusters of mitochondria are attracted and contacted to the nuclear envelope, signs of chromatin condensation is evident, suggesting the structural nature of PCD induction (Lord et al., 2011). While most mitochondrial clusters are recorded in the cytosol of cell, there are some unpublished evidences to suggest they

are also present in the vacuole (Lord et al., 2011). This might be as a result of selective elimination of damaged mitochondria via mitophagy or another quality control pathway.

1.3.7 Plant PCD and abiotic stress factors

There are many abiotic stressors (pollution, UV light, salinity, and extreme temperature etc.) that contribute to oxidative stress in plant cells. Every plant cell actively produces reactive oxygen species (ROS) at low levels when they use aerobic metabolism for energy production, which leads to the formation of various kinds of ROS by-products inside the cell such as: O_2^-, H_2O_2, $HO^{\cdot}$, etc. These ROS by-products (resulting from incomplete reduction or excitation of molecular oxygen) are produced mainly in mitochondria and chloroplasts, and have ability to damage proteins, lipids and DNA in plant cells. Oxidative stress occurs when the production and transient accumulation of ROS exceeds the natural antioxidant defense mechanism in cells, which eventually leads to cell damage and ROS-dependent PCD (Gadjev et al., 2008). Therefore, production and removal of such by-products are highly regulated in normal plant cells (Møller, 2001). There are numerous examples of ROS being involved as a signaling compound in various processes (over different developmental stages) of plants, such as stress responses, defense and PCD (Gechev et al., 2006).

Recent evidence demonstrates that the biological action of ROS signaling depends on multiple factors, including site of production, extent and strength of the signal, developmental stage of the plant, and the presence of other signaling molecules such as nitric oxide (NO) and plant hormones (Lam et al., 2001; Gechev et al., 2006; Gadjev et al., 2008). For example, although mitochondrial ROS production is much lower than that in chloroplasts due to the presence of alternative oxidase (AOX), mitochondrial ROS is found to be far more important for plant PCD (Robson and Vanlerberghe, 2002; Jones et al., 2006). Also, it is now widely accepted that low concentrations of ROS play a protective role against oxidative and abiotic stresses, while high concentrations lead to PCD (Gechev et al., 2002; Vranova et al., 2002; Gechev et al., 2006). According to some arguments, ROS may act as signaling molecules to initiate the mitochondrial permeability transition (Garcia-Perez et al., 2012). All these above mentioned observations, lead to the conclusion that mitochondria are the organelles driving plant PCD by generating ROS as a signaling molecule.

Similar to ROS, the term reactive nitrogen species (RNS) is used to designate nitric oxide (NO) and related molecules that cause nitrosative stress. NO is a free radical, and in animals it is formed by nitric oxide synthase (NOS) using arginine as a substrate. However, in plants there is no direct evidence to support the presence of NOS. There are a few established sources for NO biogenesis in plants, including reduction of nitrite by nitrate reductase (NR) in an enzymatic pathway, and by using nitrite as a terminal acceptor of mitochondrial electron transport chain (Modolo et al., 2005; Flores et al., 2008). While the direct role of NO in plant PCD is unknown, there is evidence to support it either working as a stress factor to initiate PCD (Jones, 2000), or acting as a signaling molecule to initiate PCD (Clark et al., 2000; Saviani et al., 2002). NO can work as a Ca^{2+} mobilizing compound and can increase the cytoplasmic Ca^{2+} concentration, which can lead to PTP via calcium-dependent protein pathways (e.g. CDPK, MAPK etc.) (Jones, 2000; Besson-Bard et al., 2008).

While some observations suggests that NO alone is sufficient to initiate PCD (Clarke, 2000; Saviani et al., 2002), there are other evidences suggesting that increased levels of ROS cause plant cells to be more susceptible to NO treatments and lead them to PCD (Jones, 2000; Gechev et al., 2006; Zago et al., 2006; Garcia-Perez et al., 2012). Furthermore, it has been found that with increased levels of NO (using NO donors), plant cells can produce more ROS than normal (Clark et al., 2000). On the other hand, it has also been found that increasing the amount of ROS can induce NO production in tobacco cells (De Pinto et al., 2006). These observations suggest that the balance of RNS and ROS production is important for plant cell survival.

1.3.8 Plant PCD and cytoskeleton

Contrasting modifications to the cytoskeletal arrangement during PCD have been identified in various animal, yeast and plant systems (Gourlay and Ayscough, 2005; Thomas et al., 2006). When actin filament turnover is increased in animal cells it has been found to be increasing the lifespan of the cell as well, when turnover decreased it triggers the apoptotic like cell death by mitochondrial dependent manner (Gourlay and Ayscough, 2005; Franklin-Tong and Gourlay, 2008). This reduced actin turnover and dynamics found to be linked with the depolarization of mitochondrial membrane, increased ROS production and cytochrome-c release leading to PCD, while increased actin dynamics is linked with reduction in ROS production (Gourlay et al., 2004). Same as with the actin depolymerization, actin stabilization also found to be triggering the

apoptosis in animal cells (Posey and Bierer, 1999). These observations suggest that the alterations to actin arrangement can trigger the mitochondria to release ROS, cytochrome c and other apoptotic factors to induce PCD (Gourlay and Ayscough, 2005).

In plants, when PCD is initiated via HR related mechanisms, the formation of actin bundles/ aggregates near to the site of infection have been observed (Smertenko and Franklin-Tong, 2011). Similar to these alterations to the cytoskeleton, treatments with the actin de-polymerizing drugs, Latrunculin B and cytochalasin D, resulted in elevated levels of PCD, indicating a direct link between PCD and actin depolymerization or alteration (Smertenko and Franklin-Tong, 2011). In addition, the actin stabilizing drug Jasplakinolide has also been shown to trigger PCD, indicating the importance of both actin stabilization and depolymerization in plant PCD (Smertenko and Franklin-Tong, 2011). Recent studies investigating the proteomic profiles of cells undergoing heat shock mediated or ROS mediated PCD in tobacco or Arabidopsis cells also revealed an inhibition of the expression of several actin related proteins (Swidzinski et al., 2002; Vannini et al., 2012).

Although the involvement of microtubules in PCD remains controversial, and even though most cell types undergoing PCD via developmental and HR mediated pathways show depolymerized and reorganized MTs in cells, the direct correlation between MT and PCD is still unclear (Binet et al., 2001; Esteve et al., 2007; Smertenko and Franklin-Tong, 2011). Apoptosis has been shown to occur in animal cells where the mitotic spindle has not formed correctly leading to erroneous chromosome segregation and a lag in cell cycle progression (Sorger et al., 1997). Experiments performed with the MT de-polymerizing drug oryzalin and stabilizing drug taxol showed that treatment did not trigger PCD when each drug was used alone, suggesting that in contrast to actin, in MTs, either MT stabilization or depolymerization does not have a direct role in plant PCD (Binet et al., 2001).

1.4. Main objectives of this thesis

Scott and Logan, (2008) found that in Arabidopsis protoplasts, when subjected to either chemical (which releases reactive oxygen species; ROS) or physical (a mild heat shock) stresses to induce cell death, an irreversible mitochondria morphology change occurred prior to cell death, which can be used as a marker for PCD in plants. The current work has two main

objectives following several hypothesis which offer new insights into plant PCD and mitochondrial dynamics during oxidative and nitrosative stress.

It has been hypothesized that the increased concentrations of NO found in arginase negative mutant plants make them more sensitive to ROS induced PCD and that they will show lower viability and high degree of plasmolysis compared to control samples. It has also been suggested that these arginase negative mutants may show different MMT than that of control samples when subjected to heat shock. My first objective in this research was to investigate the possible role of mitochondrial localized NO on PCD initiation, mitochondrial dynamics and MMT during heat-shock induced cell death, which will be further discussed in Chapter Three in this thesis.

My second objective was to study the cytoskeletal dynamics alongside mitochondrial dynamics during Arabidopsis PCD, which will be discussed in Chapter Four. This second objective is based on several hypotheses. Although mitochondrial morphology change is observed with heat-shock, there has been no study conducted to see the correlation between the cytoskeletal change and mitochondrial morphology. One of my hypotheses was that by disrupting actin and microtubule cytoskeleton it is possible to pheno-copy the mitochondrial clustering and cessation behavior observed with heat shock. To address this hypothesis, my objective was to use cytoskeletal disrupting drugs, such as Latrunculin B and Oryzalin to disrupt the Arabidopsis cytoskeleton and observe the mitochondrial and cytoskeletal dynamics.

Since it has been hypothesized that the mitochondrial clusters might move on microtubules (Logan et al., 2003; Logan, 2006), my second objective in this category was to identify the possible correlation between microtubules and mitochondria, during mitochondrial cluster formation.

CHAPTER 2

2. MATERIALS AND METHODS

Common molecular biology and cell biology techniques were performed as described by Sambrook et al. (2001) or according to the manufactures' instructions. Protocols which were significantly altered from previously published works are described below.

2.1 Plant material and labeling

2.1.1 Development of Arabidopsis lines to visualize microtubule plus ends and mitochondria

Arabidopsis lines expressing fluorescence proteins for both mitochondria and cytoskeletal elements were used for this experiment. To develop the experimental tool to enable visualization of microtubule plus ends together with mitochondria, Arabidopsis wild type line Colombia (Col-0) was stably transformed with a binary vector harboring microtubule end binding protein (EB1b). The vector used, pCAMBIA1300 binary vector (see appendix, Fig. 6-1) with a CaMV 35S promoter harboring either GFP or RFP AtEB1b (p35S GFP:AtEB1b or p35S RFP: AtEB1b), was a kind gift from Dr. Jaideep Mathur , (Mathur *et al.* (2003).

1.1.1.1 Preparation of electrocompetent *Escherichia coli* cells for the transformation

Escherichia coli electrocompetent cells were grown by inoculating 10 µl of a previously made aliquot of competent cells into 10 ml of LB medium. This culture was grown overnight at 37 ^{o}C, and then 500 µl of competent culture was inoculated on 500 ml of LB medium, and incubated at 37 ^{o}C with shaking until optimal growth was obtained (OD_{600nm} = 0.5). Then the cultures were centrifuged using a bucket-rotor refrigerated centrifuge (Beckman Avanti Centrifuge J-25) at 4000 x *g* for 15 min at 4 ^{o}C. Cell pellets were washed in 500 ml of ice cold sterile water. This wash step was repeated twice and the final pellet was resuspended in 10 ml of 10% (v/v) glycerol and dispensed into 50 ml falcon tubes followed by a centrifugation step at 4000 x *g* for 15 min (at 4 ^{o}C). The resulting pellet was resuspended in 1.5 ml ice cold 10% (v/v) glycerol and dispensed 50 µl aliquots, frozen with liquid nitrogen and stored at -70^{o}C.

1.1.1.2 Preparation of electro-competent *Agrobacterium* cells

Electrocompetent *Agrobacterium tumefaciens* (strains GV3101) cells were prepared according to the following protocol. A single Agrobacterium colony was inoculated on 500 ml of YEP liquid medium containing kanamycin and gentamycin and incubated at 28 ^{o}C to an OD_{600} of about 0.5 (early to mid-log phase). Following incubation, cultures were chilled on ice and centrifuged at 4000 g for 15 min (at 4 ^{o}C) in bucket-rotor refrigerated centrifuge (as above). Cell pellets were washed in 500 ml of 1 mM 4-(2-hydroxyethyl)-1-piperazineethanesulfonic acid (HEPES) (pH 7.4). This was repeated twice and the final pellet was resuspended in 10 ml of 1 mM HEPES and dispensed into 50 ml falcon tubes followed by a centrifugation step at 4000 *g* for 15 min (at 4 ^{o}C). This was resuspended in 1.5 ml ice cold glycerol (10% v/v), dispensed 50 µl aliquots, frozen with liquid nitrogen and stored at -70^{o}C.

1.1.1.3 *Escherichia coli* transformation with recombinant plasmids

Electrocompetent *E. coli* cells were transformed by electroporation using the following protocol. Electrocompetent *E. coli* cells were thawed at room temperature and immediately placed on ice, 40 µl of competent cells were transferred to a pre-chilled electroporation cuvette on ice. Approximately 2 µl of plasmid in TE buffer was mixed with the competent cells in cuvette and transformation was carried out at 1.44 kv (130-200 w, 5 ms) using a single pulse electroporation system. Cells were immediately resuspended in 1 ml of SOC medium (Hanahan, 1983) and incubated for 1 hour at 37^{o}C with shaking. Cultures were spread on LB agar plates containing the appropriate antibiotics and incubated at 37^{o}C overnight.

1.1.1.4 Plasmid DNA Isolation, purification and confirmation of recombinants

A single (transformed) bacterial colony from each plate was inoculated on 15 ml of LB and incubated overnight at 37^{o}C. Plasmid DNA was isolated using E.Z.N.A Plasmid Mini Kit I (Omega Bio-Tek, U.S.A., Ref. No. D6943-02), according to the manufacture's guidelines. Bacterial cells were pelleted by centrifugation at 10,000 x *g* for 1 min at room temperature (RT); then pellets were resuspended completely, by adding 250 µl of Solution I containing RNase A solution and vortexing thoroughly. The suspension was transferred to a 1.5 ml microcentrifuge tube and 250 µl of Solution II was added, to obtain a clear lysate. Then 350 µl of Solution III was added and mixed by inverting tubes till a flocculent white precipitate formed. After centrifugation at 13,000 x *g* for 10 min at room temperature; a compact white pellet was formed.

A HiBind DNA Mini Column was prepared by adding 100 µl of Equilibration Buffer and subsequent centrifugation at 13,000 x *g* for 1 min in a 2 ml collection tube. The cleared supernatant (from the above step) was added to a prepared HiBind DNA Mini Column. The lysate was passed through the column by centrifugation at 13,000 x *g* for 1 min in a 2 ml collection tube, flow-through was discarded. Then 500 µl of Buffer HB was added, to wash the column by centrifuging at 13,000 x *g* for 1 min at RT. After this protein contamination removal step, the column was washed twice with 700 µl of DNA Wash Buffer. The column was centrifuged at 13,000 x *g* for 1 min at RT and dried by centrifugation at 13,000 x *g* for 2 min. The column was placed in a 1.5 ml microcentrifuge tube and 75 µl of pre-heated (65^{o}C) Elution buffer was added, directly on the column matrix followed by 1 min incubation period. After centrifugation at 13,000 x *g* for 1 min at RT purified plasmids were obtained. The concentration and quality of DNA was determined, using the spectrophotometer at 260/280 nm.

To confirm the transformation, restriction enzyme digestion was performed, as described in the protocol accompanying the restriction enzymes KpnI, and NotI, (New England Biolabs, Beverly, MA).

1.1.1.5 *Agrobacterium* transformation with recombinant plasmids

Electroporation was used as the method of transformation with 100 ng of plasmid DNA in 40 µl of electro-competent *Agrobacteria* prepared as described in 2.1.1.2. Following electroporation using the manufacturer's recommended settings, 1 ml of SOC medium was added to the cells and this solution then transferred to a 15 ml Falcon tube which was then incubated for one hour at 28 ^{o}C before plating 100 µl on YEP-agar plates containing appropriate antibiotics. These YEP plates were incubated over two nights at 28^{o}C. Then single colony from each plate was inoculated on 10 ml of YEP medium containing antibiotics and incubated at 28^{o}C with shaking.

Plasmid DNA was extracted using E.Z.N.A Plasmid Mini Kit I (Omega Bio-Tek, U.S.A., Ref. No. D6943-02) as described previously but with the 2x volumes of solutions I, II and III. The resulting plasmid DNA was quantified and subjected to restriction digestion using Not I and Kpn I restriction enzymes to confirm the transformation.

1.1.1.6 Transformation of Arabidopsis plants using Agrobacterium floral dip method

Arabidopsis Colombia ecotype (Col-0) plants were transformed using modified

"*Agrobacterium* floral dip method" (Clough and Bent, 1998). Resulting stably transformed (screened and selected up to T_2 generation) lines (EB1b-GFP and EB1b-RFP) were (separately) crossed with Arabidopsis lines expressing mitochondrial targeted fluorescence proteins (either 43C5 (pBINmgfp5-atpase) (Logan and Leaver, 2000) or mito-mCherry (Logan DC, unpublished).

2.1.2 Development of Arabidopsis lines to visualize whole microtubules and mitochondria

To visualize the relationship with whole microtubule and mitochondria, lines expressing the microtubule-binding domain of the mammalian MAP4 gene (Mathur and Chua, 2000) fused to mCherry (mCherry-MAP4, Logan DC, unpublished) was crossed with a Arabidopsis line expressing mitochondrial GFP (line 43C5; Logan & Leaver, 2000).

2.1.3 Development of Arabidopsis lines to visualize actin microfilaments and mitochondria

To visualize the actin cytoskeleton and mitochondria a double transgenic Arabidopsis line expressing mCherry fused to the actin binding domain (ABD) of mouse talin (mCherry-mTalin) and mito-GFP was used (Logan DC, unpublished).

2.1.4 Development of arginase-negative mutant lines to visualize actin microfilaments and mitochondria

To visualize mitochondria in arginase negative mutant lines (*argh1-1* and *argh 2-1*) obtained from Flores et al.,(2008), Agrobacterium mediated transformation method was used to generate Arabidopsis mutant lines expressing mito-GFP (Boldt and Logan, unpublished). Seeds (T_2 generation) from this stable transformation received by the author, and further screening was carried out to choose best expressing plants (T_4 generation).

2.2 Growth of Arabidopsis lines

Seeds were surface sterilized in a 1.5 ml microfuge tube by immersion in 1 ml of 80% (v/v) ethanol (mixed by inversion for 5 min then decanted), followed by 1 ml of 1.50% NaOCl (household bleach; 3 NaOCl: 10 water, v: v) mixed as previous and then decanted, and then finally washed three times with 1 ml of sterile distilled water. The seeds were spread on a

MS agar plate containing 0.43% (w/v) 1x MS salts, 0.8% (w/v) type M agar, 1% (w/v) sucrose and 0.05% (w/v) MES, pH 5.8. The plates were stored in a refrigerator at 4^{o}C for 3 days to synchronize germination.

After the stratification, Petri dishes were placed in a growth chamber (16 hr light, 8 hr dark cycle at 23^{o}C). Petri dishes containing plants to be used for root hair observations were set in an upright position from the beginning to allow the seedlings to grow roots on the surface of the plate.

2.3 Plant crossing

In all plants chosen as females all secondary bolts were removed, and on the main bolt, all siliques and open buds were removed. On this main bolt, the three largest closed buds were retained and all others removed. Using ethanol sterilized needle-nosed forceps and a low power dissecting microscope flowers were emasculated including removal of the sepals and petals, leaving only the carpels intact. From the plants chosen to be male (or pollen donating) flowers that are visibly shedding pollen were chosen, they were detached and the convex surface of the anthers brushed against the female plant's stigma to transfer the pollen. After crossing, any newly developed inflorescences were removed from the female plant to aid the identification of the crossed flower. Siliques containing F_1 seeds were collected when mature, but before opening, and stored desiccated at -20^{o}C until use.

2.4 Microscopy and image analysis

2.4.1 Static, Z-stacks and time-lapse imaging

Arabidopsis mitochondria were examined in both intact root hairs and root epidermis cells in region of differentiation of 10 day old seedlings. To get static and time-lapse images, the whole plants were mounted on a standard glass slide (75 mm x 25 mm, 1 mm thick, Ted Pella Inc.), in 0.1% agar, and then covered by a glass coverslip (Cover glass No. 1.5; VWR). The coverslip was pressed very gently onto the slide covering the whole root (but leaving the leaves and stem exposed) to remove air-bubbles.

2.4.2 Static and time lapse epifluorescence image acquisition

Static and time lapse images were collected using wide-field epifluorescence microscopes, either Zeiss Axio Imager Z1 (Zeiss, Oberkochen, Germany) microscope coupled with a Zeiss AxioCam MRm monochrome cooled-CCD camera or an Olympus BX61 (Olympus America) microscope equipped with a QImaging Rolera-MGi+ EMCCD camera (Surrey, BC) was used.

Olympus BX61 epifluorescence microscope was used with 100 x lens with 1.40 numerical aperture plan-apochromat oil -immersion objective, and fluorescence light is separated from the excitation light using a combination of a dichroic mirror (FF562-Di02-25x36) and a bandpass filter FF01-543/22- 25 to visualize red fluorescent signals or Brightline GFP-3035B to visualize green fluorescent signals. All above filter cubes were by Semrock (Rochester, NY, USA). Pictures were taken with MetaMorph Basic system (Advanced Scientific, Meraux, Louisianna) release 7.7.10.

Zeiss Axio Imager Z1 epifluorescence microscope was used with 63 x lens with 1.40 numerical aperture plan-apochromat oil -immersion objective. Green and red fluorescent signals were visualized using filter set no. 38 (BP 470/40, FT 495, BP 525/50) or filter set no. 43 (BP 550/25, FT 570, BP 605/70) (ZEISS, 3 Jena, Germany) respectively. Pictures were taken with AxioVision Software (Rel 4.4; Carl Zeiss, Göttingen, Germany).

All the single channel time-lapse images were taken with one second intervals and all the two channel images with a 5 second interval between images (if not otherwise specified).

2.4.3 Confocal Z-stack image acquisition

A confocal laser-scanning microscope LSM510 META/ConfoCor2 system (Carl Zeiss MicroImaging GmbH) equipped with a 63x Apochromat water-immersion objective lens with numerical aperture = 1.4 was used to collect *Z*-stacks. Green fluorescent signals were detected using an argon laser with a 488 nm excitation filter and an emission range of 505-530 nm and red fluorescent signals were detected using a HeNe laser with an excitation of 543 nm and an emission of 617 nm. Data were captured by the Carl Zeiss LSM 510 software version 4.2 (Carl Zeiss).

2.4.4 Three-dimensional reconstructions and image analysis

1.1.1.7 Image deconvolution and rendering

Time-lapse movies and and *Z*-stacks were deconvoluted using Autodeblur software (AutoQuant v2, Media Cybernetics). Time-lapse images were analyzed, rendered and data extracted using IMARIS 7.4.2 software (Bitplane, Zurich, Switzerland).

1.1.1.8 Identification of mitochondrial/cluster movements

To track mitochondria with time, Imaris autoregressive motion algorithm was used with 0.5 μm as estimated mitochondrial diameter to identify individual mitochondria (see the appendix). Thereafter the same mitochondrion present at each time point was linked to a single track by means of automatic track detection. If one particular mitochondrion disappeared within consecutive time-lapse images (e.g. the mitochondrion had moved out of the field of view), the detection algorithm set to search it in five consecutive frames with maximum radius of 2 μm from its last spot. Mitochondria which were continually present for more than 16 seconds (or frames) within a total 30 seconds of sampling time were used for the further statistical analysis to avoid mitochondria which were no longer visible due to moving deeper into the tissue. Mitochondrial clusters were identified by using a similar algorithm (see the appendix).

1.1.1.9 Identification of mitochondrial movements – a different approach

In order to show moving mitochondria, two images of the same field of view were taken 30 seconds apart with identical settings. Those two images were pseudo-colored as red and green and merged to get a composite image using NIH ImageJ (available at rsb.info.nih.gov/ij/) software. Thus, if mitochondria moved within the 30 second time period, they can be easily identified as separate colors (red or green), but if a given mitochondrion did not move it can be identified as yellow (merged).

2.5 Protoplast isolation

Seedlings were grown in a growth chamber (as described above) for 14-18 days. Using a biosafety cabinet to maintain aseptic conditions, the healthy leaves from 15-20 plants were removed using flame-sterilized scissors and placed on a sterile surface (an upturned Petri dish lid). Each leaf were sliced with a new, flame-sterilized razor blade into 4-6 pieces and transferred to a new 9 cm plastic Petri dish containing 15 ml of sterile 0.5 M mannitol. The leaf fragments

were then washed in this solution for approximately one hour. After one hour, the mannitol solution were removed with a pipette and replaced with 15 ml of Protoplast Enzyme Solution (PES; 0.4 M mannitol, 0.33% (w/v) cellulase 'onozuka' R-10, 0.17% (w/v) pectinase, 3 mM MES, 7 mM $CaCI_2$, pH5.7). The Petri dish were sealed with Nescofilm (Bando Chemical IMD Ltd., Osaka, Japan) and attached to an orbital shaker. Digestion was allowed to proceed overnight in the dark, with continuous gentle mixing (~ 40-50 rpm). After digestion, the protoplast solution was removed from the Petri dish using a large-bore sterile pipette and sequentially filtered through 100 and 40 µm nylon mesh sieves to remove tissue fragments. The filtered solution was placed into a 15 ml plastic centrifuge tube (Falcon type) and centrifuged at 50 x *g* in a swing-out rotor for 10 minutes at room temperature to pellet the protoplasts. The supernatant was decanted and replaced with 10 ml of 0.5 M mannitol. The protoplasts were gently resuspended by inversion, washed, and centrifuged as before. This wash process was repeated once more using fresh 0.5 M mannitol and the protoplasts pelleted as before. The washed protoplasts were resuspended in a small volume of 0.5 M mannitol (usually 100-200 µl) and transferred to a microfuge tube. The concentration of protoplasts was then measured using a haemocytometer and adjusted to between 10^5 and 10^6 protoplasts ml^{-1} with additional 0.5 M mannitol.

2.6 ROS-inducing heat treatments

For heat treatments, 100 µl of protoplast suspension in a microfuge tube was placed in a pre-heated recirculating RM6 Lauda water bath (Postfach, Germany) at 45°C for ten minutes, while the control sample was kept at room temperature for the same time period. Following treatment, the sample was removed from the water bath and incubated for the required period of time. For root hairs, 10-day old seedlings were transferred to a small Petri dish (35x10 mm) containing 300 µl sterile ultra-pure H_20, lid were replaced and sealed using Nescofilm ® (Nippon Shoji Kaisha Ltd, Osaka, Japan), and plates were carefully transferred to a water-bath (Lauda- Postfach, Germany) at 42°C for 1.5 hours. The control sample was kept in room temperature for same length of time. After the treatment, each seedling was transferred to a MS agar plate and incubated in the vertical position.

2.7 Cell viability measurements

The vital stain fluorescein diacetate (FDA) (Sigma) was used as described by McCabe and Leaver (2000). A 0.1% (w/v) stock solution (in acetone) was stored at -20 °C. The stock was diluted to 0.002% (w/v) final concentration with 0.5M mannitol immediately prior to use. Protoplasts were incubated in FDA for five minutes prior to visualization. Any intact protoplast that did not show FDA fluorescence was deemed to be dead. For root hair viability measurements, SYTOX orange (Invitrogen) was used. Seedlings were incubated in SYTOX (diluted up to 670 nM final concentration with ultra-pure water from the DMSO stock) for five minutes prior to visualization. Any intact root hairs that did not show SYTOX fluorescence were deemed alive. Cell viability readings were recorded up to 72 hr after every treatment.

2.8 Mitochondrial morphology, cell counts, and dynamics

Protoplasts and /or root hairs were examined by epifluorescence microscopy, and any protoplast and /or root-hair in which more than half of the individual mitochondria were greater than twice the wild-type mean plan area were considered abnormal. Protoplasts or root hairs with this abnormal mitochondrial morphology were said to have undergone a mitochondrial morphology transition (MMT). Around 100 protoplasts / root hair were measured for each experimental repeat (three replicates for each time-point and treatment), and the percentage of protoplasts or root hairs that had undergone a MMT were calculated. Samples treated with heat shock were compared with non-heat shocked control samples to determine any correlation between mitochondrial dynamics and the initiation of PCD. Mitochondrial dynamics and MMT were compared between control and heat treated samples of each genotype.

2.9 Identification of programmed cell death

To determine whether or not cell death occurred due to PCD or uncontrolled necrosis, cytoplasmic shrinkage (plasmolysis) was used as a PCD marker. Cytoplasmic shrinkage within root hairs was identified by Differential Interference Contrast (DIC) microscopy. Dead root hairs which are showing positive fluorescence in SYTOX (or negative FDA), after the staining were examined by DIC microscopy in order to determine the percentage of dead cells that were also plasmolyzed.

2.10 "NO" effect on PCD and mitochondrial morphology

2.10.1 Quantification of NO accumulation in arginase-negative mutants

In order to evaluate the NO concentration in arginase negative mutants compared to that in wild type sample fluorometric NO determination method was used. In this method, 4-amino-5-methylamino- 2', 7'-difluorofluorescein (DAF-FM) diacetate (D-23844, Molecular Probes, Eugene, OR, USA) was used. Stock solution (in DMSO) was diluted with ultra-pure H_2O to 10 µM final working solution and 5 day old Arabidopsis seedlings were incubated for 30 min followed by a washing step. DAF fluorescence was detected using a Nikon SMZ 1500 zoom stereomicroscope (Nikon, Melville, NY) equipped with a Nikon 1.0 x WD 54 objective lens camera and GFP filter cubes.

2.10.2 The relationship between NO production and sensitivity to ROS-induced PCD of arginase-negative mutants

Cell death and plasmolysis percentages both without heat shock and after the heat shock were compared with the control sample (mito-GFP line 43C5) and arginase negative mutant lines (*argah* 1-1 and 2-1 expressing GFP). Additionally, these data were compared with the results obtained from Arabidopsis 43C5 line treated with the synthetic NO donor sodium nitroprusside (SNP; 12.5 µM, 10 days).

2.11 Drug treatments

Stock concentrations of 30 mM Oryzalin and 2 mM Lat-B were prepared in 100% ethanol (EtOH). Each stock solution was diluted with ultra-pure H_2O to the appropriate final concentration just before use. Ethanol control solutions were made with the same dilution factor of the stock solvent. When experiments performed with different concentrations, the lowest dilution factor of solvent was used for the control.

2.12 Data analysis

Data were analyzed by ANOVA using a MIXED model in SAS 9.2 (SAS Institute, Cary, NC) software. Treatments (heat shock, time, drug treatments were considered fixed factor while replication (how many times an individual experiment performed) were considered random

factors. Prior to analysis, data were tested for normality and homogeneity of variance. Means were separated using Fisher' LSD and declared significant at a probability of 0.05.

CHAPTER 3

3. INVESTIGATING THE ROLES OF MITOCHONDRIAL DYNAMICS AND REACTIVE OXYGEN AND NITROGEN SPECIES IN PLANT PROGRAMMED CELL DEATH

3.1 Introduction

There is a wide range of programmed cell death processes identified in plants, including PCD induced by biotic factors, such as pathogen attack (hypersensitive response) and PCD induced by abiotic factors such as heat shock (HS) and mimicked by various chemicals. Heat stress can change the cellular redox equilibrium of plants, leading to oxidative damage, which will eventually lead to PCD (Vacca et al., 2006; Gao et al., 2008). Mitochondria and chloroplasts are the major site of ROS production in plant cells, and there is evidence that ROS produced in mitochondria is critical to PCD induction (Gechev et al., 2006).

As described in chapter one, mitochondria are highly dynamic organelles, but there is little information about mitochondrial dynamics during plant PCD. In a previous study, Scott and Logan (2008) suggested the mitochondrial morphology transition (swelling) is an early indicator for plant PCD event. In that study, cell death was induced by treating with a heat shock or ROS-inducing chemical (methyl viologen, hydrogen peroxide or s-triazine), and the experiment was done with Arabidopsis leaves and/or protoplasts. Both *in-planta* mitochondria and protoplast mitochondria exhibited abnormal mitochondria morphology after ROS (chemical and heat) treatments. These morphological changes were ROS-specific, and ROS scavengers not only alleviated the morphological changes but also decreased the rate of cell death. It has also been found that ROS inhibits plant mitochondrial movements inside the plant cells (Zhang and Xing, 2008).

Soon after cellular ROS levels increase, changing calcium ion fluxes were observed in the cells (Harper et al., 2004). As a result, solutes (up to about 1.5 kDa) can rush through the inner

membrane and accumulate in the mitochondrial matrix (this is also known as mitochondrial permeability transition-mPT) (Lord and Gunawardena, 2012). Cytosolic calcium flux and mPT are found to be the main causes of mitochondrial morphology transition, cessation of movements, and subsequent cell death (Scott and Logan, 2010; Lord and Gunawardena, 2012).

Treatment of Arabidopsis leaves with methyl viologen (a ROS-producing chemical) for 4 hours caused mitochondria to cluster (Scott and Logan, 2008), a phenotype also observed with protoplasts treated with methyl jasmonate (MeJA), a signaling compound that induces ROS production in plants (Zhang and Xing, 2008). Although the morphology is not completely similar, the mitochondrial clustering behavior observed with ROS treatment is similar to the mitochondrial-friendly mutation (Logan et al., 2003). It has been hypothesized that this clustering mitochondrial behavior may be due to some deformation of cytoskeletal elements or mitochondrial membranes (see chapter 4), and clustered mitochondria might be collected and targeted for destruction via mitophagy.

As described in chapter one, although there is some published evidence relating to mitochondrial morphology changes in response to ROS-induced PCD, no study has been published examining mitochondrial dynamics and PCD under conditions of elevated levels of RNS (particularly NO) in plant PCD. Similar to the ROS production, RNS are also generated in mitochondria, chloroplasts and peroxisomes in plants (Planchet et al., 2005; Corpas et al., 2009; Gas et al., 2009). There are some speculations about mitochondrial localized plant nitric oxide synthase (NOS) which produces NO by an L-arginine oxidizing pathway, but to date no such enzyme has been discovered (Guo et al., 2003; Shi et al., 2012). However, in Arabidopsis genome the presence of AtNOS1 gene was identified (Guo et al., 2003), but later renamed as nitric oxide associated 1 (AtNOA1) since its functionality as NOS could not verified (Guo and Crawford, 2005). Conversely, mounting evidence supports NOS-like activities in plants, where NO is produced either from an enzymatic complex by using arginine as a substrate, or indirectly as a byproduct of an arginine dependent reaction (Corpas et al., 2006; Corpas et al., 2009).

In my experimental system, I used *Arabidopsis thaliana* lines that have mutations in two homologus arginase structural genes (ARGAH1 and ARGAH2), which result in increased NO accumulation (Flores et al., 2008). Arginase is a mitochondrial protein degrading L-arginine to L-ornithine and urea. The increased levels of NO in arginase-negative mutants are suggested to

be due to a nitric oxide synthase (NOS) like activity, generating NO directly from arginine (Arg) in plant mitochondria (Flores et al., 2008). Previous research performed using NO donors (Roussin's black salt and sodium nitroprusside) showed that elevated levels of NO (0.70 nmol min^{-1} for six hours) is sufficient to induce PCD in plant cells without high ROS levels (Clarke, 2000). However, in that experiment they did not record mitochondrial morphological changes prior to NO-induced PCD, so we still do not know whether the morphological changes observed with ROS-induced PCD are universal among other PCD inducers or not. On the other hand, NO synthesis from arginine is still hypothetical. In this study I compared mitochondrial morphological changes, mitochondrial dynamics, and arrangements between *argah* mutants, the wild type treated with SNP and negative control (wild type 43C5).

This study uses *Arabidopsis thaliana* protoplasts and root hairs were used here as experimental model systems. For over 25 years, protoplasts have been used as an experimental system for cell and molecular biology, including investigation of cell organelles, cell wall regeneration, membrane fusion, virology etc. Protoplasts are relatively efficient when subjected to chemical and physical treatments like heat, and are also easy to image with microscopes due to the lack of cell walls and cell layers. Root hairs, on the other hand, provide another excellent research tool due to their presence at the surface of the root and away from the plant body. Root hairs are less fragile than protoplasts, and their lack of a cuticle layer allows physical and chemical treatments to reach the cell. Root hairs become visible on seedling roots shortly after seed germination (5-6 days), thereby allowing rapid and efficient tests to be performed (Grierson and Schiefelbein, 2002).

The purpose of the present work is to unravel whether the mutation of arginase genes in Arabidopsis affects the cellular redox levels and mitochondrial dynamics upon the initiation of heat shock induced PCD. With the use of fluorescence-tagged mitochondria and various microscopy techniques combined with state of the art image analysis algorithms, differences in mitochondrial dynamics were observed *in vivo*.

3.2 Results

The effect of heat shock-induced PCD initiation on Arabidopsis mitochondria was observed and documented using Arabidopsis mesophyll protoplasts and root samples. Initially,

Arabidopsis protoplasts and seedlings were subjected to various heat stress levels (37, 42 and 55^{o}C for various time periods) in order to determine the most effective temperature and time combination for protoplasts and root hairs. However, after the preliminary studies, it was clear that the viability of protoplast samples deteriorated with time even without the heat shock. As a result, all the viability tests and cell plasmolysis counts presented in this document were done using Arabidopsis root hairs after the 42^{o}C for one and half hours heat shock, which was similar to the temperature and temporal ranges tested to induce Arabidopsis PCD by previous researchers (Schramm et al., 2006; Charng et al., 2007).

3.2.1 Cell death and plasmolysis percentages increased with heat shock and increased levels of NO

3.2.1.1 Mutations in two homologous arginase structural genes resulted in increased NO accumulation

Arginase-negative mutants (*argah 1-1* and *argah 2-1*) found to have a significant difference in root morphology from the wild types (Fig. 3-1) which was also observed in a previous study (Flores et al., 2008).

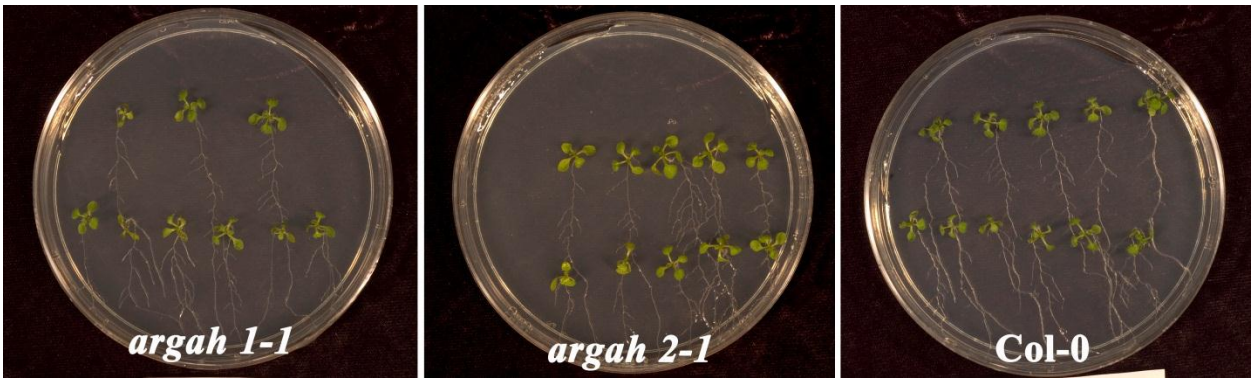

Figure 3-1. Arabidopsis plants of each genotype (*argah1-1* and *argah2-1* and Columbia (Col-0)) samples. Seedlings were grown on vertical plates in MS medium for 10 days.

To detect the NO accumulation pattern of arginase mutants and the wild type, a DAF-FM fluorescence detection method was employed in the presence of NO. According to the results, *argah 1-1* and *argah 2-1* plants showed higher levels fluorescence intensity, compared to wild type plants (Fig.3-2).

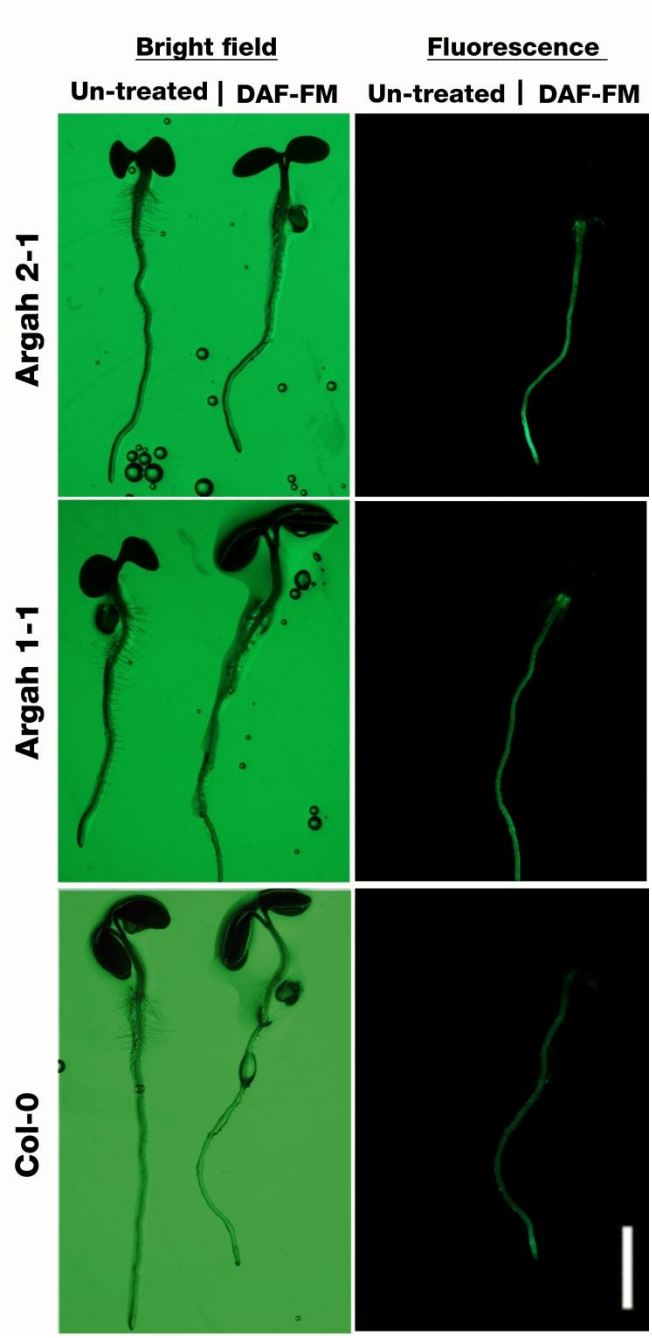

Figure 3-2. DAF fluorescence images showing nitric oxide levels in each genotype (*argah 1-1*,*argah 2-1* and Col-0 Wild type) samples comparatively. The same seedlings were captured with bright field (left images) and with florescence emission (right images). Samples showing as untreated were not treated with DAF staining procedure, and samples showing as DAF were treated. All plants were grown on vertical plates in MS medium for 3 days. For each genotype, the image is a representative sample of 30 seedlings observed in each of the experiment repeated 3 times. Bar = 3mm.

3.2.1.2 Temporal measurement of cell death and plasmolysis

It was clear that root hair cells in Arabidopsis plants that were subjected to heat shock lose their viability more rapidly than those in control samples. This cell death was statistically significant ($P \leq 0.05$, n = 3; 47 ± 1.8 % in all heat-treated samples, 10 ± 1.8 % in control) when compared to those in control samples in all viability testing points in time (24 hours, 48 hours and 72 hours; Fig.3-3). The cell death percentages rose in a consistent rate in HS samples and reached up to 63 ± 3 % in 72 hours, while in control samples it only reached up to 13 ± 3 %.

A consistent increase in the percentage of plasmolyzed cells with time was also observed in heat shocked samples, and the percentage of plasmolyzed cells was significantly higher in heat treated samples than the non-treated samples at all three time points. All points in time showed a significant and gradual increase in both cell death and plasmolysis percentages in HS samples, while there was no detectable difference in control samples with time. The Pearson correlation coefficient was used to determine the relationship between cell death and plasmolysis percentages, and a 94 % correlation (n= 72) was detected.

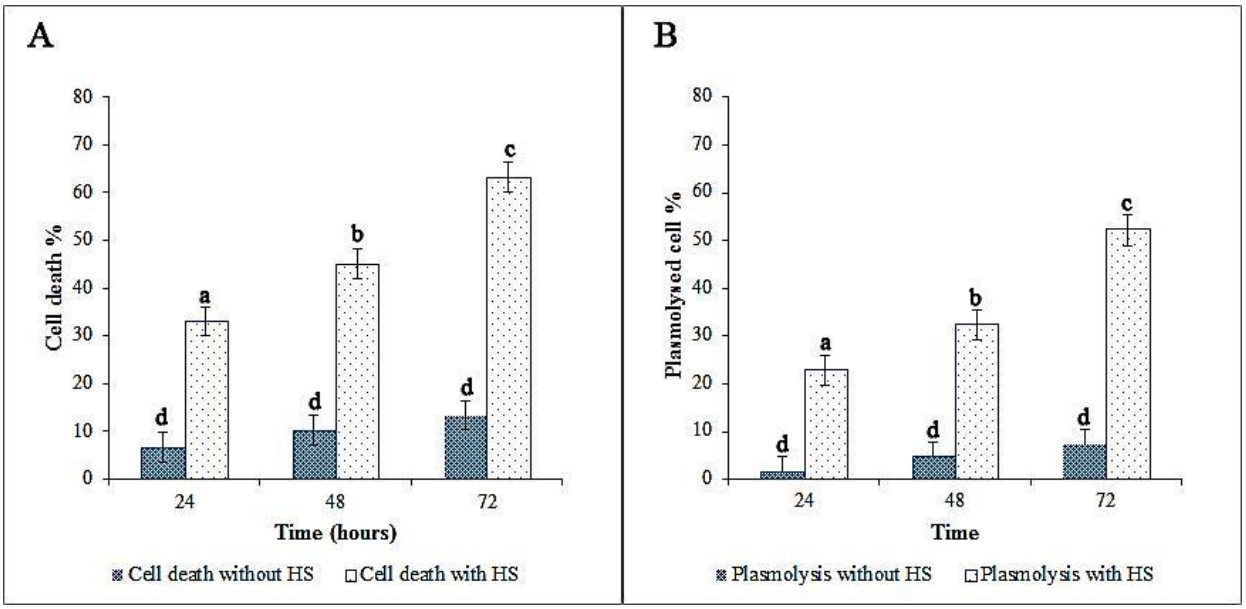

Figure 3-3. Effect of heat shock (HS) on overall (A) percentage of dead cells and (B) percentage of plasmolyzed cells over time (in hours) observed in Arabidopsis root-hair cells. Data presented are means of three independent experiments; error bars represent the standard errors of the means. Different letters above the bars indicate significant differences ($P \leq 0.05$) between treatments as indicated by a Fisher's least-significant difference test.

3.2.1.3 Genotypic effects on cell death and plasmolysis

There was a significant difference in cell death percentages between wild type (WT) sample, SNP-treated WT (WT-SNP), and the *argah1-1* sample; however, no significant difference was detected between the WT and *argah2-1* samples (Fig. 3-4). The cell death percentage showed an overall 16 ± 2.5% increase in the SNP-treated WT than that in untreated WT (where cell death was 25.33 ± 2.5%), while there was an 10 ± 2.7% reduction in cell death rate in *argah1-1* plants in the 72 hour observation period.

On the other hand, only the SNP-treated WT showed a significant difference in the percentage of plasmolysed cells from the WT (Fig. 3-4; 20 ± 2.7 in SNP-treated compared to 15.9 ± 2.7% in WT). The gap between cell death percentages and plasmolysis percentages was highest in the *argah2-1* sample, and lowest in the *argah1-1* sample, indicating the majority of cell deaths in *argah1-1* sample are due to PCD (lower the gap means more cells are dead by PCD).

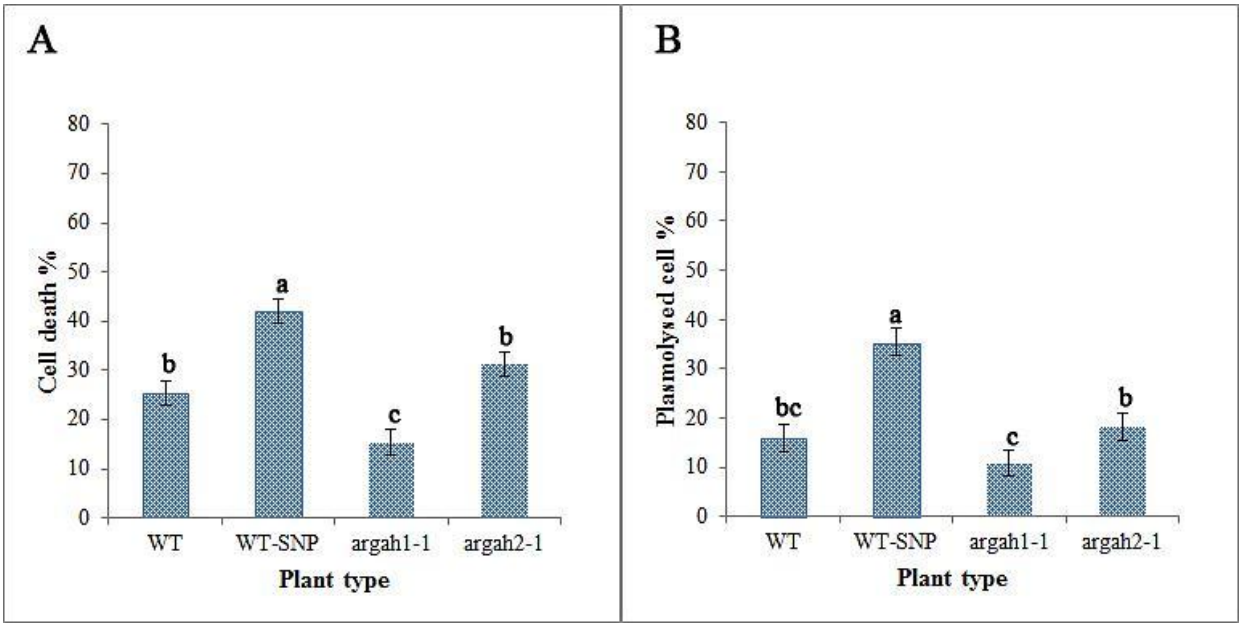

Figure 3-4. Cell death (A) and plasmolysis (B) of WT (43C5), WT-SNP (43C5+SNP), *argah1-1* and *argah2-1* samples of Arabidopsis root-hair cells in 72 hours of observation period. Data presented are means of three independent experiments; error bars represent the standard errors of the means. Different letters above the bars indicate significant differences ($P \leq 0.05$) between treatments as indicated by a Fisher's least-significant difference test.

When the non-heat-treated samples are considered, only the SNP-treated WT showed a significant difference (10 ± 3.5% increase) in dead cell percentage compared to WT (which was 7.1 ± 3.5%) in 72 hour observation period. However, in the heat-treated samples, all samples other than the *argah2-1* sample showed a significant difference from the WT (Fig 3-5). The cell death percentage in heat-treated WT samples increased by 23 ± 3.5% upon SNP-treatment while there was a 20 ± 3.5% reduction in *argah1-1* sample, compared to the wild type.

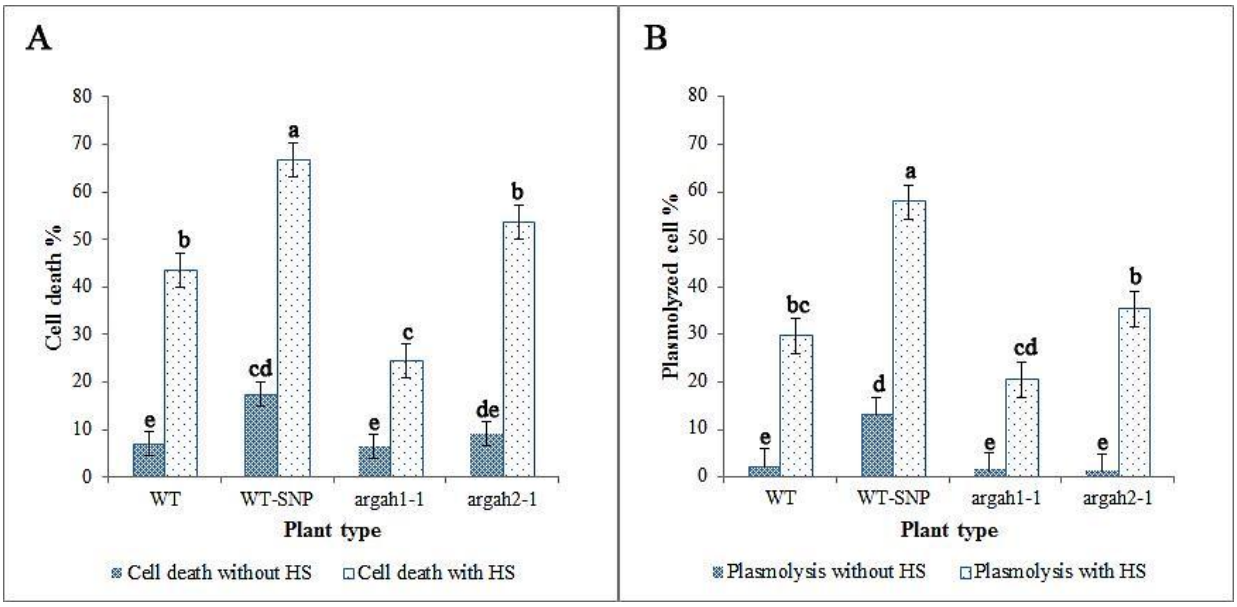

Figure 3-5. Effect of heat shock on (A) cell death and (B) plasmolysis of different samples of Arabidopsis root-hair cells with and without heat shock. Different letters in the graph denote differences at $P \leq 0.05$ between treatments as indicated by a Fisher's least-significant difference test. Data presented are means of three independent experiments; error bars represent the standard errors of the means.

Again, the SNP-treated WT (non-heat shocked) sample showed a significant increase (11 ± 3.7% increase) in percentage plasmolysis than the other non-heat-treated samples, and it was also the only sample that showed a significant increase (28 ± 3.7%) in plasmolyzed cell percentage when heat treated (Fig. 3-5).

3.2.2 Mitochondrial dynamics and morphology changed with heat shock and increased cellular NO concentration

In order to identify moving mitochondria, two images were captured 30 seconds apart using same settings and same field of view. Those two images were pseudo-colored as red and green and merged to get a composite image. If mitochondria moved within the 30 second period, they can be easily identified as separate colors (red or green), but if a given mitochondrion did not move, it can be identified as yellow/orange (merged). With protoplast and root cell experimental systems, it was clear that with mild heat shock, mitochondrial morphology changes permanently within one hour (Fig. 3-6 and 3-7). These swollen mitochondria then clustered with time (usually within 5 min after the heat shock), and reduction of mobility was observed, but the negative controls did not show any change in morphology, distribution or mobility (Fig. 3-6 and 3-7).

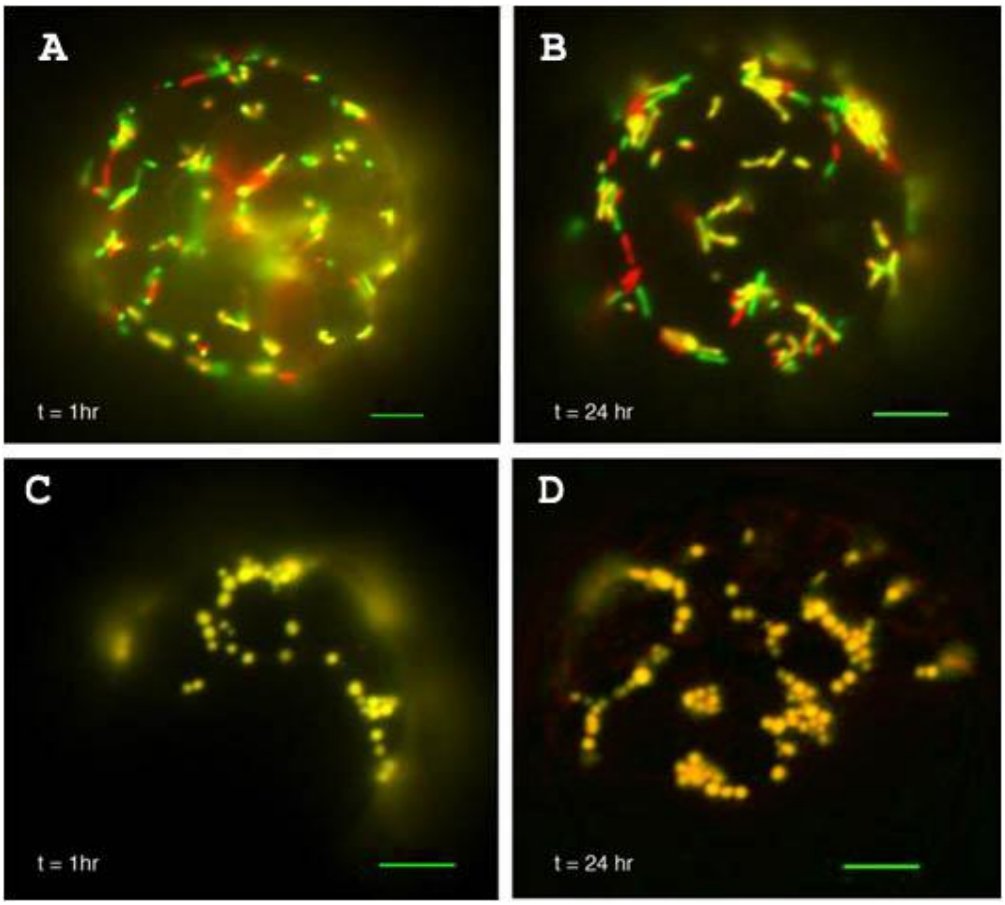

Figure 3-6. Abnormal mitochondrial morphology observed in wild type Arabidopsis mesophyll protoplasts after 45°C heat shock for 10 min. Images (A) and (B) showing control protoplasts after 1 hour and 24 hours respectively, (C) and (D) showing heat-shocked protoplasts after 1 hour and 24 hours

respectively. Each image is a composite of two micrographs captured 30 seconds apart that have been differentially pseudo-colored to allow for detection of movement. Each image is a representative sample of more than 100 protoplasts, the experiment repeated 3 times. Bar = 5µm

Change in mitochondrial morphology, aggregation, and cessation of movement after heat shock were universal among all the observed plant samples (Fig. 3-7). Mitochondria in heat shocked samples began to cluster (5-15 mitochondria per cluster) within 5 minutes to one hour, regardless of the sample type. However, after 24 hours, all heat shocked samples had very big clusters (20-40 mitochondria).

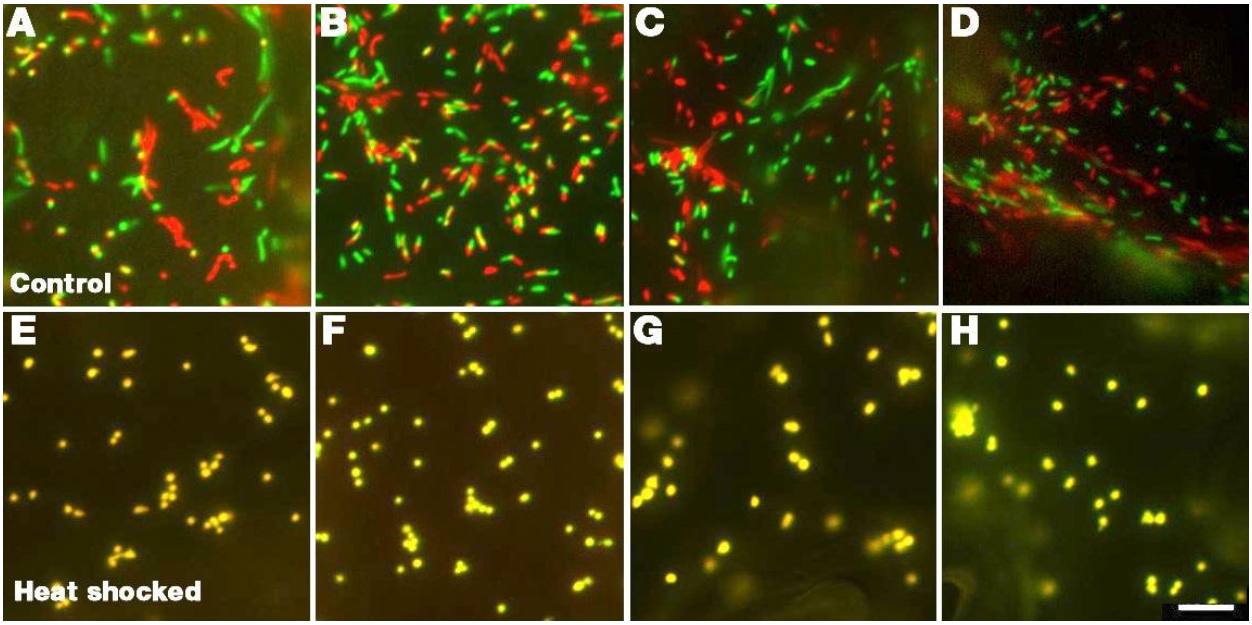

Figure 3-7. Mitochondrial morphology change and cessation of movement observed one hour after the heat shock (42°C for 1.5 hours). Image (A) 43C5 negative control (B) 43C5 SNP control, (C) *argah* 1-1 control (D) *argah* 2-1 control , (E) 43C5 heat treated, (F) 43C5 SNP heat treated (G) *argah* 1-1 heat treated (h) *argah* 2-1 heat treated. Each image is a representative sample of more than 50 root epidermal cells, the experiment repeated 3 times. Bar = 5µm.

While mitochondria in all the control samples showed normal morphology and movement for up to 72 hours (Fig. 3-8), mitochondria in heat shocked samples were swollen, clustered (Fig. 3-9), and comparatively immobile (see Table 3-1) at all the observed points in time (one to 72 hours).

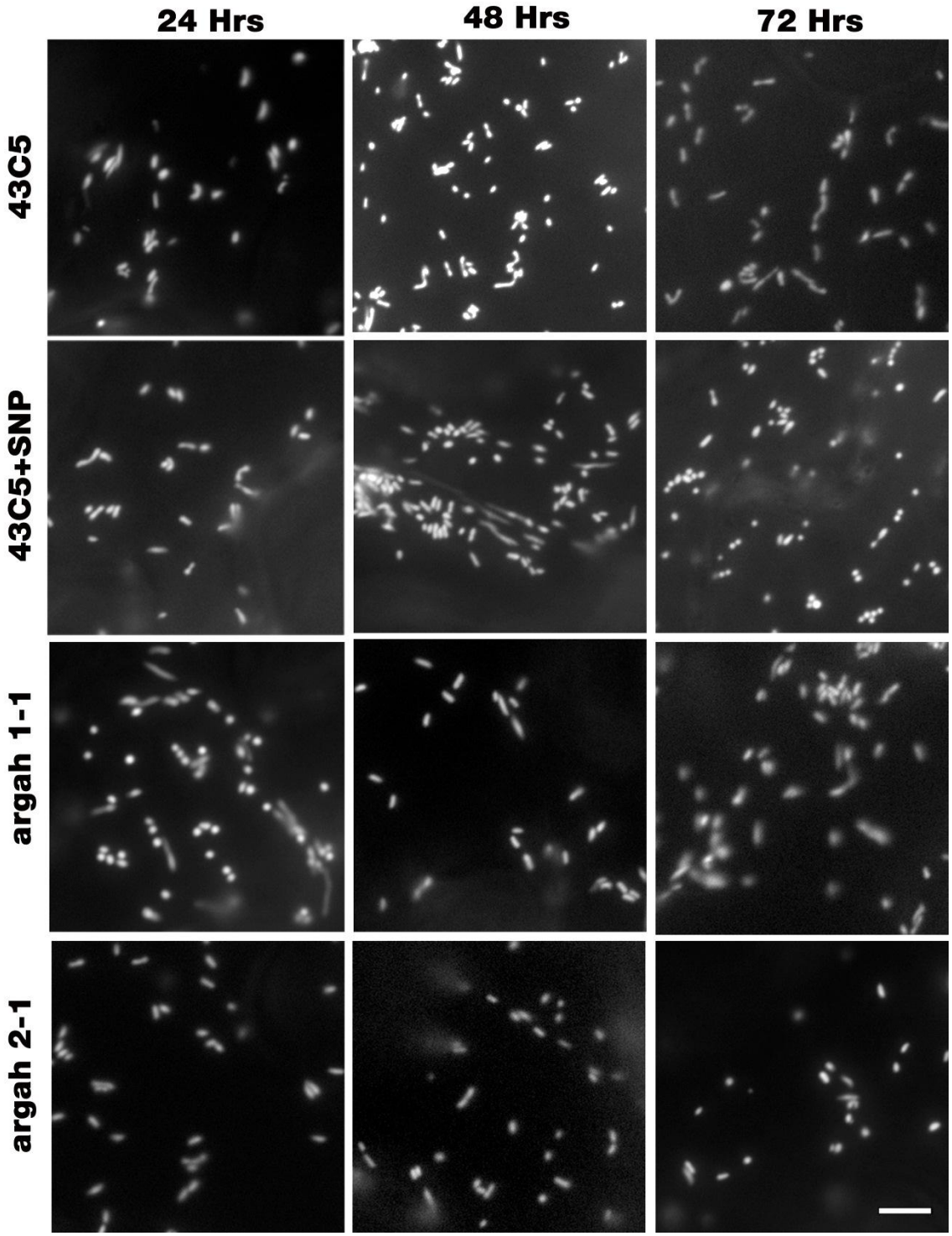

Figure 3-8. Mitochondrial morphology and distribution observed in the 43C5 wild type, 43C5 SNP, *argah 1-1*, *argah* 2-1 control samples at 24, 48 and 72 hours. Each image is a representative of more than 50 cells, the experiment repeated 3 times. Bar = 5µm.

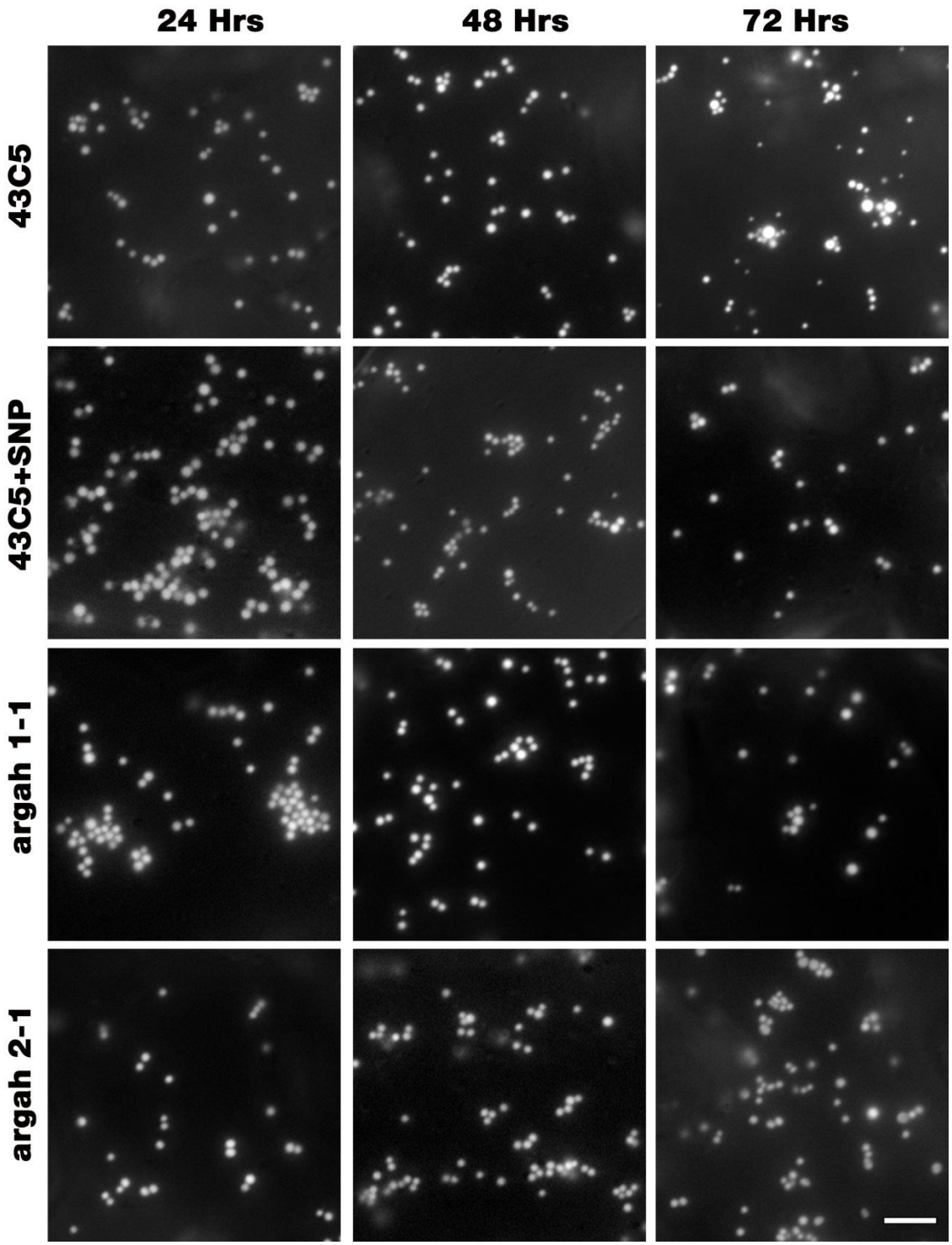

Figure 3-9. Mitochondrial morphology change and clustering behaviour observed after the heat shock (42°C for 1.5 hours). All images taken at 24, 48 and 72 hours after the heat shock. Images showing 43C5 wild type, 43C5 SNP, *argah 1-1*, *argah* 2-1 heat-treated samples. Each image is a representative sample of more than 50 cells; the experiment repeated 3 times. Bar = 5µm.

As shown in Fig 3-7, mitochondria in heat shocked samples showed little or no movement one hour following heat shock compared to the control samples. To better understand the changes in mitochondrial dynamics after heat shock in each sample, time-lapse images were collected (one second interval) for up to 30 seconds and individual mitochondria were tracked using Imaris automated tracking software. With this tracking software, each mitochondrion can be traced temporally throughout sequential frames (30 frames in this case = 30 seconds). To each identified mitochondria, a unique identity was assigned by the software to track its movements with time. Using this identity, the software can calculate the path of each individual mitochondrion, which is termed the "track" in this document.

Using the individual mitochondria tracks, several mitochondrial motility parameters were calculated and compared between heat-treated and control samples. The parameters were: average mitochondria velocity, mitochondrial meandering index, average mitochondria acceleration, average mitochondria displacement, average mitochondria speed, average track displacement length, average track length, average maximum track speed and track speed means.

Table 3-1 Characteristics of mitochondrial dynamics in control and heat treated samples showing significant differences. The standard errors of the means (n = 4) and significant differences (P < 0.05) between treatments as indicated by a Fisher's least-significant difference test.

	Without heat shock				With heat shock			
Mitochondria velocity	0.08	±	0.01	µm/s	0.01	±	0.01	µm/s
Meandering index	0.33	±	0.01		0.26	±	0.01	
Mitochondria acceleration	0.20	±	0.01	µm /s^2	0.01	±	0.01	µm /s^2
Mitochondria Displacement	38.5	±	2.6	µm ^{2}	0.06	±	2.4	µm ^{2}
Mitochondria speed	0.50	±	0.01	µm/s	0.01	±	0.01	µm/s
Track Displacement Length	5.46	±	0.2	µm	0.12	±	0.2	µm
Track Length	16.4	±	0.5	µm	0.5	±	0.5	µm
Track Speed Max	2.10	±	0.05	µm/s	0.06	±	0.05	µm/s
Track Speed Mean	0.70	±	0.02	µm/s	0.01	±	0.02	µm/s

To establish a baseline for the mitochondrial movement behaviors of a normal cell, a set of non-heat-treated samples of 43C5 wild type, 43C5 SNP, *argah 1-1* and *argah 2-1* samples were analyzed alongside the heat-treated samples.

There was a significant difference between non heat treated samples and heat treated samples in mitochondrial velocity, acceleration (change in the mitochondria velocity over time), displacement, speed (average instantaneous speeds of the mitochondria), track displacement length (the distance between first appearance of the mitochondria (t1) and the last appearance (t30) position), track length (the total length of displacements within the mitochondrial path/track), and maximum and mean track speeds.

The meandering index was obtained by dividing the displacement from the origin (within 30 seconds or 30 frames) by track length such that an index = 1 means that the mitochondria was displaced in a straight line). The median meandering index value for the control sample was 0.34 ± 0.02 (n = 4), which suggested that the mitochondrial migration in control samples was significantly more directional compared to that in heat-treated samples (0.26 ± 0.02).

CHAPTER 4

4. ACTIN, MICROTUBULE AND MITOCHONDRIA DYNAMIC REORGANIZATIONS DURING ARABIDOPSIS PCD

4.1 Introduction

Plant mitochondria are very dynamic organelles, which need to move (in order to meet) and maintain a cellular distribution that supports proper functioning (Scott and Logan, 2007). As far as mitochondrial movements and distribution are concerned, the cytoskeleton (composed of microtubules and actin) plays a major role. Indeed, it has been recorded that mitochondria in growing Arabidopsis root hairs, can move through the cytosol at speeds up to 10 μm s^{-1} using the cytoskeleton (Zheng et al., 2009). The organization and correct functioning of cytoskeletal elements are crucial to plant cell survival, as they govern various aspects of life including cytoplasmic streaming, cargo and organelle transport, cell division, maintaining cell shape, cell signaling, plant morphogenesis, and programmed cell death. Microtubules play a major role in most animal and yeast mitochondrial movement (Heggeness et al., 1978; Boldogh and Pon, 2007; Frederick and Shaw, 2007). In contrast, actin plays a major role in *Saccharomyces cerevisiae* (budding yeast) and plant mitochondrial movement (Kohler et al., 1997; Hermann and Shaw, 1998; Van Gestel et al., 2002; Doniwa et al., 2007; Frederick and Shaw, 2007).

According to a previous study, treatment of Arabidopsis leaves with methyl viologen (a bi-pyridyl herbicide that produces superoxide by donating electrons to oxygen) for 4 hours caused mitochondria to cluster (Scott and Logan, 2008). This phenotype was also observed in other studies when Arabidopsis protoplasts were subjected to various PCD-inducing chemicals and treatments. Such as, with methyl jasmonate (MeJA) (a signaling compound that induces ROS production) (Zhang and Xing, 2008), with UV treatment to induce PCD (Gao et al., 2008), and also in lace plant protoplasts when PCD induced by a heat shock (Lord and Gunawardena, 2011). Cessation of mitochondrial movements after PCD induction has also been observed in various systems including Arabidopsis protoplasts (Gao et al., 2008; Zhang et al., 2009), Arabidopsis

leaf disks (Yoshinaga et al., 2005), tobacco BY-2 cells (Vacca et al., 2006) and in lace plant protoplasts (Lord and Gunawardena, 2011). Mitochondrial morphology transition, inhibited motility, and subsequent cell death (PCD) are found to be dependent on cytosolic calcium flux and mPT (Scott and Logan, 2008; Lord and Gunawardena, 2012). In animals, mPT has been shown to be an early indicator for apoptosis (and PCD) even hours before other cell death markers such as DNA fragmentation and chromatin condensation appear (Kroemer et al., 1997).

However, accordping to Yoshinaga et al. (2005), 2, 3- butanedione monoxime (BDM), an acto-myosin inhibitor, caused a round and swollen mitochondrial morphology and inhibited the motility of mitochondria and cytoplasmic streaming, similar to the effects of ROS treatment. Similar observations were made using Arabidopsis leaf epidermal cells and tobacco cells treated with BDM or actin-depolymerizing drug Latrunculin B (Lat-B) (Van Gestel et al., 2002; Doniwa et al., 2007). Treatment with Lat-B resulted in mitochondrial clusters that were very similar to the clusters observed with heat shock and ROS treatments (Van Gestel et al., 2002). However, the microtubule-disrupting drugs propyzamide or oryzalin does not cause any significant change in mitochondrial movements or arrangement (Van Gestel et al., 2002; Doniwa et al., 2007). These observations indicates a possible link between physical stresses such as heat treatment, ROS-inducing chemicals, destruction of cytoskeletal compounds (most probably the actin cytoskeleton), and mitochondrial morphology transition, and arrangement into clusters. Hence the cessation of mitochondrial movement maybe a potential early indicator for plant PCD.

However, no published research was found reporting investigations of the direct connection between this cessation of mitochondrial movement, cluster formation; it's regulation by the cytoskeleton and the involvement of these processes in PCD. As discussed previously, the aberrant mitochondrial behavior during PCD may be due to some deformation or modification of cytoskeletal elements or mitochondrial membranes, and clustered mitochondria might be collected and targeted for destruction via mitophagy. While it has been demonstrated that the reorganization of the actin cytoskeleton induces plant PCD, still no published studies could be found to indicate the link between microtubule deformation and PCD (Smertenko and Franklin-Tong, 2011).

In this study I have aimed to address some of the basic questions, such as the similarity of clusters formed after PCD induced by ROS or physical stress (for example, heat shock), with the

mitochondrial clusters formed due to cytoskeletal depolymerization; the relationship between these cytoskeletal-disintegrating drug-induced cluster formation with the Arabidopsis PCD; how these clusters arrange with cytoskeletal elements such as actin filaments and microtubules; and how these clusters move with respect to cytoskeletal elements and their interaction with the plus ends of MT.

To answer these questions, I used heat shock to induce PCD and mitochondrial cluster formation in Arabidopsis cells, observing the reorganizations and changes to the MT and actin cytoskeletons with emphasis on mitochondrial morphology, arrangement, and movement changes. Then I depolymerized the individual components of the cytoskeleton using chemical treatments (Lat –B and Oryzalin), to determine if they reproduced the same morphological and behavioral changes from heat shock treatment.

4.2 Results

4.2.1 Effects of mild heat shock on mitochondrial movements and cytoskeletal dynamics

As discussed in the previous chapter, there was a mitochondrial morphology transition, cessation of movement, and clustering behavior observed with mild heat shock (42^{o}C for 7 min). To determine the relationship of changing mitochondrial dynamics with the cytoskeletal components, different Arabidopsis lines (stable double transgenic) expressing a mitochondrial targeted fluorescent reporter gene together with either an actin (mito-GFP/mTalin-mCherry) or microtubule fluorescent reporter (mito-GFP/MAP4-mCherry).

Within 5 minutes after the heat shock, mitochondria became clustered, and actin filaments appeared to be shorter and fewer in number compared to the control sample (Fig. 4-1). These mitochondrial clusters were observed to be moving along the remaining actin filaments. Clusters became larger within 15 minutes in the heat shocked sample, while there was no detectable difference in the control sample. Following treatment, only a few remaining actin filaments were observed in the cells (Fig. 4-1, indicated by white arrows), while some of the actin filament fragments made disk-like or globular-shaped objects that were closely associated with mitochondrial clusters (indicated by white circles). Within 30 minutes, mitochondrial clusters became very large (15- 20 mitochondria per cluster), while almost all actin filaments

disappeared. These mitochondrial clusters were associated with globular actin debris, and appeared to be mostly sessile at this point. Little change was observed in the mitochondrial clusters between 30 minutes to one hour after the heat shock, while new actin filaments began to regenerate (indicated by black arrows).

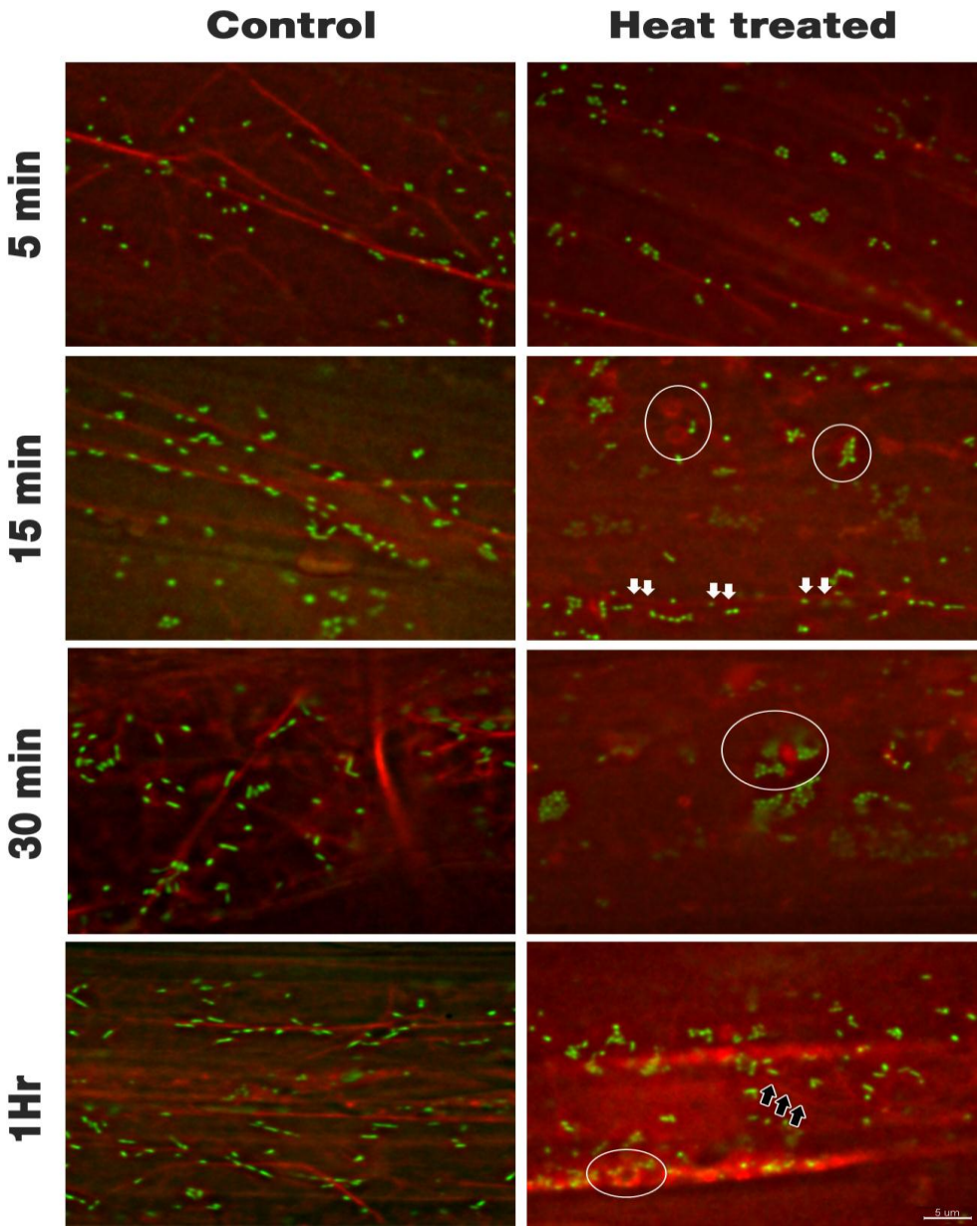

Figure 4-1. Alteration in the morphology and arrangement of mitochondria with respect to the changes of actin filaments in Arabidopsis root epidermalcells following a mild heat shock. The mito-GFP/mTalin-mCherry line was heat shocked at 42^{o}C for 7 min. All images were taken after the HS in time intervals as indicated in the figure. Mitochondria are shown in green and actin in red. Disk-like or globular-shaped objects are indicated by white circles, remaining actin filaments observed after the HS indicated by white

arrows, and actin filaments regenerating after the HS indicated by black arrows. Images are representatives of five independent experiments. Bar = 5 µm.

The 3D reconstructed image (Fig. 4-2), demonstrates that mitochondrial clusters are very closely apposed (likely connected) to the remaining actin filaments, while some large clusters are completely detached from actin filaments, some small clusters appear connected to short fragments.

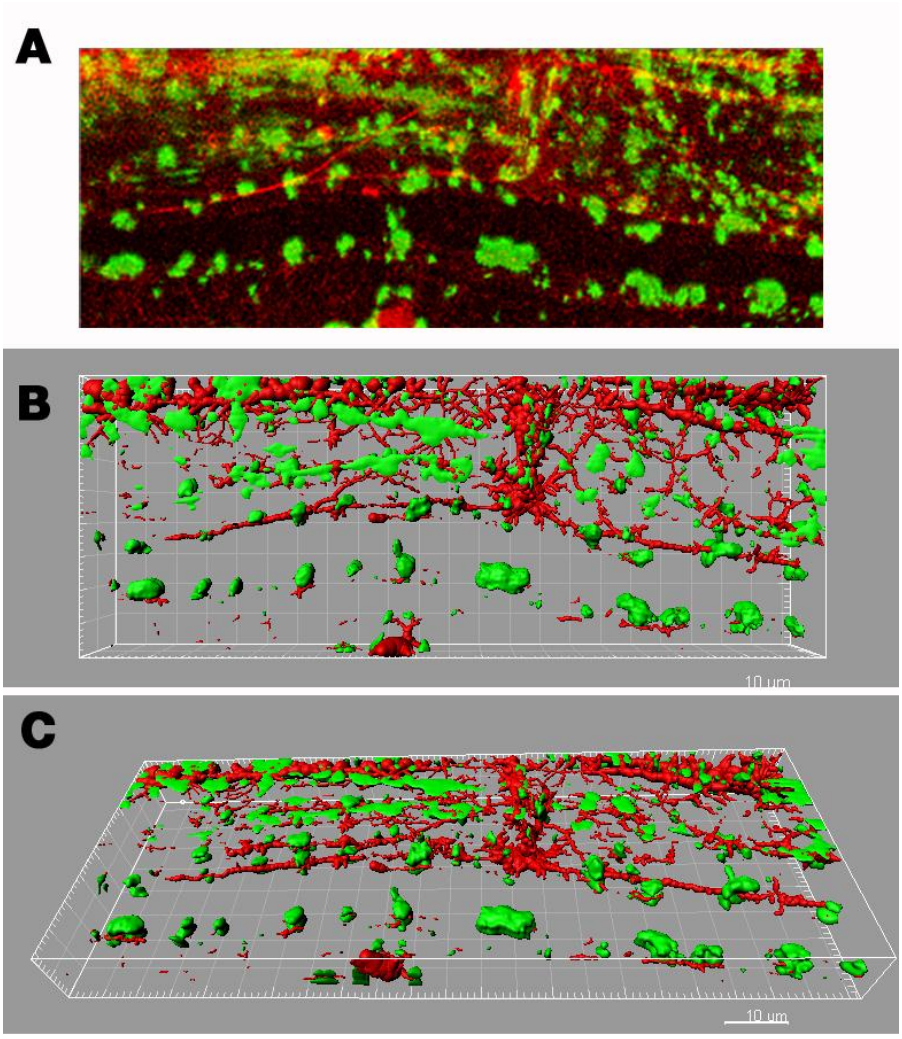

Figure 4-2. Effects of mild heat treatment on actin cytoskeleton, mitochondria morphology and movements. The mito-GFP/ mTalin-mCherry line was heat shocked at 42^{o}C for 7 min. Image (A) raw image (Z-stack) taken by confocal microscope, showing a maximum intensity projection, the front view (B) and the view in 45 degrees angle (C) are 3D reconstructed images (Imaris, Bitplane) showing actin (red) and mitochondrial clusters (green). Bar = 10 µm.

The same effect was observed in the Arabidopsis line expressing microtubule reporter gene (mito-GFP/ MAP4-mChery) following a heat shock: mitochondria showed a clustering behavior, while microtubules were fewer in number and were arranged abnormally compared to the control sample (Fig. 4-3, white arrows). After 15 minutes, it was clear that these mitochondrial clusters were growing larger and moving slowly. However, same as in the control samples, there was not any observable connection between the remaining microtubules and mitochondrial cluster movements. Within 30 minutes after the heat shock, most of the microtubules had disintegrated, with only short fragments visible under the microscope (Fig. 4-3, white circles). Mitochondrial clusters were mostly immobile and didn't show any significant change after this time point. One hour after the heat shock, only few fragments of microtubule remained in the heat shocked sample while no significant change was observed in the control sample, in terms of mitochondrial dynamics or the microtubule arrangement.

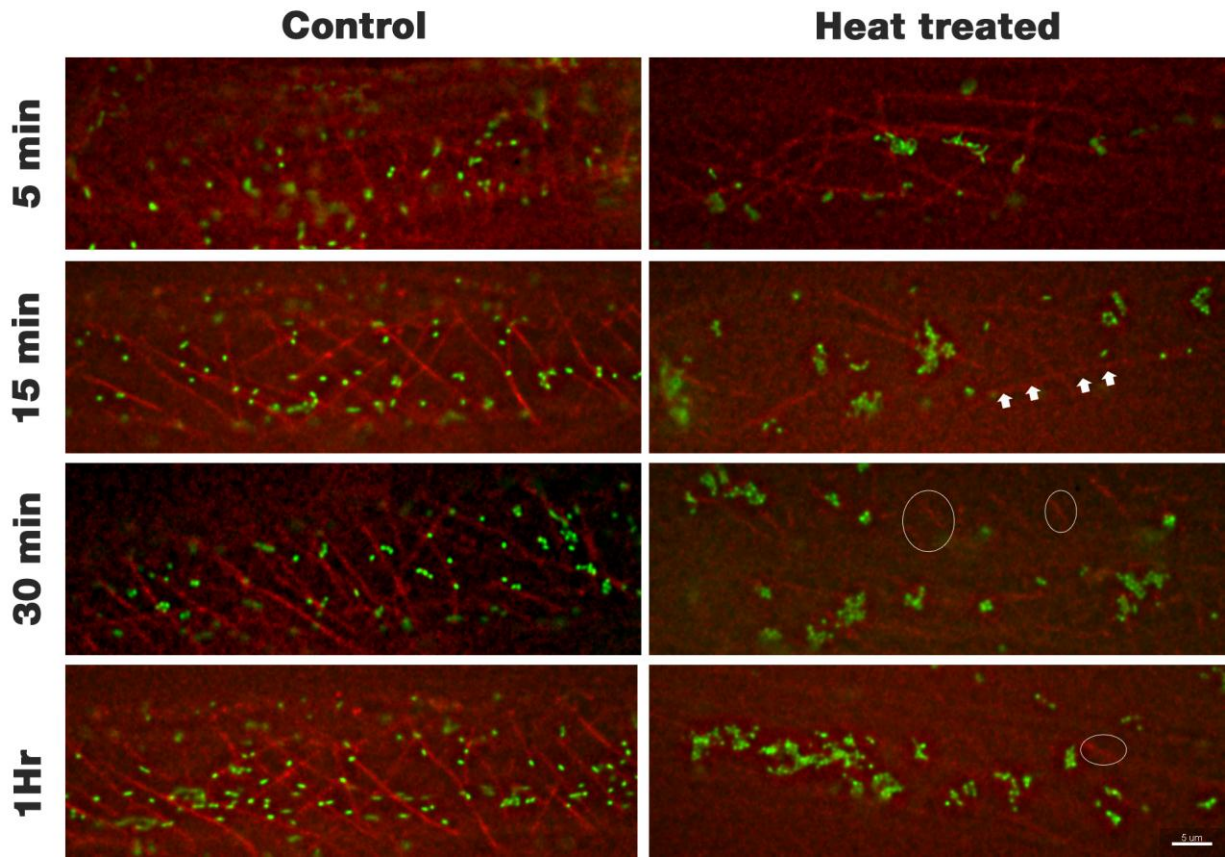

Figure 4-3. Alteration in the morphology and arrangement of mitochondria with respect to the changes of microtubules in mild heat shocked Arabidopsis root epidermis cells following a mild heat shock. The mito-GFP/MAP4-mCherry line was heat shocked at 42^{o}C for 7 min. All images were taken after the heat

shock in time intervals as indicated in the figure. Mitochondria are shown in green and microtubules in red. Microtubules that remained after 15 minutes of treatment are indicated by white arrows, and microtubule fragments remaining after 30 minutes of treatment are indicated by white circles. Images are representatives of four independent experiments. Bar = 5 μm.

To test the hypothesis that mitochondrial clusters moved on microtubules in a plus-end-directed manner, an Arabidopsis line expressing a microtubule plus end reporter and a red mitochondrial reporter (mito-mCherry/EB1b-GFP) was subjected to heat shock. Following heat shock this line also showed similar mitochondrial clustering and movement changes observed in microtubule and actin lines (Fig. 4-1 and 4-3). However, the microtubule plus end behavior (Fig. 4-4) with heat shock was different from the whole microtubule behavior observed with MAP4 line (Fig. 4-3). Within 5 minutes after the heat shock, the plus ends of the microtubules appeared to be closely associated with the mitochondrial clusters (Fig. 4-4, few microtubule plus ends were indicated with an arrow), while no such interactions were observed in the control sample in the entire one hour observation period. Following heat shock these microtubule plus ends were detected as ring- or disk-shaped structures (Fig. 4-4, indicated by circles) associated with mitochondrial clusters in some samples and moving along with the clusters. There were similar observations 15 minutes after the heat shock, where fewer plus ends were detected than in the control sample. These plus ends totally disappeared 30 minutes after the heat treatment, and were not observed again in the whole observation period (up to one hour) (Fig. 4-4).

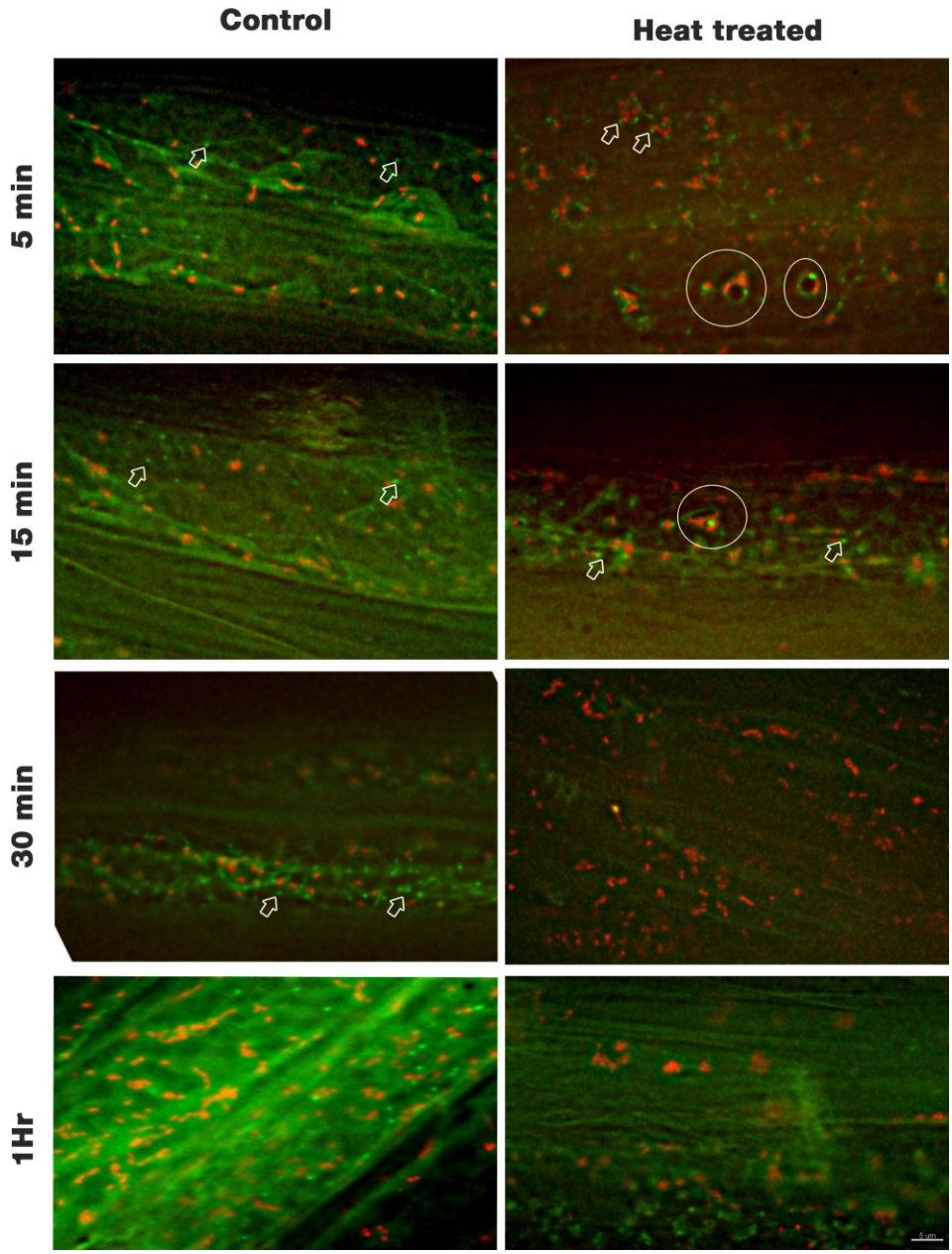

Figure 4-4. Alteration.s in the morphology and arrangement of mitochondria with respect to the changes of microtubule plus ends in mild heat shocked Arabidopsis root epidermis cells. The mito-mCherry / EB1b-GFP line was heat shocked at 42^{o}C for 7 minutes. All images were taken after the heat shock in time intervals as indicated in the figure. Microtubule plus ends are shown in green and mitochondria in red. Few representative microtubule plus ends indicated by white arrows, microtubule plus ends forming ring- or disk-shaped structures appeared after the treatment were indicated by white circles. Images are representative of four independent experiments. Bar = 5 µm.

Heat shocked samples showed a significant reduction in speed of movement of mitochondrial clusters, while untreated samples showed a 0.67 ± 0.12 µm/s average cluster speed, heat treated

samples showed a 0.02 ± 0.09 µm/s average cluster speed. This was also clearly visible in the comparison of speeds and cluster areas of heat shocked and un-treated samples (Fig. 4-5).

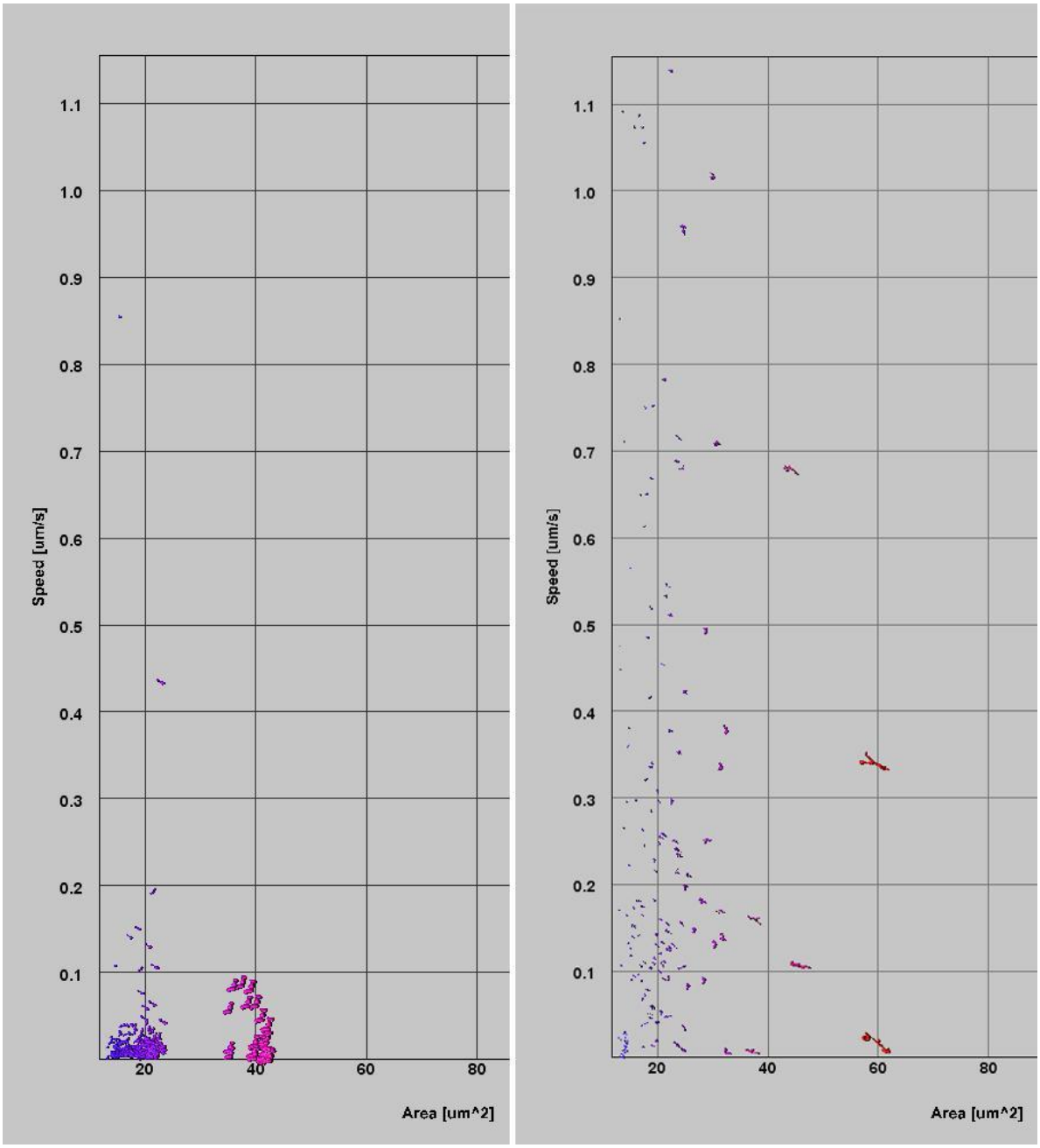

Figure 4-5. A comparison of mitochondrial cluster speeds (in Y axis, µm/s) and cluster area (in X axis, μm^2) of heat shocked (the graph in left side) and un-treated (right side) randomly selected Arabidopsis 43C5 line cells (representative for 4 cells per treatment). Clusters were identified and statistic generated using Imaris software. Cluster speeds and area were calculated over 30 seconds (one image per second). Clusters are proportionate to the actual image data set. Bar = 30 µm.

4.2.2 Effects of actin cytoskeleton disruption on mitochondrial movements

In higher plants the actin microfilament has been found to play a major role in mitochondrial motility (Zheng et al., 2009). It has been shown by the experiments described earlier that when both actin and microtubules are depolymerized by the heat treatment, mitochondrial clusters stop moving. In order to see more clearly what cytoskeletal element causes this clustering behavior and movement change, each cytoskeletal element was depolymerized separately in the following experiments.

As a base line for the other observations especially with the mitochondrial cluster morphology and dynamics, in order to determine whether mitochondrial dynamics change with the disruption of the actin cytoskeleton in Arabidopsis, double transgenic Arabidopsis line stably expressing mito-GFP/mTalin-mCherry was treated with 2 µM Latrunculin B (with 0.1% v/v ethanol as the solvent) for different time periods (10 min to 3 hours). From microscopic observation of the first experiment, F-actin was clearly depolymerized, but in the solvent only (ethanol 0.1% v/v) controls, F-actin remained unaffected (as shown by the short arrow heads along intact actin cable in Fig. 4-1 A and C). These observations were expected and in accordance with previously published works (Sampathkumar et al., 2011) . Increasing incubation time in Lat-B led to a more extensive depolymerization of the actin network. This depolymerization effect grew more obvious over time (see thin arrows showing fragmented F-actin in Fig. 4-1 B and depolymerized actin in Fig.4-1 D).

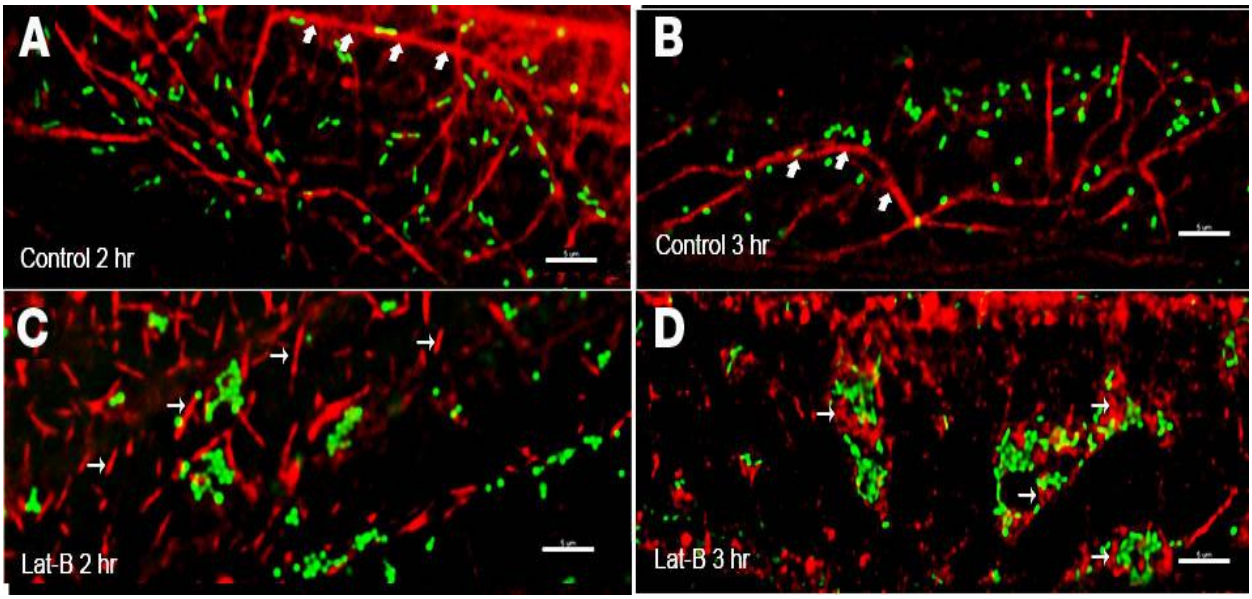

Figure 4-6. Mitochondrial morphology change and clustering behavior observed in mito-GFP/mTalin-mCherry line treated with 2 µM Lat-B. (A) Mock treatment with 0.1% (v/v) ethanol (EtOH) after 2 hours, (B) mock treatment with 0.1% (v/v) ethanol (EtOH) 3 hours (C) 2 hours with Lat-B treatment and (D) 3 hours with Lat-B treatment. Mitochondria are shown in green color and actin in red, short arrow heads indicating intact actin cables, while thin arrows showing fragmented F-actin or depolymerized actin. Images are representatives of four independent experiments. Bar = 5 µm.

Although the changes to the mitochondrial dynamics with actin depolymerization were obvious, for the benefit of numerical analysis, mitochondrial movements were also tracked and statistically analyzed, as described in chapter 2, both in leaf epidermal cells and root epidermal cells (in region of differentiation).

When mitochondrial instantaneous speeds (µm/s) were compared on tracked mitochondria in Lat- B or mock treatment with 0.1% (v/v) ethanol (EtOH), there was a significant difference ($P < 0.05$) in speeds (Fig. 4-7 A) in leaf epidermal cells. However, there was not any significant change on mitochondrial speed detected in root epidermal cells (Fig. 4-7 B, as the same letters above the two bars indicate that there is no significant difference between means).

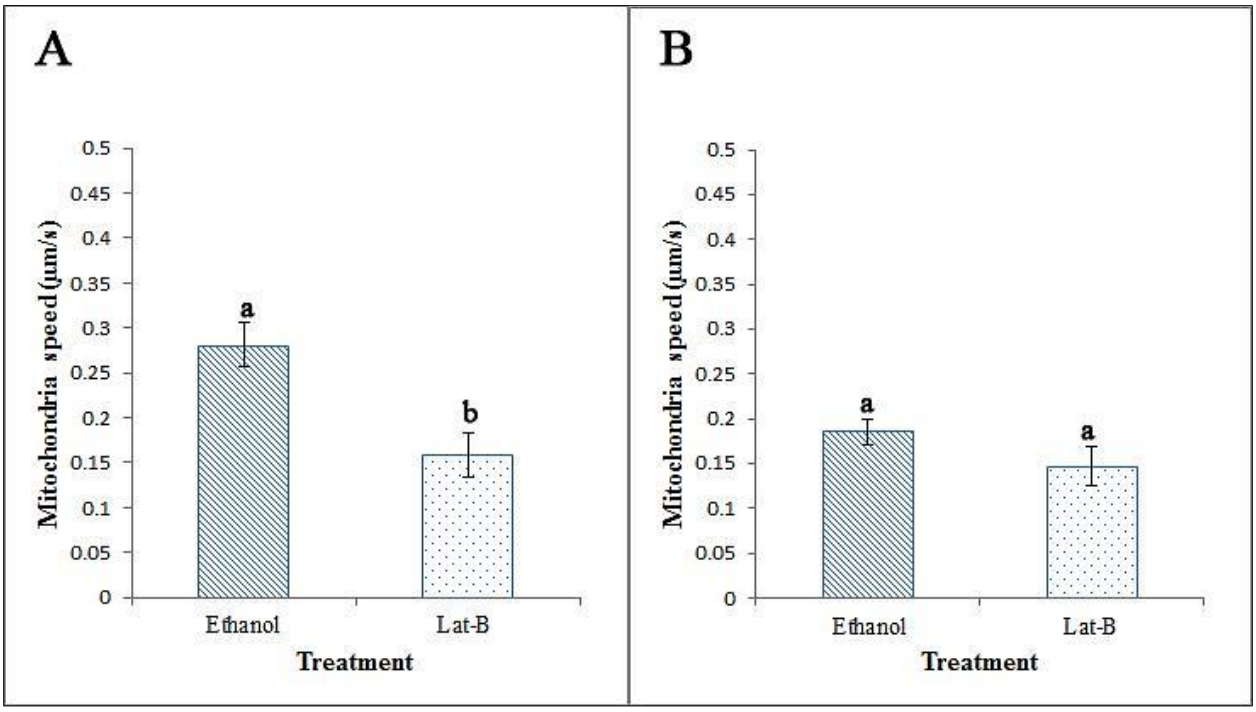

Figure 4-7. The effect of the actin depolymerization on average mitochondrial speed in mito-GFP/mTalin-mCherry line treated with 2 µM Lat-B and mock treatment with 0.1% (v/v) ethanol (EtOH) up to 3 hours. (A) Leaf mitochondria and (B) root mitochondria. Error bars represent the standard errors of the means (n = 6 cells). Different letters above the bars indicate significant differences ($P \leq 0.05$) between treatments as indicated by a Fisher's least-significant difference test.

The mitochondria in leaf epidermis cells of, Lat-B treatment showed 0.12 ± 0.02 µm/s (n = 6 cells) speed reduction (on average) than those of the mock treatment with ethanol. Leaf cells and root cells both displayed significant reduction (7.8 ± 1.8 µm reduction in leaves and 2.95 ± 1.2 µm reduction in roots) in average mitochondrial displacement (distance between the mitochondria's first and last position in the cell) with 2 µM Lat-B treatment, compared to the mock treatment with 0.1% (v/v) ethanol (EtOH) (Fig. 4-8).

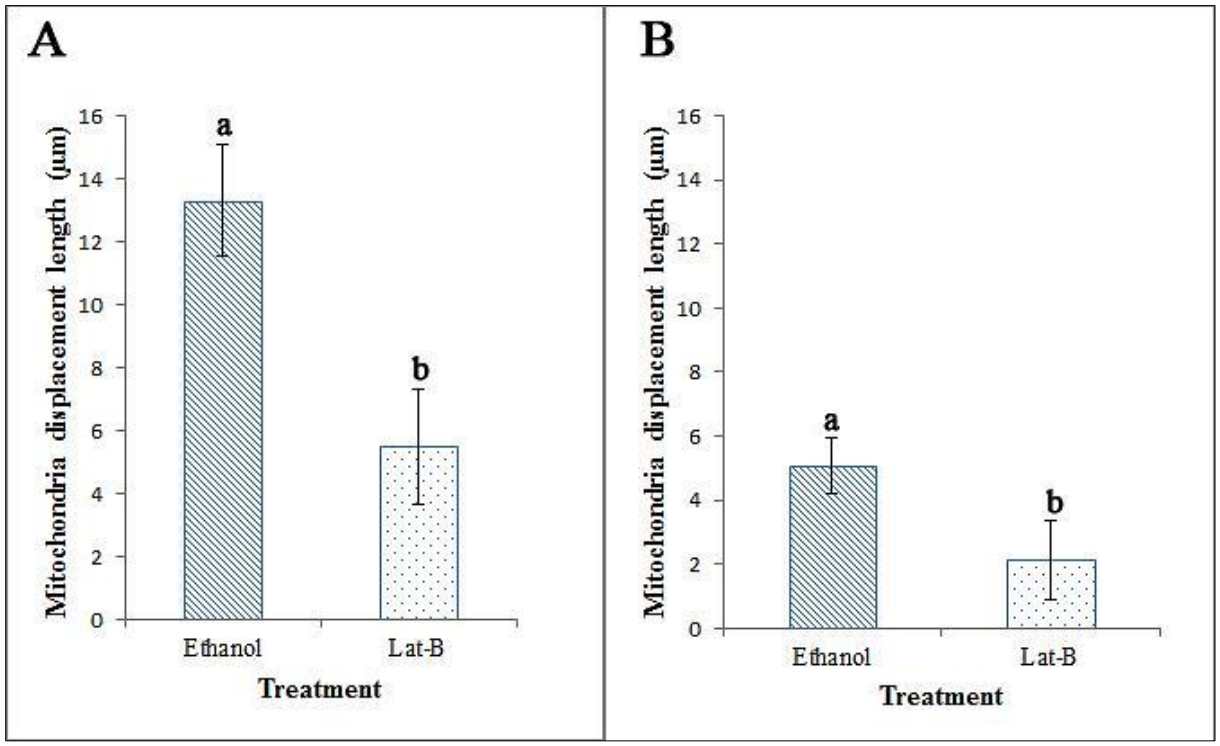

Figure 4-8. Comparison of average mitochondrial displacement lengths in mito-GFP/mTalin-mCherry line treated with 2µM Lat-B and mock treatment with 0.1% (v/v) ethanol (EtOH) up to 3 hours. Graph (A) showing leaf mitochondria and (B) showing root mitochondria. Error bars represent the standard errors of the means (n = 6). Different letters above the bars indicate significant differences ($P \leq 0.05$) between treatments as indicated by a Fisher's least-significant difference test.

In the comparison of mitochondrial track lengths in leaf cells, a similar pattern was observed (Fig.4-9 A). However, in root cells, although there was a significant difference in mitochondrial displacement between Lat-B treated sample and mock treatment with ethanol, the reduction of mitochondrial track length was insignificant (Fig. 4-9 B).

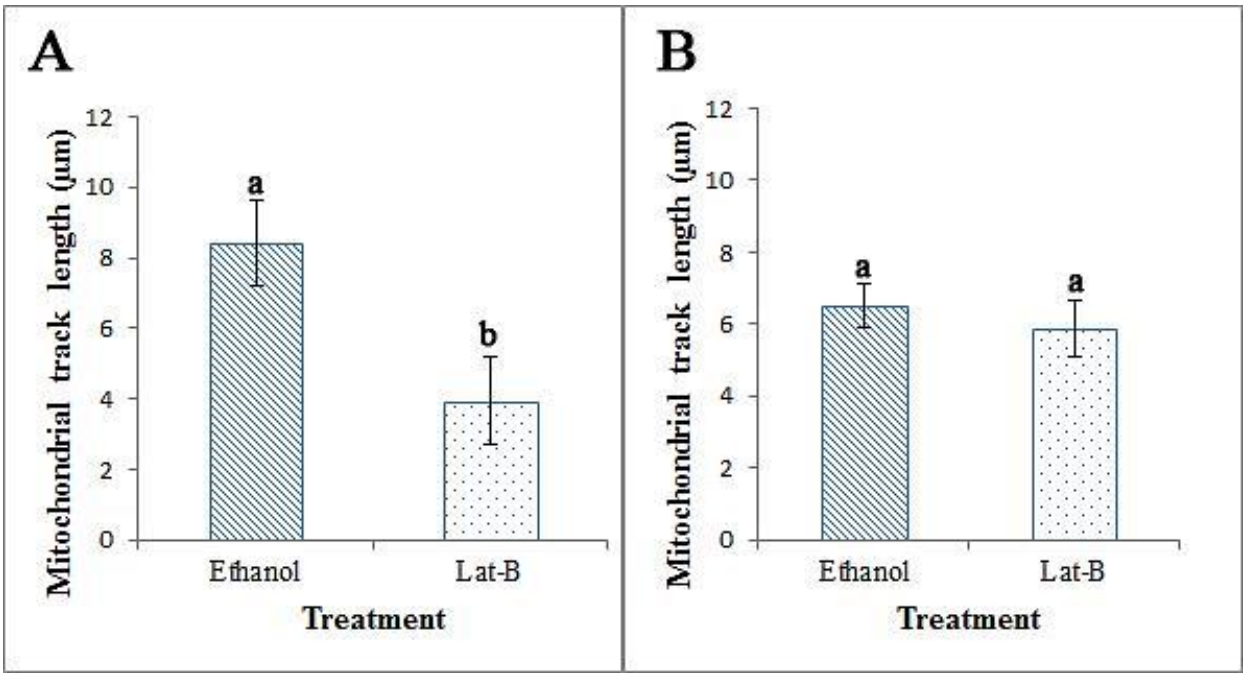

Figure 4-9. Comparison of average mitochondrial track lengths in mito-GFP/mTalin-mCherry line treated with 2µM Lat-B and the mock treatment with 0.1% (v/v) ethanol (EtOH) up to 3 hours. (A) Leaf mitochondria and (B) root mitochondria. Error bars represent the standard errors of the means (n = 6 cells). Different letters above the bars indicate significant differences ($P \leq 0.05$) between treatments as indicated by a Fisher's least-significant difference test.

In terms of the meandering index developed (mitochondrial track displacement over the track length), there was a significant difference between the Lat-B treated sample and the mock treatment with ethanol (EtOH) for both root and leaf samples (Fig. 4-10). Meandering indices for individual time points were similar except for the 10 min index, indicating the significant and irreversible change of mitochondrial movement after 10 minutes of Lat-B treatment (Fig.4-11).

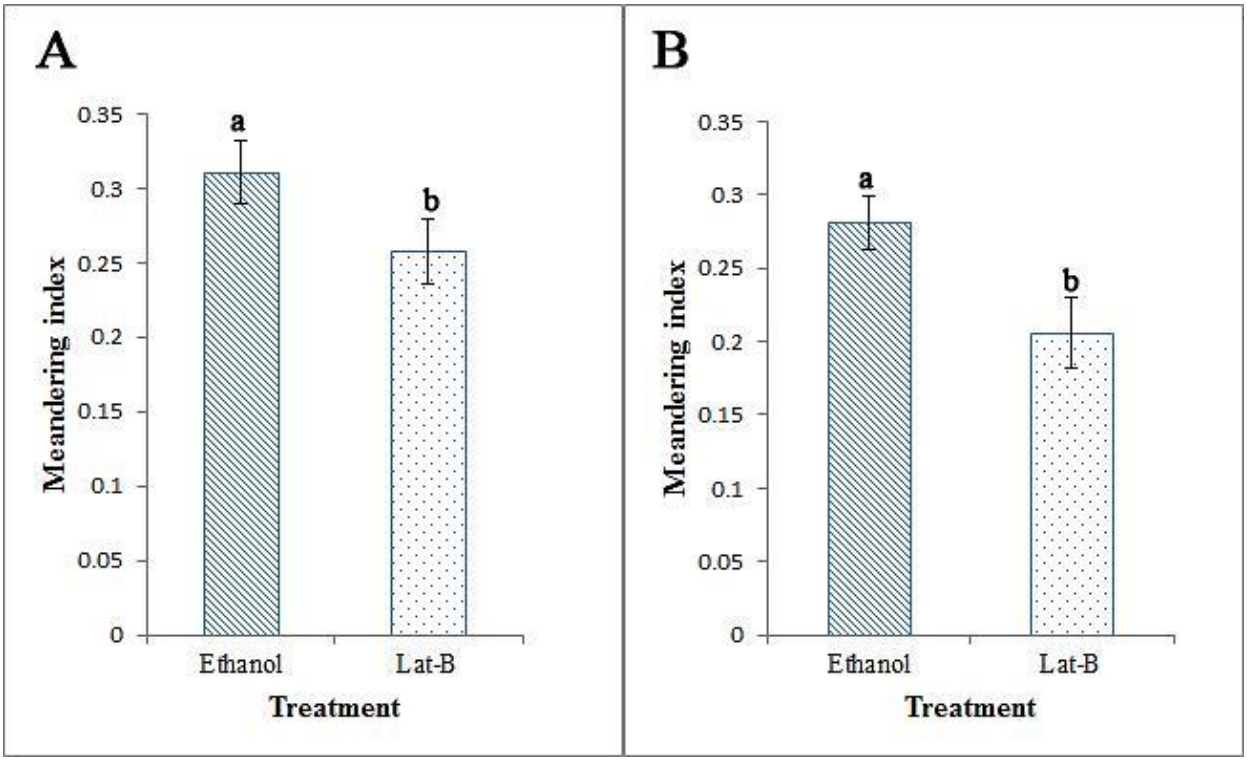

Figure 4-10. Meandering index developed for mito-GFP/mTalin-mCherry line treated with 2 µM Lat-B and the mock treatment with 0.1% (v/v) ethanol (EtOH) up to 3 hours. (A) Leaf mitochondria and (B) root mitochondria. Error bars represent the standard errors of the means (n = 6 cells). Different letters above the bars indicate significant differences ($P \leq 0.05$) between treatments as indicated by a Fisher's least-significant difference test.

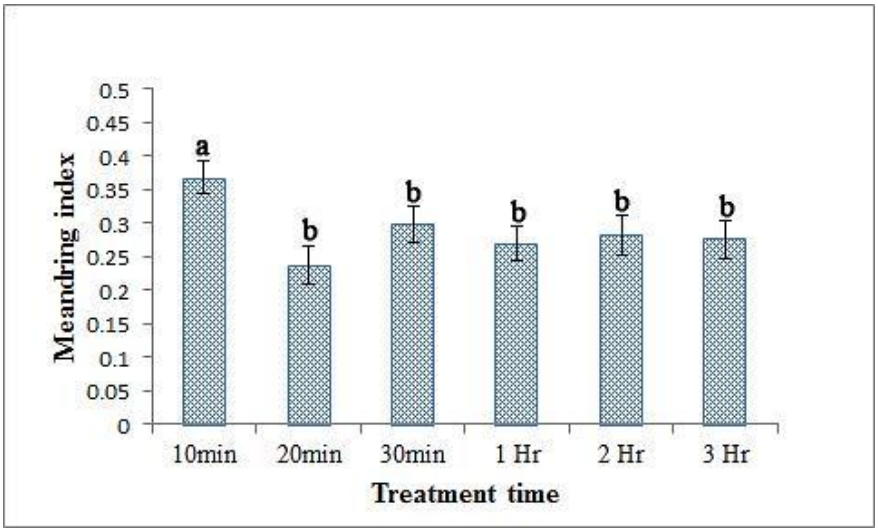

Figure 4-11. Mitochondrial meandering index in Arabidopsis leaf mesophyll cells treated with Lat-B for different times. Error bars represent the standard errors of the means (n = 6). Different letters above the

bars indicate significant differences ($P \leq 0.05$) between treatments as indicated by a Fisher's least-significant difference test.

4.2.3 Effects of actin cytoskeleton disruption on mitochondrial arrangement and distribution

With microscopic observation, it was clear that after the Lat-B treatment, mitochondrial arrangement changed significantly and individual mitochondria began to cluster with time (Fig.4-6). These clusters were compact and appeared to move along the remaining actin filaments (Fig. 4-12).

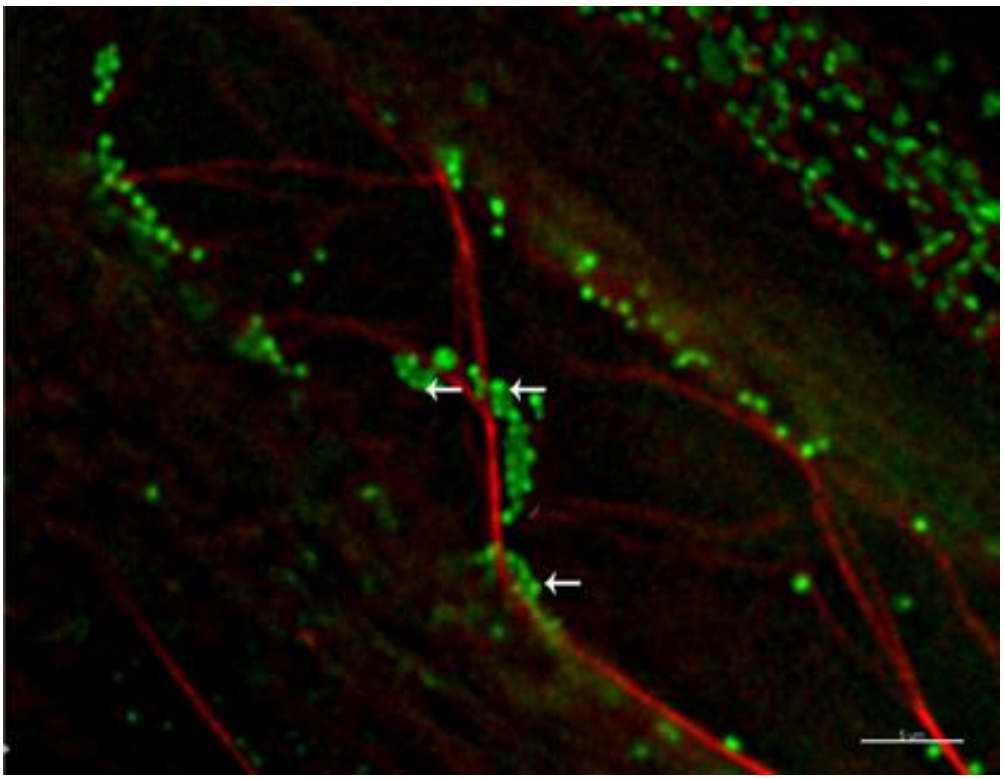

Figure 4-12. Clusters of mitochondria moving along actin cable in mito-GFP/mTalin-mCherry line treated with 2 µM Lat-B. Image was taken after 2 hours of Lat- B treatment. Mitochondria are shown in green and actin with red; clusters are indicated with white arrows. Bar = 5 µm.

To compare changes, the mitochondrial movements were also tracked and statistically analyzed. Although mitochondrial clusters were observed in the mock treated sample with ethanol and 2 µM Lat-B treatments, much larger clusters were observed with Lat-B treatment (9.8 ± 2.6 µm larger than the clusters in mock treated samples with ethanol on average).

A significant difference was also detected in the speed of cluster movements between the 2 µM Lat-B treated sample (0.08 ± 0.01 µm/s) and the mock treated sample with ethanol (0.14 ± 0.01µm/s). Mitochondrial cluster speeds were generally higher in both the mock treated sample with ethanol and 2 µM Lat-B treatments for up to 30 minutes, but it was significantly slower with 2 µM Lat-B treatment after one hour (Fig. 4-13) and remained slower up to 3 hours.

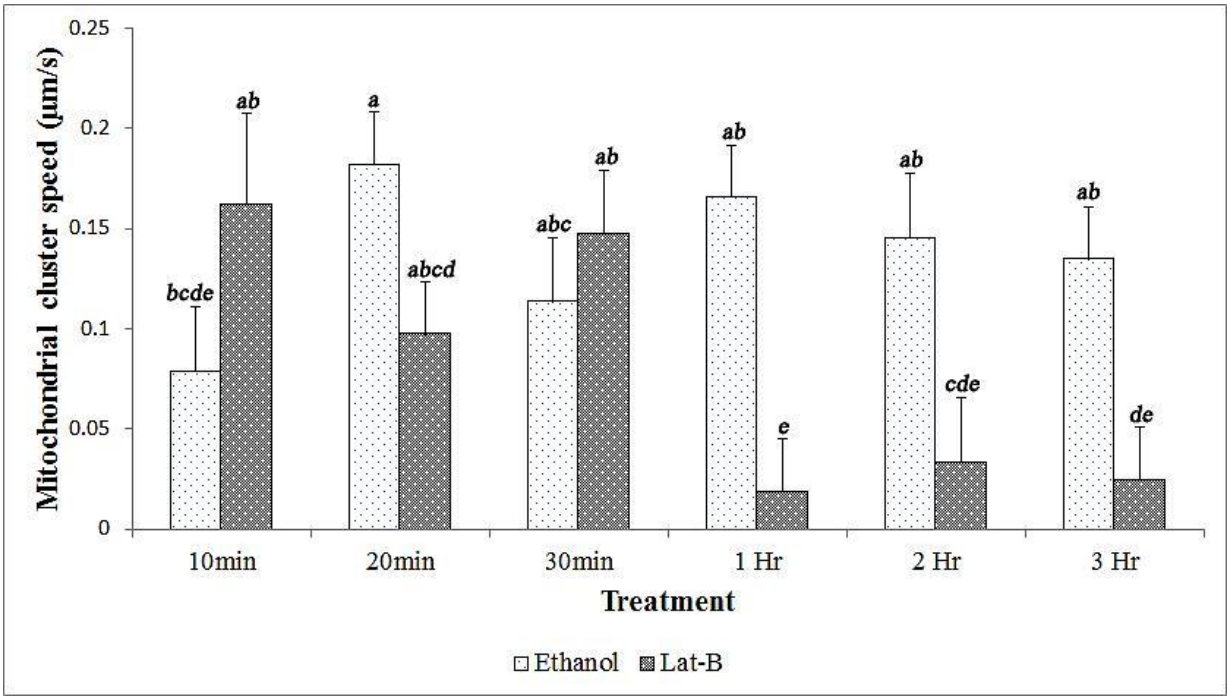

Figure 4-13. The effect of the actin depolymerization on average mitochondrial cluster speed in mito-GFP/mTalin-mCherry line treated with 2 µM Lat-B and the mock treatment with 0.1% (v/v) ethanol (EtOH). Error bars represent the standard errors of the means (n = 6 cells). Different letters above the bars indicate significant differences (P<0.05) between treatments as indicated by a Fisher's least-significant difference test.

Although with 2 µM Lat-B treatment- clusters started to appear within 10 minutes of treatment time, they became bigger after one hour time period (Fig. 4-14). Meanwhile clusters became slow-moving after one hour (Fig. 4-13) and cluster arrangement tightened with time (Fig.4-6 D and 4-14).

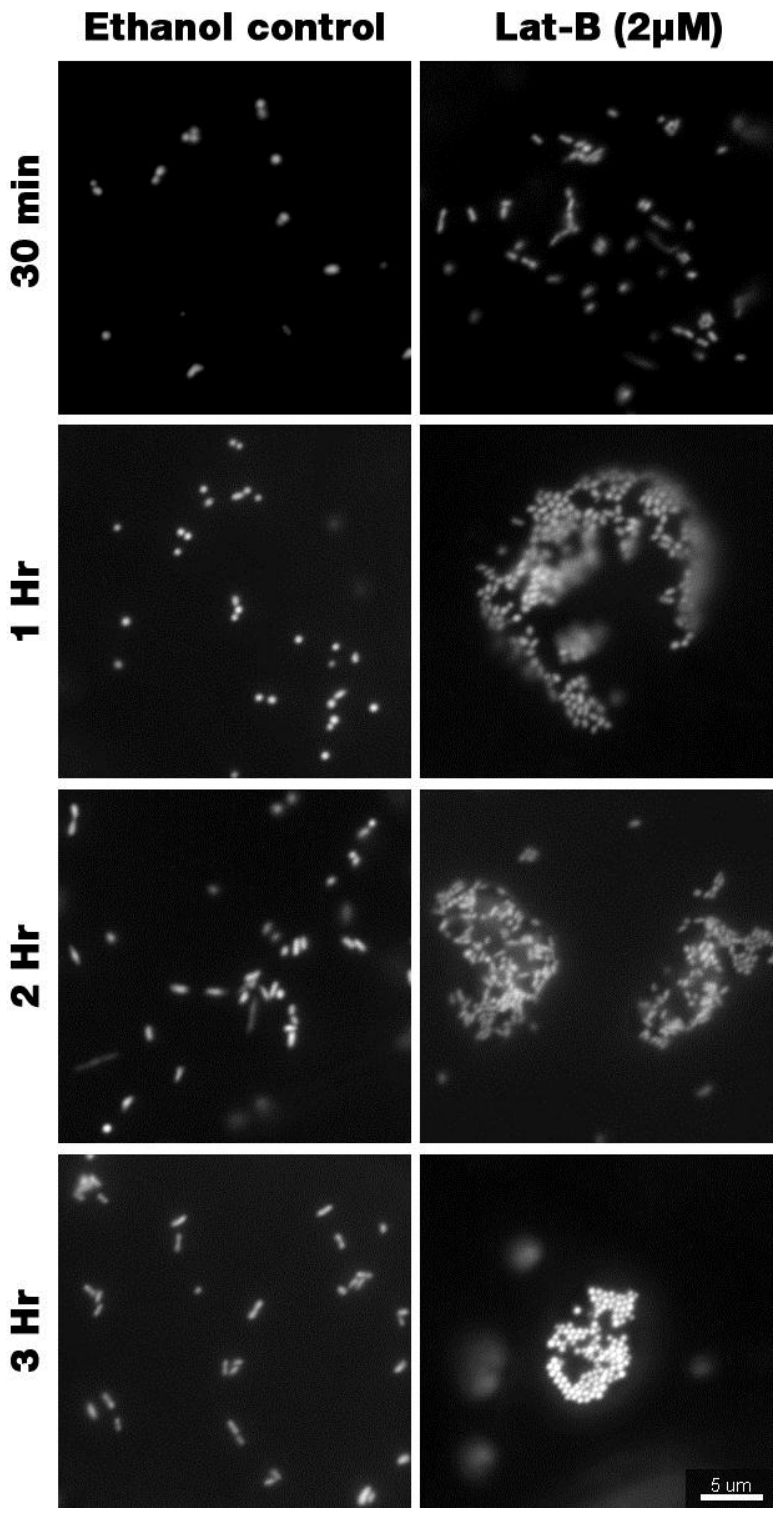

Figure 4-14. Mitochondrial morphology change and clustering behaviour observed with respect to time in mito-GFP/mTalin-mCherry line treated with 2 µM Lat-B or 0.1% v/v mock treatment with ethanol. Bar = 5µm

With respect to the average area of mitochondrial clusters, there was a significant increase of cluster area with Lat-B treatment compared to the mock treatment with ethanol. The average cluster area of the Lat-B samples (at 3 hr time point) was 26.95 ± 2.5 μm^2 while it was only 17.09 ± 3.2 μm^2 in the mock treatment with ethanol.

Figure 4-15 shows 2D reconstruction (in a randomly chosen sample) of mitochondrial clusters that appeared after 2 hours of 2 µM Lat-B treatment and 0.1% (v/v) mock treatment with ethanol. The data show that clusters with an area larger than 80 μm^2 were relatively immobile, while small clusters (area less than 60 μm^2) showed comparatively fast movement (Fig. 4-15 A). Almost every rare transient cluster that appeared in mock treated sample with ethanol (which they also do in untreated cells) showed comparatively high-speed movements (Fig. 4-13 and Fig. 4-15 B).

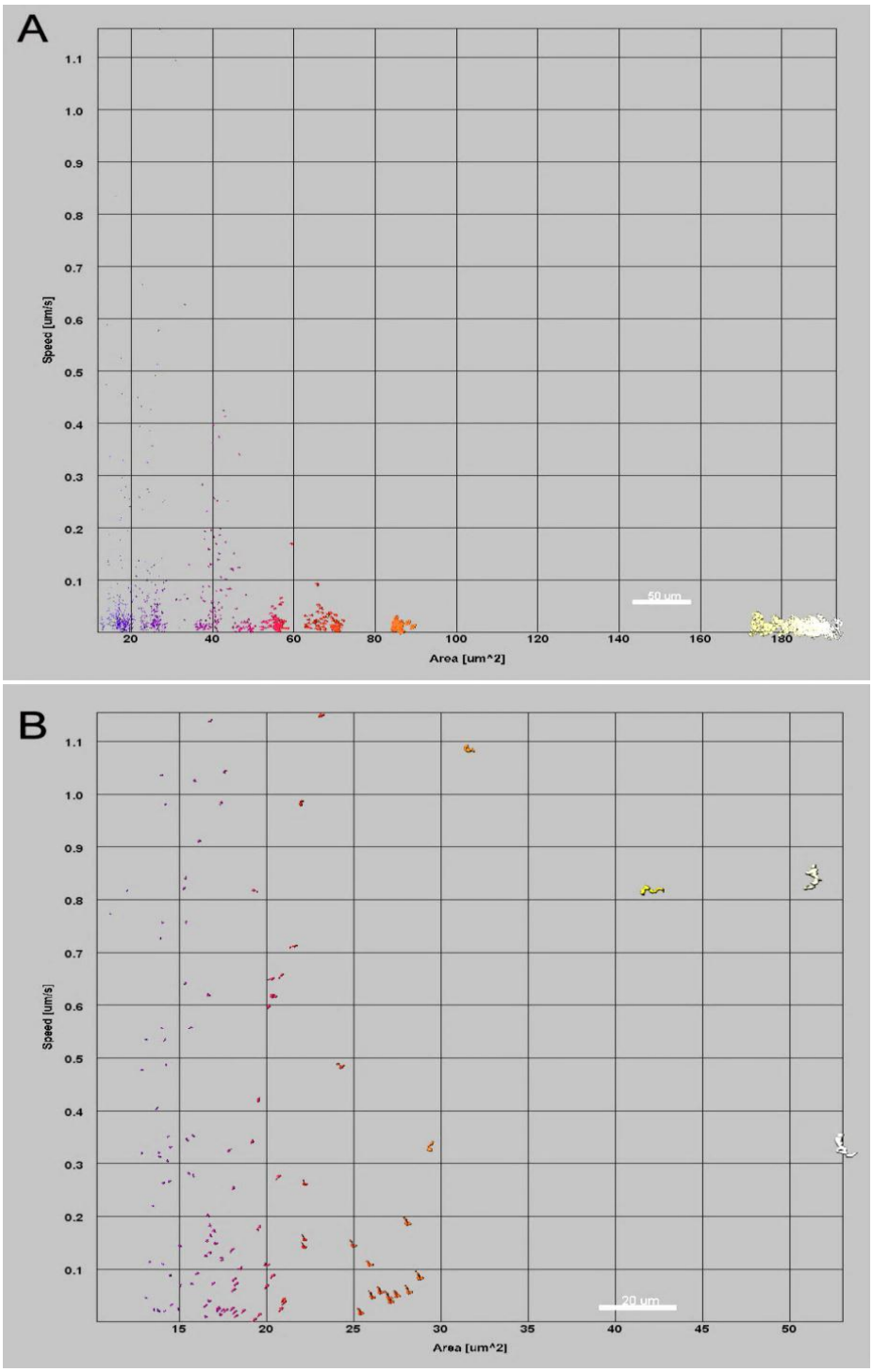

Figure 4-15. A comparison of mitochondrial cluster speeds (in Y axis, µm/s) and cluster area (in X axis, μm^2) of (A) 2 µM Lat-B treated and (B) mock treated with 0.1% (v/v) ethanol (randomly selected) Arabidopsis 43C5 line cells. Cluster identified and statistic generated using Imaris software. Cluster speeds and area were calculated over 30 seconds (one image per second). Clusters are proportionate to the actual image data set. Bar in graph A is 50 µm and the bar in graph B is 20 µm.

4.2.4 Effects of microtubule cytoskeleton disruption on mitochondrial movements

To see the effect of MT depolymerization with mitochondrial movements, Arabidopsis line expressing both mitochondria and MT tagged fluorescence protein (mito-GFP/MAP4-mCherry line) was used. In untreated samples (Fig 4-16), mitochondria appeared to move on a different plane than MT (0.8 µm distance on average).

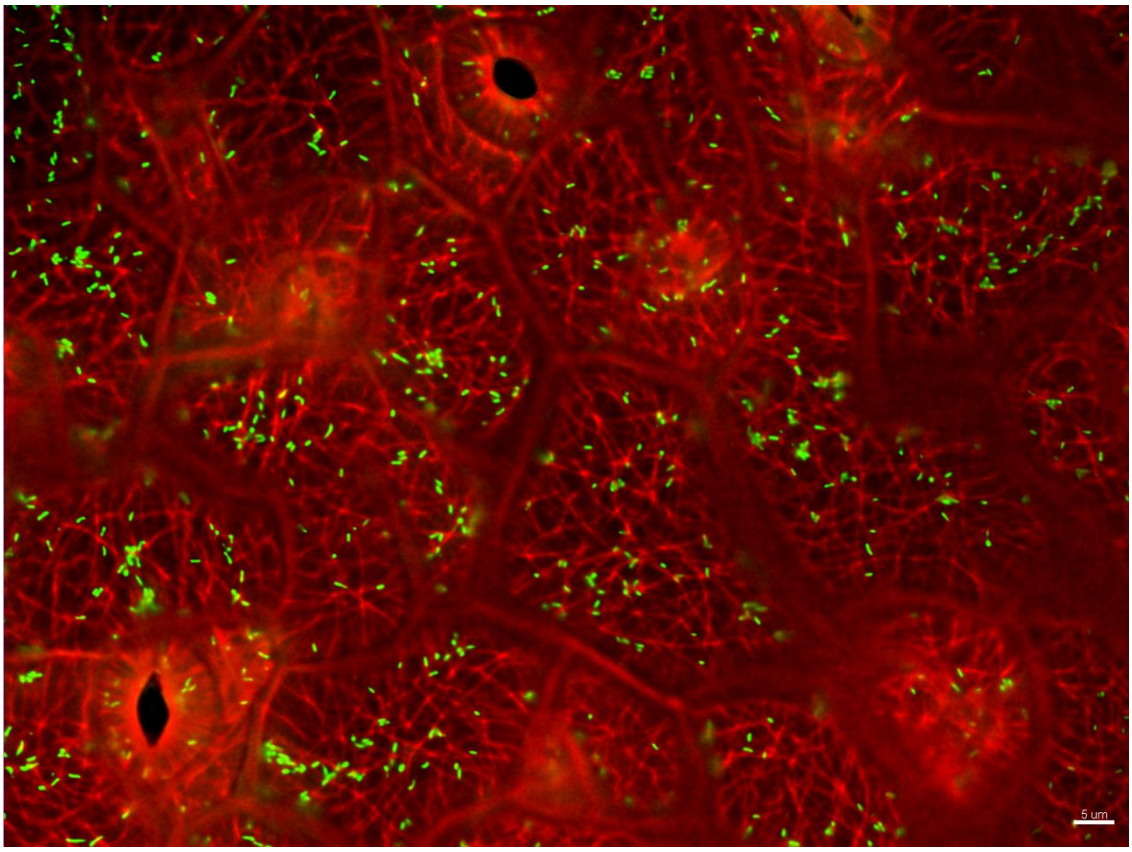

Figure 4-16. The appearance of mitochondria and microtubules in Arabidopsis mito-GFP/MAP4-mCherry leaf epidermis cells, mitochondria shown in green and microtubules in red. Bar = 5µm.

When mito-GFP/MAP4-mCherry line was treated with MT-disrupting drug oryzalin, as expected, microtubules were totally depolymerized in treated sample (Fig. 4-17), while most microtubules remained intact in the mock treatment 0.1% (v/v) ethanol (EtOH). However, no obvious mitochondrial morphology change was observed in up to 3 hours (Fig. 4-18). Other aspects of mitochondrial movements were also unchanged, such as speed, acceleration, and

displacement. However, there was an increase in average cluster area in the oryzalin treated sample (19.89 ± 1.12 μm^2) compared to the mock treatment with ethanol (15.45 ± 1.39 μm^2).

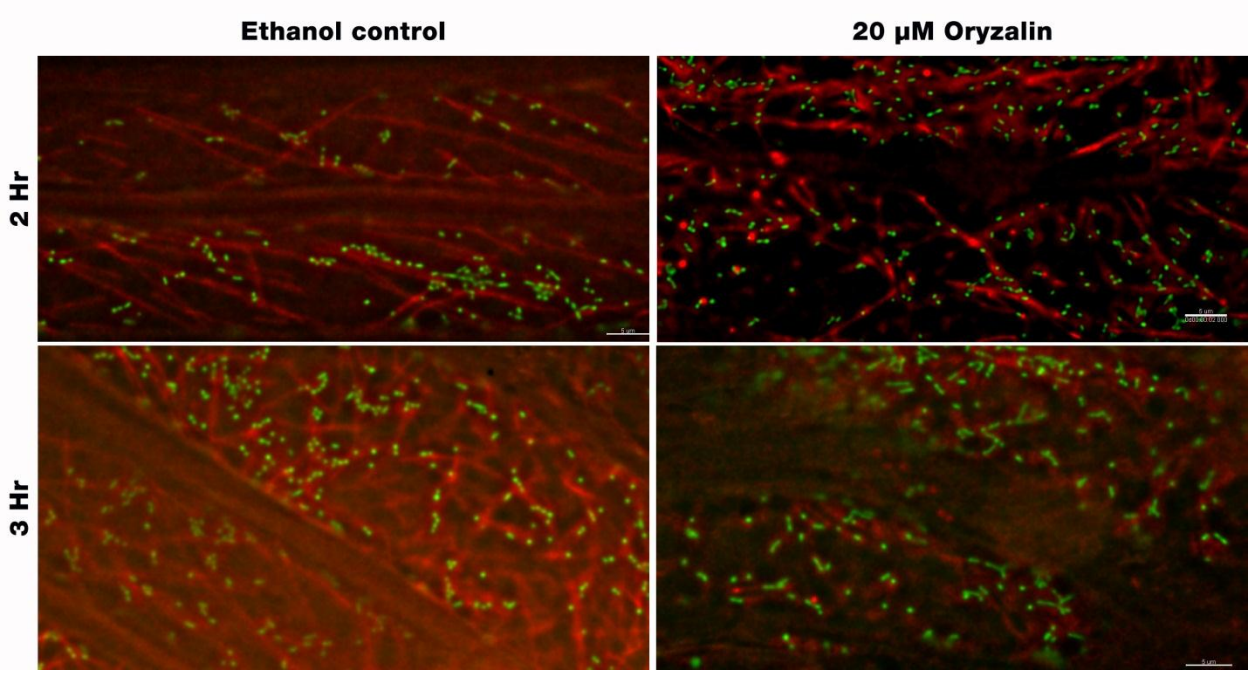

Figure 4-17. Effects of 20 μM oryzalin and mock treatment with 0.1% (v/v) ethanol (EtOH) on mitochondria arrangement and movement with time. Mito-GFP/MAP4-mCherry line used to visualize microtubules and mitochondria, mitochondria shown in green and microtubules in red. Bar = 5μm.

This average cluster area increase was comparatively very low with that observed in the Lat-B treated sample (Fig 4-15). These clusters also showed a significant increase in mitochondrial meandering index, 0.50 ± 0.05 in the oryzalin-treated sample compared with that in the mock treatment with ethanol (0.34 ± 0.05).

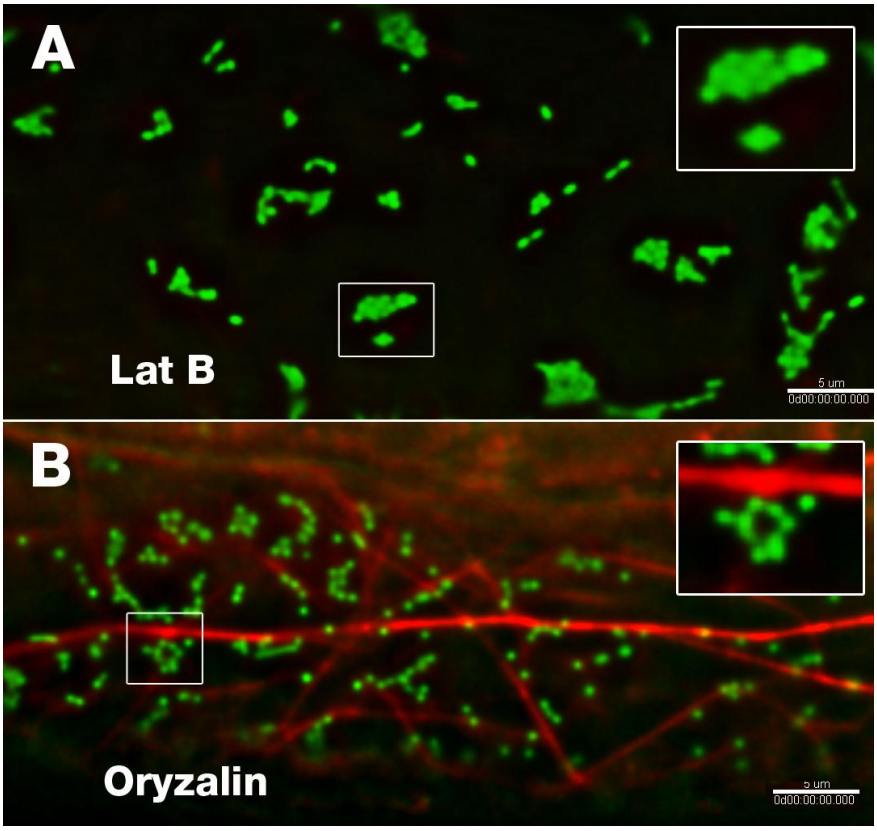

Figure 4-18. Effects of oryzalin and Lat-B treatments on mitochondria morphology and movements in the Mito-GFP/mtalin-mCherry line. Images are (A) with 2 µM Lat- B treatment, and (B) with 20 µM oryzalin treatment. The inset shows double magnified clusters. All images were taken after 3 hours of treatment. Images were representatives of more than 30 observed samples. Mitochondria are shown in green and actin in red. Bar = 5µm.

Although with both Lat-B and oryzalin treatments, mitochondria became clustered, there were significant morphological and volumetric differences in mitochondrial clusters between the two treatments. In Lat-B treated samples mitochondrial clusters were more abundant, tightly packed and individual mitochondria in the cluster seem normal in size (Fig. 4-18 A). But in oryzalin-treated samples, mitochondria became swollen and clusters appeared loosely packed (Fig 4-18 B), while most of these mitochondrial clusters were rare and transient in nature.

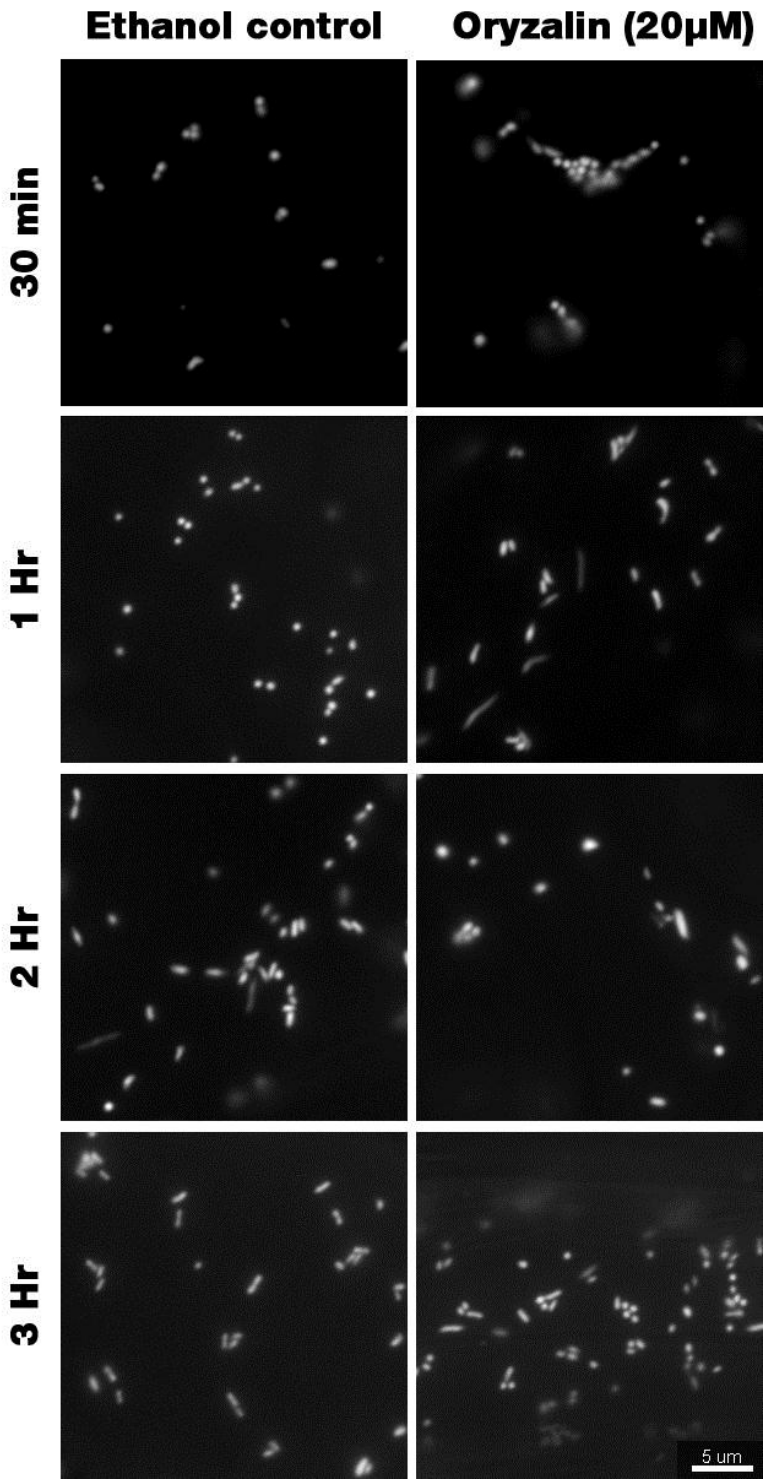

Figure 4-19. Mitochondrial morphology change and clustering behaviour observed with respect to time in mito-GFP-mCherry-MAP4 line treated with 20 µM Oryzalin or mock treatment with 0.06% (v/v) ethanol (EtOH). Bar = 5µm.

4.2.5 Effects of cytoskeleton disruption on PCD induction

To evaluate the effect of actin and MT cytoskeleton depolymerization on PCD initiation, following experiment was carried out with Arabidopsis seedlings. They were treated with either cytoskeleton-disrupting drug (2 µM Lat-B or 30 µM oryzalin) or mock treatment with ethanol for up to 72 hours. Arabidopsis root hairs were used to determine cell viability and plasmolysis.

The cell death data (Fig. 4-20), showed that there was a significant increase in dead cells in Lat-B treated samples at every observation point (24, 48, and 72 hours). The increment of the cell death percentage with Lat-B treatment was 47% from 24 to 48 hours, and increased up to 88% in total at 72 hours. Both the mock treatment with ethanol and oryzalin-treated samples had less than 25% of dead cells up to 72 hours. In the oryzalin-treated sample, increment of dead cells from 24 hours to 48 hours was very low (6%) compared to the Lat-B sample. However, there was a 40% increment in the final 24 hours, which increased up to 64% in total at 72 hours.

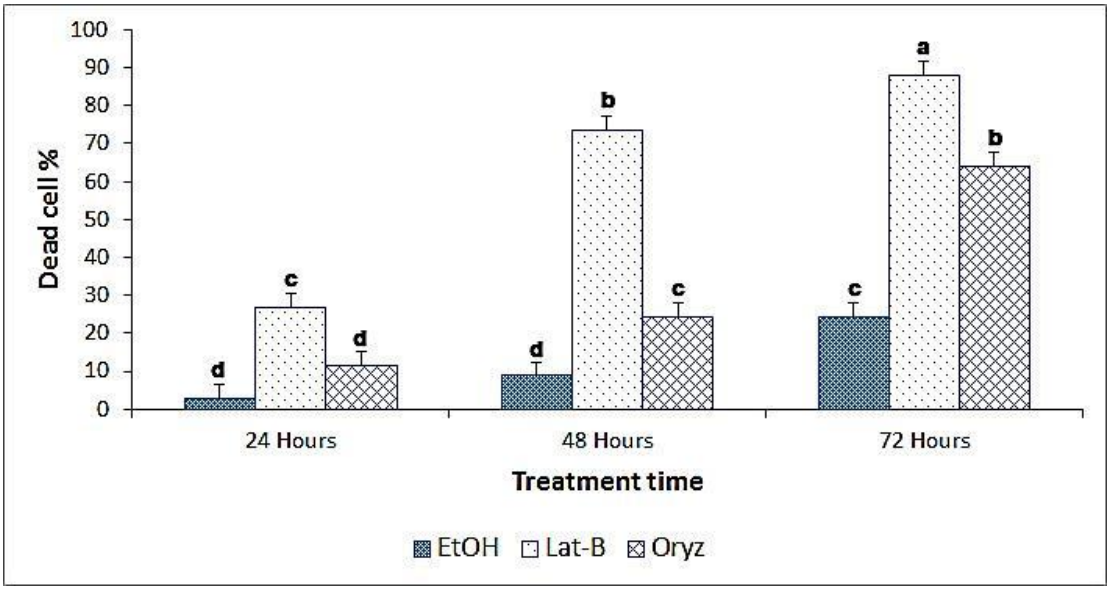

Figure 4-20. Cell death percentages of Arabidopsis mito-GFP (43C5) line treated with 2 µM Lat-B, 30 µM oryzalin or the mock treatment with 0.1% (v/v) ethanol (EtOH). Error bars represent the standard errors of the means (n = 3). Different letters above the bars indicate significant differences ($P \leq 0.05$) between treatments as indicated by a Fisher's least-significant difference test.

Plasmolysis data also showed a similar pattern with these cytoskeleton destructing drugs (Fig. 4-21). Treatment with Lat-B resulted in significant increases the percentage of plasmolysed cells at all-time points. The increment of the cell plasmolysis percentage with Lat-B treatment

was 42% from 24 to 72 hours, and increased up to 85% in 72 hours. Just as in cell death percentages, both the mock treatment with ethanol (EtOH) and oryzalin-treated samples showed less than 25% cell plasmolysis up to 48 hours. The Oryzalin-treated sample showed only a 9% increment from 24 to 48 hours, and a 44% increment from 48 to 72 hours, resulting in 60% of cells plasmolysed in 72 hours. According to the Pearson correlation coefficient analysis, there was a 99% correlation (n = 27) between cell death and plasmolysis percentages.

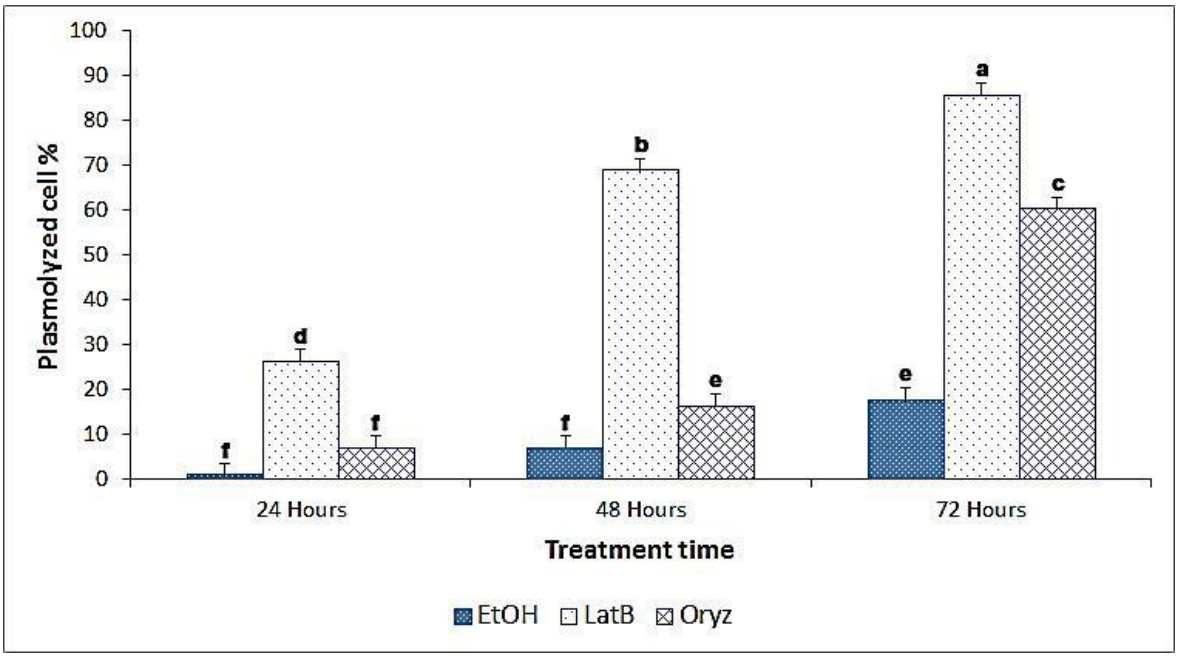

Figure 4-21 Cell plasmolysis percentages of Arabidopsis mito-GFP (43C5) line treated with 2 µM Lat-B, 30 µM oryzalin and the mock treatment with 0.1% (v/v) ethanol (EtOH). Error bars represent the standard errors of the means (n = 3). Different letters above the bars indicate significant differences ($P<0.05$) between treatments as indicated by a Fisher's least-significant difference test.

Regarding mitochondrial clustering morphology, significantly larger clusters were observed in Lat-B treated sample compared to the mock treatment with ethanol, though the cluster morphology did not change with time (Fig. 4-22). However, the oryzalin treated sample did not show much difference either on mitochondrial morphology or arrangement, compared to the mock treatment with ethanol (EtOH) (Fig. 4-23).

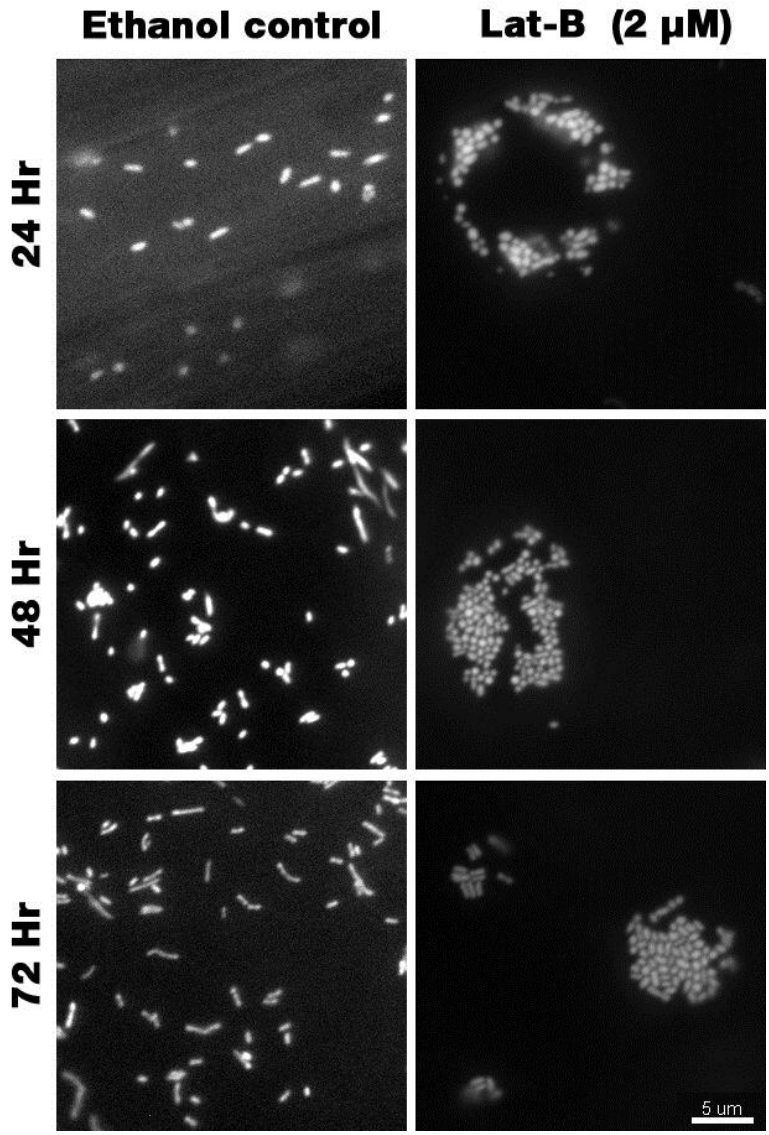

Figure 4-22. Mitochondrial morphology change and clustering behaviour observed with respect to time in Arabidopsis 43C5 line treated with 2 µM Lat-B or 0.1% (v/v) mock treatment with ethanol. Bar = 5 µm.

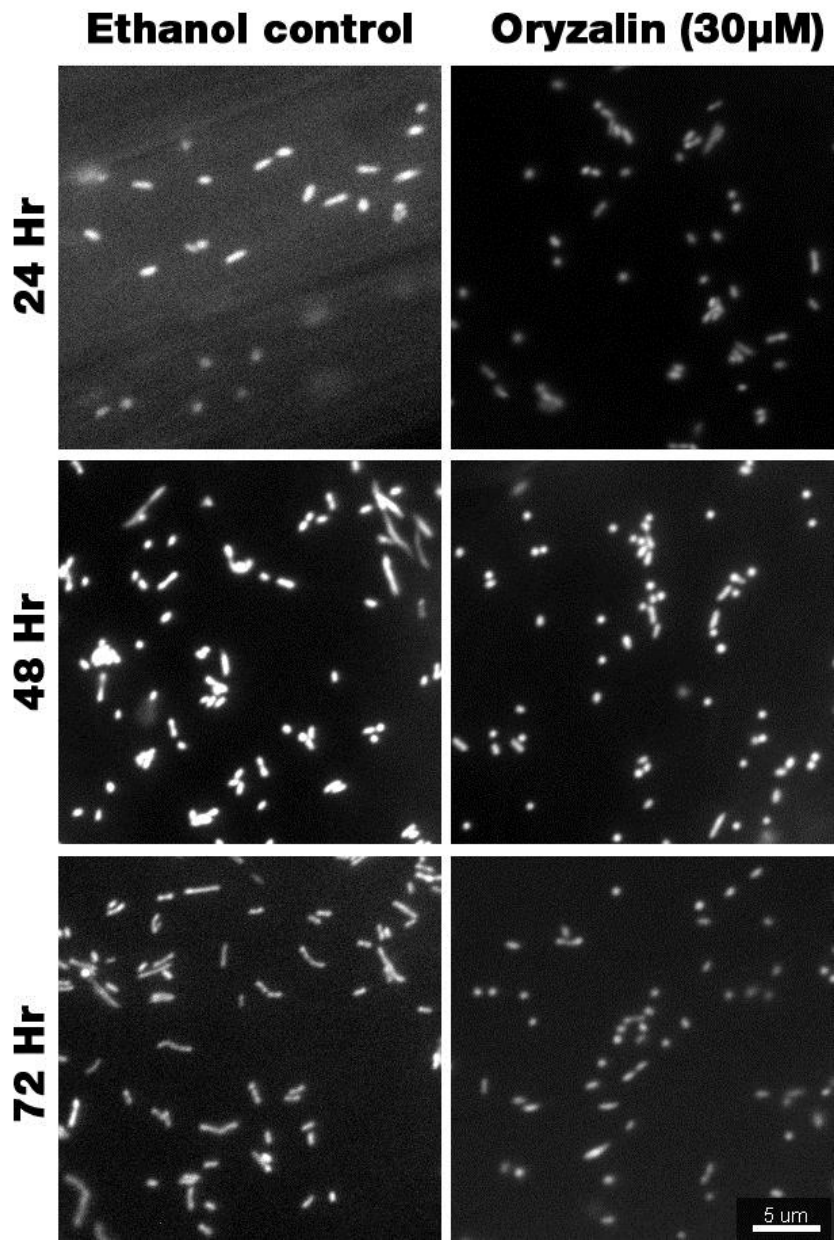

Figure 4-23. Mitochondrial morphology change and clustering behaviour observed with respect to time in Arabidopsis 43C5 line treated with 30 µM oryzalin or mock treatment with 0.06% (v/v) ethanol. Bar = 5 µm.

Various changes that happen to mitochondrial dynamics with these cytoskeletal-disrupting drugs were also tracked as described previously. According to the statistical analysis, significant differences were observed with the Lat-B treatment over 72 hours, in mitochondrial acceleration (0.08 ± 0.02 µm/s^2 reduction), mitochondrial speed (0.20 ± 0.04 µm/s reduction), mitochondrial displacement (9.87 ± 1.9 µm^2 reduction), track length (6.3 ± 1.1 µm reduction), and meandering

index (0.12 ± 0.01 reduction). However, with the 30 µM oryzalin treatment (up to 72 hours), no significant change was shown in such mitochondrial dynamics, only a (0.05 ± 0.01) increase in meandering index. Interestingly, no significant effect on mitochondrial dynamics was detected with temporal changes of the drug treatment.

4.2.6 Mitochondrial cluster association with the plus ends of MT

To show the interaction between mitochondria and MT plus ends, an Arabidopsis line dual-labeled with EB1b and mito-mCherry was used (mito-mCherry/EB1b-GFP). In the un-treated plants, no interaction was observed between MT plus ends and mitochondrial dynamics (Fig. 4-24).

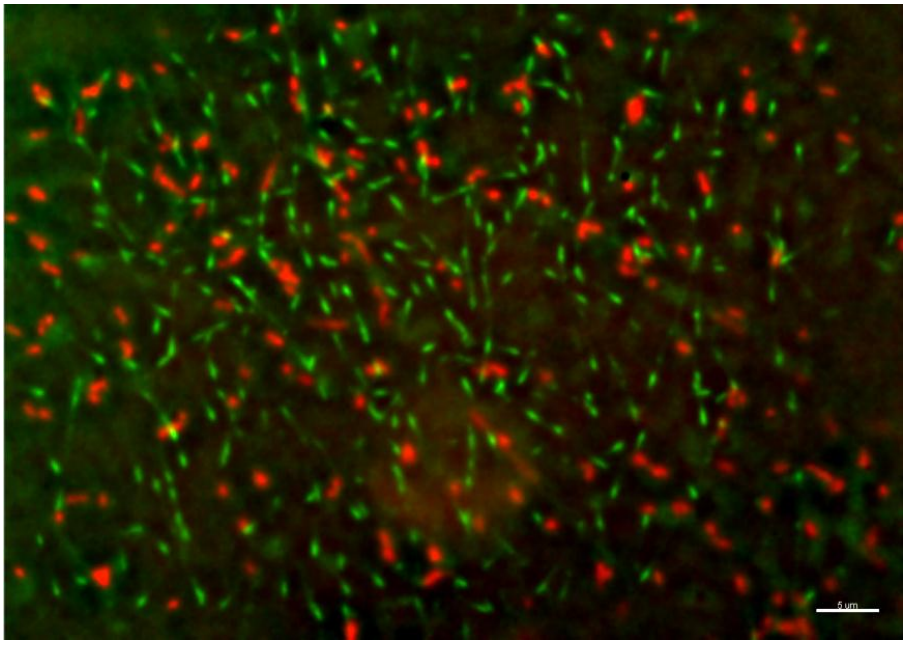

Figure 4-24. Arabidopsis line (mito-mCherry/EB1b-GFP) showing microtubule plus ends (EB1b) in green and mitochondria (mito.mCherry) in red. Bar = 5 µm.

To determine the effect of actin depolymerization and mitochondrial cluster formation with respect to MT plus ends, mito-mCherry/ EB1b-GFP line was treated with 2 µM Lat-B for 2 hours. No interaction was detected between MT plus ends (EB1b) and mitochondrial clusters. Microtubule plus end (EB1b) morphology did not change with the actin depolymerization (Fig. 4-25).

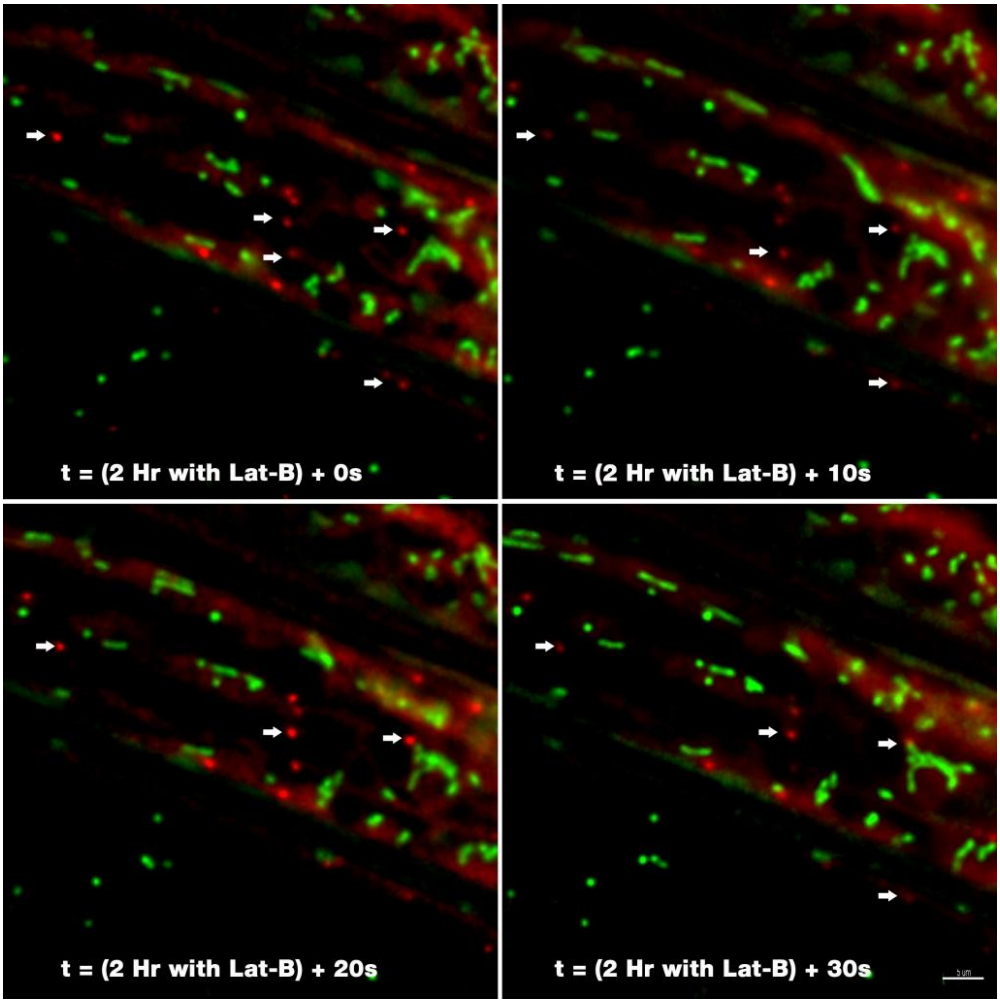

Figure 4-25. Effects of actin depolymerization on mitochondria morphology and microtubule plus end interaction. The mito-mCherry/EB1b-GFP line was treated with 2 µM Lat-B for 2 hours. All Images were taken after 2 hours of Lat-B treatment, each frame 10 seconds apart. Mitochondria are shown in green and MT plus ends in red, with arrow heads showing MT plus ends. Bar = 5 µm.

To determine the effect of microtubule depolymerization and mitochondrial dynamics with respect to MT plus ends, EB1b-mito.mCherry line was treated with 20 µM oryzalin for 2 hours. Microtubule plus end (EB1b) morphology (see Fig.4-24 for untreated sample) completely changed with the oryzalin treatment (Fig. 4-26). Microtubule plus ends (EB1b) became smear-like around the moving mitochondria. Some mitochondria were observed to be embedded in this smear. Most of the mitochondria observed to be moving (as also shown by statistical analysis) without any change (Fig. 4-26, some moving mitochondria were indicated by a white circle).

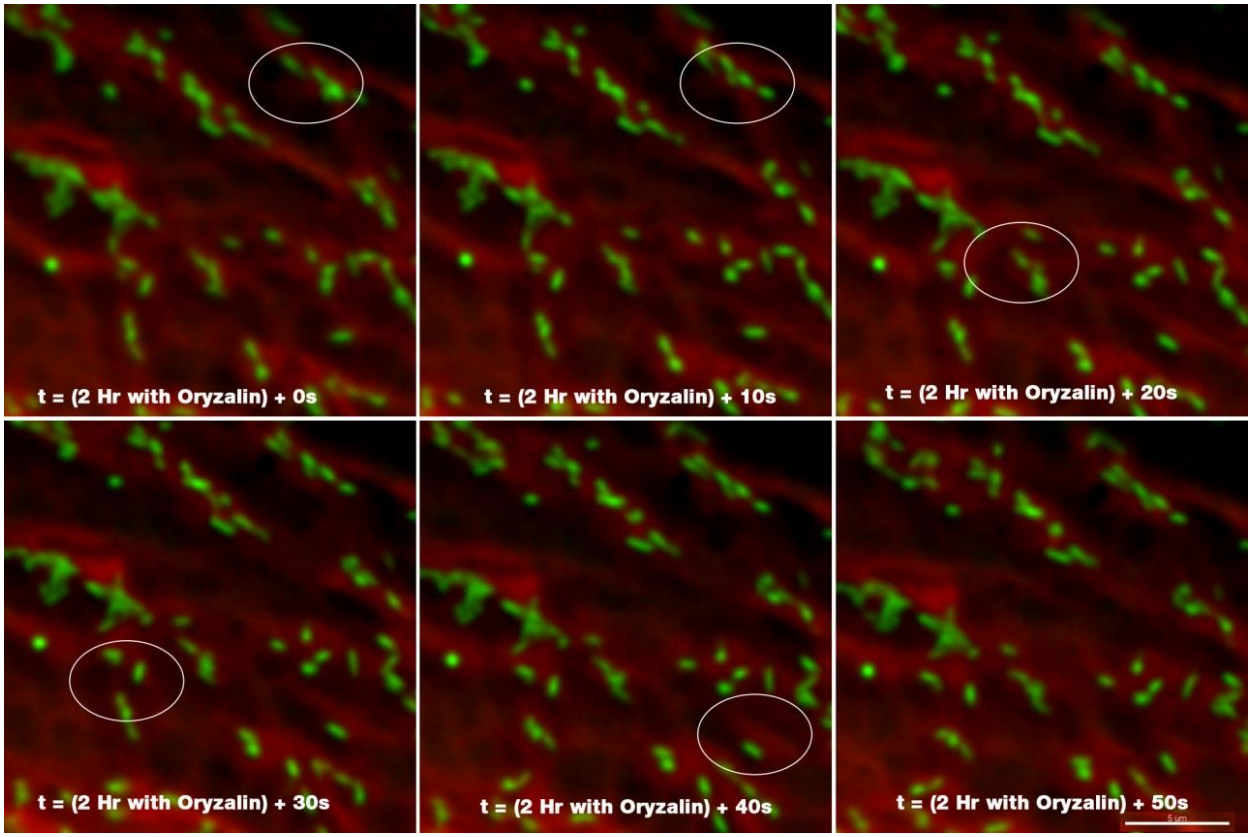

Figure 4-26. Effects of microtubule depolymerization on mitochondria morphology and microtubule plus end arrangement. The mito-mCherry/EB1b-GFP line was treated with 20 µM oryzalin treatment. All Images were taken after 2 hours of oryzalin treatment, each frame 10 sec apart. Mitochondria are shown in green and MT plus ends in red (smear). Some moving mitochondria are indicated by a white circle. Bar = 5 µm.

This effect was also clearly visible with the sample treated up to 24 hours with 15 µM oryzalin (Fig. 4-27). Mitochondria showed no difference in movement or morphology, but microtubule plus ends (EB1b) were not observable, and instead showed smearing fluorescence.

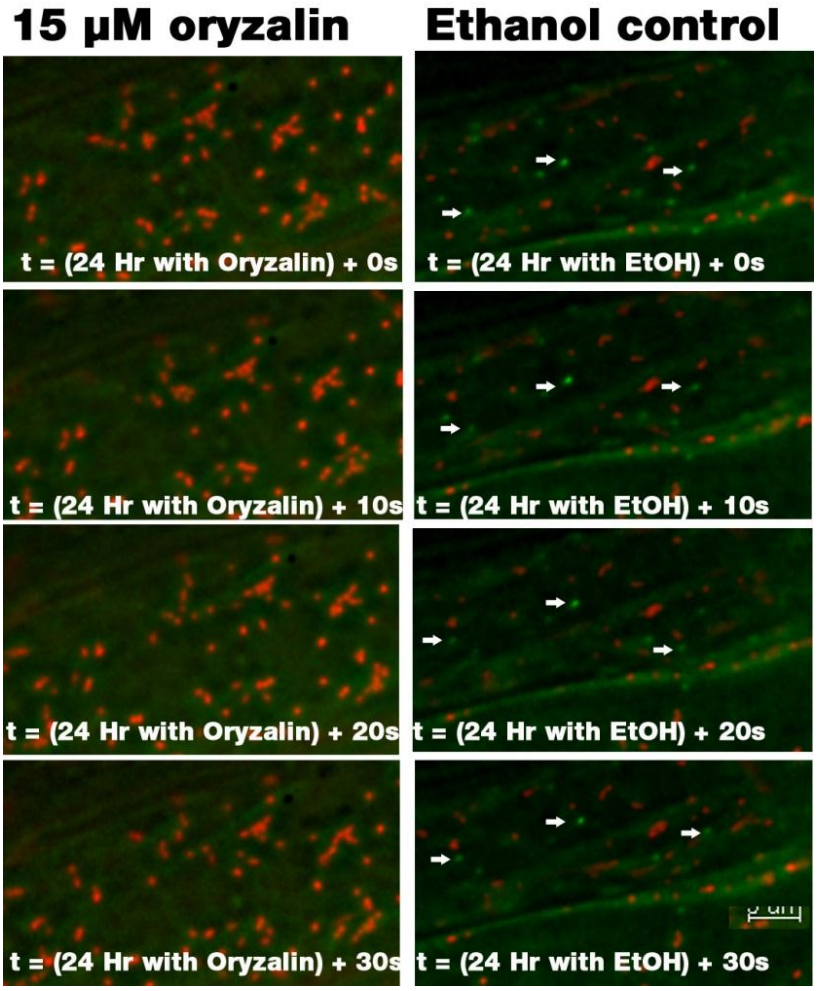

Figure 4-27. Effects of microtubule depolymerization on mitochondria morphology and microtubule plus end interaction. The mito-mCherry/EB1b-GFP line was treated with 15 µM oryzalin and mock treatment with 0.1% (v/v) ethanol (EtOH). All images were taken after 24 hours of treatment, each frame 10 sec apart. Mitochondria are shown in red and MT plus ends in green (shown in pointed arrow). Images are representative of three independent experiments. Bar = 5 µm.

As shown in Figure 4-24, microtubule plus ends (EB1b) did not exhibit any connection with mitochondria in the control sample (see Fig. 4-28 A); in fact, they appeared to be in two different focal planes. After mild heat treatment (42^{o}C for 7 minutes), these microtubule plus ends (EB1b) appeared to move with swollen mitochondrial clusters (Fig. 4-28 B).

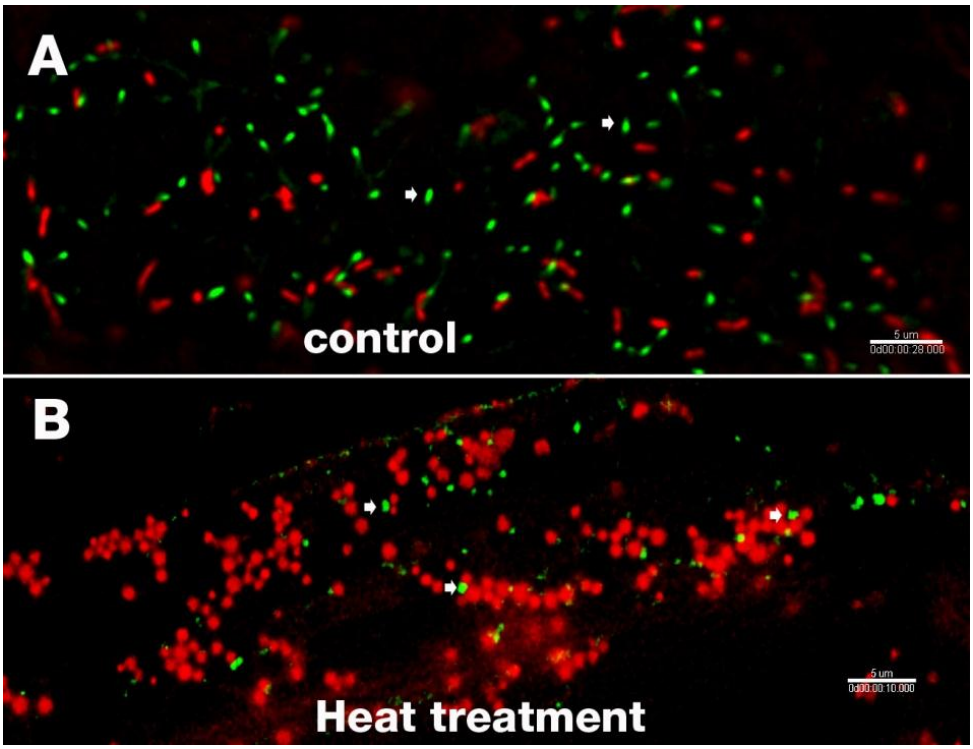

Figure 4-28. Effects of mild heat treatment (42^{o}C for 7 minutes) on microtubule plus ends and mitochondrial morphology and movement. Arabidopsis mito-mCherry/EB1b-GFP line was used to visualize microtubule plus ends and mitochondria. Image (A) negative control, (B) after 7 min heat treatment. All images were taken 5 min after end of the treatment. Mitochondria are shown in red and microtubule plus ends are in green. White arrows indicate few representatives MT plus ends. Images are representative of five independent experiments. Bar = 5µm.

CHAPTER 5

5 DISCUSSION

5.1 Heat shock induced PCD with increased levels of nitric oxide, changes in mitochondrial dynamics

In animals, nitric oxide is well known to play a major role in various physiological processes, but in plants there is less information regarding this matter. In the experiment explained in chapter three, I tried to test the effects of both natural and artificially increased NO levels in Arabidopsis cells. This effect of increased levels of NO was recorded with respect to mitochondrial morphology and dynamics with or without heat shock induced PCD. In order to determine the NO concentration in arginase negative mutants, DAF- FM staining method was followed as described in chapter 2 and 3.

The fluorescence intensity difference detected between arginase negative mutants and the wild type can be considered as an indicator of different NO levels present in each genotype observed. This observation concurs with the previous observations by Flores *et al.* (2008). In this study (described in chapter 3) aimed to understand the action of increased levels of NO on cell viability and PCD alongside with the effects of heat shock (HS).

5.1.1 Cell viability changes with heat shock and increased NO concentration

Cell death and plasmolysis data presented here indicate that heat shock at 42^{o}C for 1.5 hr is an efficient inducer of PCD in Arabidopsis root hair cells. A clear difference was observed, both in mitochondrial morphology and motility within one hour after the treatment, and the difference was irreversible at least over the following 72 hr. Heat shock increased both cell death and plasmolysis in a consistent pattern with time, while both were steady in non-heat-treated control samples (Fig. 3-3). A correlation of 94 % between cell death and plasmolysis percentage was a strong indication that those cells had not undergone a necrosis-type cell death, but rather had undergone PCD.

In the previous research done by Flores *et al.*,(2008), they have found that, when transgenic wild-type plants expressing promoter :: GUS construct, ARGAH1T :: GUS and ARGAH2 ::

GUS were compared, ARGAH1 :: GUS was found to be expressing in the entire cotyledon extending to the mid hypocotyl towards to the root tip, while ARGAH2 :: GUS showed a more localized expression. They have made a similar observation when arginase negative mutants stained with DAF-FM staining method to detect NO. There was high intensity florescence detected on hypocotyl- root junction of *argah1-1* plants while *argah 2-1* plants showed a higher signal in cotyledons, upper hypocotyl, and roots indicating more NO accumulation than in *argah1-1*.

In the present study, when the overall cell death percentages (with and without HS) are considered, the *argah2-1* line did not show any significant difference either in cell death percentage or in plasmolysis percentage from the WT. On the other hand, although there were significant differences in cell death percentages between wild type and *argah 1-1*, no significant difference was detected in overall plasmolysis percentages (Fig 3-4). The difference observed here may be due to the differences of localized accumulation (tissue specific) of NO between two arginase negative mutants. However, the SNP-treated WT caused significant change in overall cell death and plasmolysis levels, indicating the effect of high levels of synthetic NO.

A similar conclusion was also reached when comparing the overall death and plasmolysis percentages with and without HS (Fig. 3-5). Cell death and plasmolysis percentages were significantly higher (17.5% and 13% respectively) in SNP-treated WT even without a HS, indicating the induction of PCD by elevated levels of synthetic NO.

The greatest cell death and plasmolysis percentages were observed in SNP-treated WT heat-treated samples. That might indicate the effects of synergistic levels of both ROS (produced from HS) and NO in PCD initiation. A similar effect was observed previously both in a hypersensitive response related experiment performed using tobacco cells treated with NO producing NOS (animal) enzyme (Durner et al., 1998) and with carrot cells treated with the synthetic NO donor SNP (Zottini et al., 2002). In both experiments cell death was induced by H_2O_2 and generated synergistic levels of cell death, just as reported in this work. Previous research with NO donors (Roussin's black salt and sodium nitroprusside) showed that elevated levels of NO (0.70 nmol min^{-1} for six hours) is sufficient to induce PCD in plant cells without high ROS levels (Clarke, 2000). As well, research with animal systems suggests that prolonged exposure to NO can prevent proper functioning of mitochondria and leads to cell death (Brown and Borutaite, 2002).

These observations also suggest either the nitric oxide concentrations found in cells of *argah* plants were not high enough to critically change any PCD event, with or without HS, or that these plants are adapted to the high levels of NO they have experienced since germination.

There might be another reason why high concentrations of NO found in *argah 1-1* and *argah 2-1* genotypes were insufficient to induce PCD. Plant mitochondria contain an additional oxidase complex, relative to other eukaryotes (present in certain prokaryotes, plants, fungi and some protozoa but not found in mammals) called the alternative oxidase (AOX) (Henriquez et al., 2009). This enzyme complex can suppress the RNS and ROS concentrations by moderating the mitochondrial membrane potential which will eventually prevent PCD (Cvetkovska and Vanlerberghe, 2012). However, when high levels of NO accumulate in the system, as with SNP-treated sample, AOX simply cannot suppress the excessive amount of NO and as a result PCD is initiated.

In *argah 1-1*, while cell death is less than that in wild type, no significant difference was found between percentage plasmolysis (Fig. 3-5), indicating that the low NO concentration in *argah 1-1* when compared with the *argah 2-1* and SNP treated WT, may have reduced necrotic cell death by some mechanism, but not PCD specifically.

5.1.2 Mitochondria morphology change with HS but not with NO levels

My observations on mitochondria morphology change with HS were similar to those reported by Scott and Logan (2008). Mitochondria morphology changes occurred rapidly (within 5 min) after the heat shock, and were irreversible up to the end of the observation period (72 hour) (Fig. 3-9), whilst in the control no change in morphology was detected (Fig. 3-8). No difference was detected either at different times of observation (24, 48 or 72 hours) or in different plant samples (43C5 wild type, 43C5 SNP, *argah 1-1*, *argah* 2-1), either in heat shocked or untreated plants. Although in mammalian cells, NO induces mitochondrial fission, resulting in fragmentation of the mitochondrial network, and cell death (Barsoum et al., 2006), no evidence supports this scenario in the plant kingdom. In my experiment, even though the concentration of NO in SNP-treated WT was enough to induce PCD with or without HS, there was no change in mitochondrial morphology observed (Fig. 3-9); indicating mitochondrial morphology change appeared with ROS induced (or HS induced) PCD is specific marker for the cell death by ROS related pathway.

5.1.3 Mitochondrial dynamics changed with HS but not with NO levels

Mitochondrial movements were analyzed in heat shocked and control samples to get a better idea on the effect of increased concentrations of NO and/or heat stress on mitochondrial movements. Data collected on mitochondrial velocity, speed, acceleration, displacement, track displacement length, and meandering index showed changes to the straightness of the mitochondrial track with treatments and time (Table 3-1).

Heat shock as a treatment caused a significant change in every mitochondrial movement indices analyzed, but there was no significant change depending on time factor or the sample factor (43C5 wild type, 43C5 SNP, *argah 1-1*, *argah* 2-1). Although there is some evidence of NO-based reduction of mitochondrial movements in animal cells such as in neurons (Rintoul et al., 2006; Zanelli et al., 2006), there is no published evidence from plants. In my experiment, I did not observe any significant movement change in arginase-negative mutants or in SNP-treated WT relative to controls. This might indicate that the presence of increased concentrations of NO alone was insufficient to change mitochondrial movements in the samples I have observed. It was clear from microscopic observation that mitochondrial movements in control samples were significantly straighter than those in heat-treated samples.

5.2 Changes in mitochondrial and cytoskeletal dynamics with heat shock

In higher plants actin microfilaments have been shown to play a major role in mitochondrial motility and positioning (Zheng et al., 2009). Although some studies have investigated changes in mitochondrial dynamics with altered cytoskeletal components (Zheng et al., 2009), this study (as described in chapter 4) focused on cytoskeletal-mitochondrial morphology and dynamics with respect to various events that occur during the process of cell death. Especially mitochondrial cluster formation and the cessation of movement after a mild heat shock. In addition, this study has investigated the cytoskeletal elements responsible for this morphology and dynamics change using drug treatments directed specifically against the actin or MT cytoskeleton. Mitochondrial morphology transition and arrangement into clusters after a mild heat shock was analyzed with the help of the Arabidopsis lines expressing both mitochondrial and cytoskeletal reporter genes.

5.2.1 Mitochondrial clustering and immobility following heat shock

From observation, it was clear that both actin and MT filaments were depolymerized and fragmented with time after the heat shock (Fig. 4-1 and 4-3). Following heat shock, the mitochondrial clusters were appeared to be associated with the remaining actin filaments. However, most of large mitochondrial clusters appeared to be completely disconnected from actin filaments, which might explain the lack of movement of these large clusters. Some intermediate-sized clusters were connected to fragments of actin filaments, and it can be assumed that they are able to move within limits set by the length of these few remaining filaments (Fig.4-2). On the other hand, microtubules observed in the mito-GFP/MAP4-mCherry line did not show any association with mitochondrial clusters in heat shocked samples (Fig. 4-3). Although the fragments of microtubules disappear with time, there was no any sign of regenerating MT as found for actin filaments.

5.2.2 Cytoskeletal disruption and mitochondrial dynamics

As expected, and observed in previous studies (Doniwa et al., 2007; Collings, 2008; Zheng et al., 2009; Sampathkumar et al., 2011), with Latrunculin B (Lat-B) treatment, actin filaments were depolymerized with time, and as a result mitochondria showed a reduction in movement soon after (speed, mitochondrial displacement length, and track length) and formed clusters (Sheahan et al., 2004). According to previous studies, although the average velocity of mitochondria in Arabidopsis root hairs was in the 0.6 to 3.4 μm s^{-1} range (Zheng et al., 2009) and 1.4 μm s^{-1} in leaf epidermal cells (Doniwa et al., 2007), I only detected 0.035- 0.045 μm s^{-1} for the control samples. One reason might be the semi-automatic tracking algorithm used to track the mitochondrial movements. It was employed to detect mitochondria that are continually present in more than 16 frames within a 30 second period, so very fast-moving mitochondria in control samples might be ignored as these left the field of view. Another reason might be that in other experiments (Doniwa et al., 2007), they ignored very slow-moving mitochondria (0- 0.3 μm s^{-1} range), and because in this experiment I did not ignore any slow-moving mitochondria, so the average might be lower.

The concentration of Lat-B (2 μM) used for this experiment was significantly lower than the concentrations (10 μM for 1 hour) used by other authors (Doniwa et al., 2007), but it was used for up to 3 hours. In the Lat-B treated samples, mitochondria were found to be associated with

remaining actin filament fragments (see arrows in Fig 4-6 C) and predominantly showed a local movement (see mitochondrial displacement in Fig 4-8), and mitochondrial clusters were arranged with the fragments of actin filaments (Fig. 4-6 D).

To evaluate the effect of actin depolymerization on mitochondria in different plant tissues, Arabidopsis leaf epidermal cells and root epidermal cells were used for this experiment. In leaf cells with Lat-B treatment, it was clear that mitochondrial speed, track speed, track length, and track displacements levels decreased significantly ($P < 0.05$) compared to the mock treatment with ethanol. In root samples, on the other hand, only the track displacement showed a significant reduction, although both mitochondrial speeds and track lengths did not show significant difference with Lat-B treatment than that in the mock treatment with ethanol (EtOH). Since this might be an indication of wiggling (or Brownian) motion of mitochondria, a meandering index (also known as track straightness) (Ellett et al., 2011) was developed to enable comparison with other samples (Fig. 4-10).

There was no significant difference detected in the meandering in the mock treatment using leaf cells or root epidermal cells, which was in the 0.25 to 0.3 range, indicating a more straight motion of mitochondria. On the other hand, root cells treated with Lat-B showed a significantly lower meandering index, indicating mitochondria in those cells predominantly exhibited a wiggling motion, which is observable with the microscope. Conversely, mitochondria in the Lat-B treated leaf sample did not show any wiggling motion, but most of the mitochondria stopped moving, which can also explain the low values of mitochondrial speeds, displacement, and track lengths, yet high meandering index because of the low number of mitochondria moving with straight trajectories. After 10 minutes, meandering index for mitochondria in leaf epidermal cells changed irreversibly to significantly lower values, indicating the effect of actin depolymerization on mitochondrial dynamics (Fig. 4-11).

Although previous observations demonstrate clearly that individual mitochondria move along actin filaments (Doniwa et al., 2007), according to my knowledge this is the first observation of mitochondrial clusters moving on actin filaments (Fig. 4-12). These clusters observed following Lat-B treatment were comparatively very large and showed different cluster morphology than those in MT de-polymerizing drug oryzalin-treated samples (see Fig. 4-15 and 4-18). These large clusters move at a lower speed (Fig. 4-15), and many were immobile. The larger the cluster, the

slower the speed of movement, was observed (e.g. after one hour of Lat-B treatment) (Fig. 4-13). It was also clear that the mitochondria in these clusters were becoming packed tightly with time (see images in Fig. 4-14) and arranged with the debris of actin filaments (Fig 4-16 D).

As expected, and according to pervious research done by different groups (Sheahan et al., 2004; Zheng et al., 2009; Scott and Logan, 2010), it was clear that in Arabidopsis, mitochondria were not moving along the MT array, which was in fact in a different focal plane (0.8 µm distance in average). When treated with the MT de-polymerizing drug oryzalin, mitochondrial morphology showed no difference (Fig. 4-19), but they began to form mitochondrial clusters, although these were not as big or compactly packed like those observed with Lat-B treatment (Fig. 4-14, 4-15). With image analysis, although a significant difference in cluster areas was detected between mock treatment with ethanol and oryzalin treatments, the difference was minute compared to cluster volumes detected with Lat-B treatment. All the other aspects of mitochondrial dynamics were normal with the oryzalin treatment, as also suggested by previous experiments (Van Gestel et al., 2002; Sheahan et al., 2004; Zheng et al., 2009).

5.2.3 Cytoskeletal disruption induced PCD

Although the disruption of cytoskeletal elements leading to PCD has been observed in many plant PCD events, such as tracheary differentiation (Zheng et al., 2010), embryo development (Brown and Borutaite, 2002), senescence (Durner et al., 1998), and hypersensitive response (Zottini et al., 2002), according to my knowledge there has been no published study of the effect of cytoskeletal disruption on mitochondrial dynamics and the initiation of PCD.

It is well known that the actin cytoskeleton reorganizes and bundles near the site of pathogen attack or the site of entry in HR mediated plant PCD (Cvetkovska and Vanlerberghe, 2012). Recent studies have suggested that changing the balance between polymerization and depolymerization of actin filaments can cause PCD in plants (Smertenko and Franklin-Tong, 2011). According to my results, there is a clear link between actin depolymerization (Lat-B treatment) and the initiation of the PCD in Arabidopsis (Fig. 4-20 and 4-21). Within 24 hours of treatment, Lat-B caused a clear increase of both cell death percentage and plasmolyzed cell percentage, indicating the initiation of PCD. On the other hand, oryzalin treatment did not increase either cell death or plasmolysis in the first 24 hours, indicating the actin

depolymerization is more critical to induce PCD and MT depolymerization is not critical or directly involve with the induction of PCD in Arabidopsis.

Unlike with actin depolymerization, the exact effect of MT depolymerization on plant PCD induction is poorly documented. Experiments performed with *Papaver* pollen indicated that MT depolymerization with oryzalin or stabilization with taxol were not enough to initiate PCD (Smertenko and Franklin-Tong, 2011). In my experiment as well, there was no sign of PCD induction in the first 24 hours when plants treated with oryzalin (Fig. 4-20 and 4-21). When treated up to 48 hours, although there was a significant increase of PCD in oryzalin-treated sample, it was not a large increase when compared with the Lat-B treated sample. However, when treated up to 72 hours, the oryzalin-treated sample showed a big increase in PCD, and dead cell and plasmolysis cell percentages exceeded 50%, while in the control sample it was less than 25%. These results indicate that although MT depolymerization could trigger PCD in Arabidopsis, it was not a quick induction like that observed in actin depolymerized samples. This might be due to the fact that MT depolymerization can affect actin filament arrangements and then change actin stability, triggering PCD. Changes to mitochondrial dynamics with actin disruption, but not with MT disruption, support this idea. Since mitochondria move on actin filaments, and the only change in mitochondrial dynamics detected in the oryzalin-treated sample was the increase in meandering index value (meaning that mitochondria move straighter in the oryzalin-treated sample than in the mock treatment with ethanol), indicating actin filament arrangements was changed with oryzalin treatment. This change might be partially due to formation of a many cytoplasmic strands after the oryzalin treatment, as suggested by Van Gestel et al.,(2002).

5.2.4 Microtubule plus end behavior and mitochondria

Observation of the EB1b line showing plus ends of MT demonstrated that in the untreated samples, MT plus ends and mitochondria did not have any interaction, and in fact were observed on two different focal planes. The actin depolymerizing drug Lat-B did not have any effect on this behavior, and mitochondrial clusters resulting from Lat-B treatment did not show any interaction with MT plus ends. However, both oryzalin and heat treatments made MT plus ends associate with mitochondrial clusters. These plus ends of MT were also moving with the mitochondrial clusters.

5.3 Conclusions and future directions

Using different genotypes and Arabidopsis reporter lines, I examined the morphological and dynamic changes to the mitochondria in plants which have high concentrations of RNS (NO) and the effects of heat shock (HS) induced PCD. My findings showed that the elevated concentrations of NO found in arginase negative mutants (*argah 1-1* and *argah 2-1*) are not sufficient to induce PCD as hypothesized, although the data from Arabidopsis plants treated with synthetic NO (SNP-treated WT sample) in this thesis as well as previous research suggested a link between high levels of NO and plant PCD (Durner et al., 1998; Clarke, 2000; Zottini et al., 2002). I used Arabidopsis root-hairs to observe and record the cell death and plasmolysis percentages. Since plant cell death could result from necrotic or PCD processes, and the viability staining method I employed (Sytox staining) was unable to detect PCD specifically (Reape et al., 2008) although it can detect dead cells, I used plasmolysed cells as an indicator of cells undergoing PCD (McCabe and Leaver, 2000).

I was unable to detect any mitochondrial morphology or dynamic difference on arginase negative mutants, which is significantly different from the WT, even with the heat shock. However, the overall effect of heat shock on mitochondrial dynamics and morphology was very clear as the data suggested in this thesis and previous research described in the introductory section.

Some of these changes previously observed with heat shock or with ROS-induced PCD, but my aim here was to study this phenomenon in detail with the help of fluorescent markers of mitochondria and of cytoskeletal elements using state of the art microscopy and image analysis tools. Although it seemed rational to suggest the involvement of the cytoskeleton in the mitochondrial morphology and dynamic changes, no previous study observed these changes with the induction of PCD in Arabidopsis. Here I tried to reproduce the clustering and abnormal mitochondrial behavior (pheno-copy) that is observed with heat shocked plants in Arabidopsis lines expressing cytoskeletal reporter genes.

For that purpose, I used two different cytoskeletal-inhibiting drugs (Lat-B and oryzalin) to de-polymerize the specific cytoskeletal component. The results showed that the treatment with Lat-B (actin-disrupting drug) closely resembles the clustering morphology observed with the

heat shock (Fig. 4-3 and 4-18), although the clusters found with Lat-B treatment are generally much bigger than that found with heat shock (Fig. 4-5 and 4-15). Although, the microtubule-disrupting drug oryzalin and the mock treatment with ethanol showed some rare transient clusters, however with careful consideration of other mitochondrial dynamic changes such as speed, displacement, and cluster morphology, it can be suggested that mitochondrial clusters observed after the heat shock may be a result of actin filament disruption.

Microtubules did not show (with mito-GFP/MAP4-mCherry line) any observable association with the mitochondria or with mitochondrial clusters as hypothesized; however, EB1b expression was observed in close proximity and moving with the mitochondrial clusters after the oryzalin treatment and heat shock. Since EB1b is a MT plus end tracking +TIP family protein (a cytoplasmic protein that attach into microtubule plus ends) (Young and Bisgrove, 2011), after the heat shock and/or depolymaraization of MT (after oryzalin treatment) it might dissociate from MT plus end, and might not represent the behavior of MT plus ends in that situation. In the other hand, these EB1b proteins are capable of interact with actin filaments via actin-associated proteins such as formin (Bisgrove et al., 2008; Deeks et al., 2010), which might explain why EB1b signals found with the close proximity with mitochondrial clusters which are attached to actin filaments after the heat shock.

Neither untreated samples nor Lat-B treated samples exhibited any connection between microtubule plus ends (EB1b) with mitochondria (or cluster). This disproves a previous suggestion that mitochondrial clusters were associated with microtubules and that mitochondrial clusters moved along the microtubule in a plus-end-directed manner (Logan et al., 2003; Logan, 2006). It might be more likely that the damaged MT plus ends are in the same confined space with mitochondrial clusters rather than associated with them and both components moving along the actin cables.

The effect of cytoskeletal motor proteins on mitochondrial cluster formation might be an interesting area to study. According to some previous observations, BDM which is an acto-myosin inhibitor, caused round and swollen mitochondrial morphology and inhibited the motility of mitochondria and cytoplasmic streaming, similar to the effects of ROS treatment (Yoshinaga et al., 2005). Although I used oryzalin to disrupt the MT and Lat-B to disrupt the actin filaments, it would be beneficial to see the overall effect of actin and MT disruption by some other drugs

too, for example nocodazole for MT depolymerization, and cytochalasins to block the actin polymerization.

Furthermore, a similar experiment with ROS inducing chemicals such as methyl viologen and s-triazine or various levels of RNS would provide further support to the present finding that will be beneficial to clear the following doubts of present research. Although I applied only a mild heat shock for a short duration, there is a chance that some vital proteins, indirectly necessary for mitochondrial movement, could be damaged. With chemically-generated ROS, we could assume that the harm to the other pathways would be negligible, and unlike in heat-shocked samples, the effect on cytoskeletal elements would be low. These proposed experiments might give a better picture of ROS-induced mitochondrial cluster formation and behavior with respect to the cytoskeletal elements.

6 APPENDIX

6.1 Binary Vector used for transformation (pCAMBIA1300)

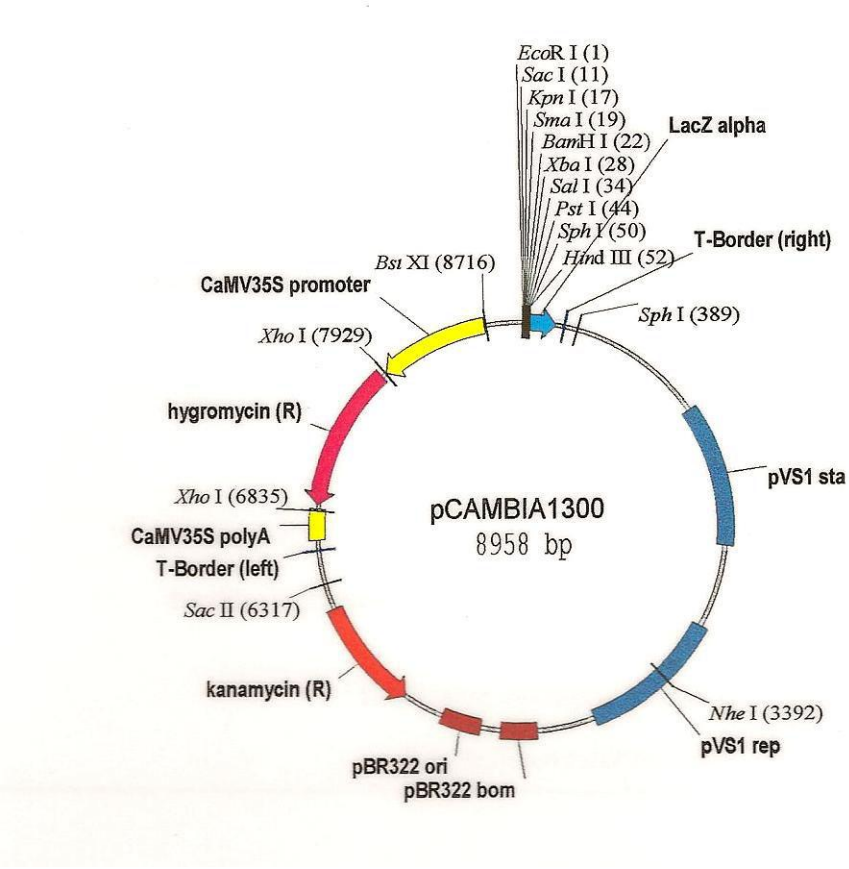

Figure 6-1 pCAMBIA1300 binary vector without the construct

6.2 Imaris algorithms used in this thesis

6.2.1 To detect mitochondria (spots) following algorithm was used

[Algorithm]

Enable Region of Interest = false

Enable Region Growing = false

Enable Tracking = true

[Source Channel]

Source Channel Index = 1

Estimated Diameter = 0.5

Background Subtraction = true

[Classify Spots]

"Quality" above automatic threshold

[Tracking]

Algorithm Name = Autoregressive Motion

MaxDistance = 5

MaxGapSize = 5

Fill Gap Enable = true

[Classify Tracks]

"Track Duration" above 16.000 s

6.2.2 To detect mitochondrial clusters, following algorithm was used

[Algorithm]

Enable Region of Interest = false

Enable Region Growing = false

Enable Tracking = true

[Source Channel]

Source Channel Index = 1

Enable Smooth = true

Surface Grain Size = 0.204

Enable Eliminate Background = true

Diameter of Largest Sphere = 3

[Threshold]

Enable Automatic Threshold = false

Manual Threshold Value = 17.143

Active Threshold = true

Enable Automatic Threshold B = true

Manual Threshold Value B = 161.22

Active Threshold B = false

[Classify Surfaces]

"Number of Voxels" above 10.000

"Volume" above 4.000 um^3

[Tracking]

Algorithm Name = Autoregressive Motion

MaxDistance = 2

MaxGapSize = 3

Fill Gap Enable = true

[Classify Tracks]

6.3 Mitochondrial Statistics

6.3.1.1 Mitochondrial Acceleration

Acceleration is the change in the mitochondrial (s) velocity over time.

Object position at time-point *i*:

$$P(i) = \begin{pmatrix} Px(i) \\ Py(i) \\ Pz(i) \end{pmatrix}$$

Acceleration vector x, y, z at time-point *i*

$$A(i) = \frac{\frac{P(i) - P(i-1)}{t(i) - t(i-1)} + \frac{P(i+1) - P(i)}{t(i+1) - t(i)}}{2 * (t(i+1) - t(i-1)}$$

Acceleration at time-point i:

a (i) = |A(i)|

Acceleration at the first and last time-point is 0.

6.3.1.2 Mitochondrial Speed

The mitochondrial speed is the instantaneous speed of the object (µm/s).

$$S(t) = \frac{\sqrt{D_{x\ (t+1,\ t-1)}^2 + D_{y\ (t+1,\ t-1)}^2 + D_{z\ (t+1,\ t-1)}^2}}{T_{(t+1)} - T_{(t-1)}}$$

$$D_X(t_1, t_2) = P_X(t_1) - P_X(t_2)$$

S (t)= instantaneous speed

S (t)= Track Speed

P_X (t) = x-position of object at time index t

T (t) = time in seconds at time point t

For the first and the last time points in the series the instantaneous speed calculation of based on the formula:

S (0)= instantaneous speed at the first time point

$$S(0) = \frac{\sqrt{D_x\ (t_1\text{-}t_0)^2 + D_y\ (t_1\text{-}t_0)^2 + D_z\ (t_1\text{-}t_0)^2}}{T(t_1) - T(t_0)}$$

$$D_x\ (t_1 t_0) = P_x(t_1) - P_x\ (t_0)$$

S (n)= instantaneous speed at the last time point

$$S(n) = \frac{\sqrt{D_{x\ (n-1,\ n)}{}^2 + D_{y\ (n-1,\ n)}{}^2 + D_{z\ (n-1,\ n)}{}^2}}{T_{(n)} - T_{(n-1)}}$$

$$D_x\ (t_n t_{n-1}) = P_x(t_n) - P_x\ (t_{n-1})$$

S (n)= instantaneous speed at the last time point

6.3.1.3 Mitochondrial Track Duration

The Track Duration is the duration between the first and last time point within the track.

$$\text{Duration} = T(t_L) - T(t_F)$$

Duration = Track Duration

T (t) = time in seconds at time point t

T_L = last time index of track

t_F = first time index of track

6.3.1.4 Mitochondria Track Length

The Track Length is the total length of displacements within the track.

$$L = \sum_{t=t_F+1}^{tL} \sqrt{D_x(t, t-1)^2 + D_y(t, t-1)^2 + D_z(t, t-1)^2}$$

L = Track Length

t_L = last time index of track

t_F = first time index of track

$$D_X(t_1, t_2) = P_X(t_1) - P_X(t_2)$$

$P_X(t)$ = x-position of mitochondria at time index t

6.3.1.5 Mitochondrial Track Straightness / meandering index

$$S = \frac{D}{L}$$

S = Track Straightness

D = Track Displacement

L = Track Length

6.3.1.6 Maximum intensity projection (MIP)

A maximum intensity projection (MIP) is a computer visualization method for 3D data that projects in the visualization plane the voxels with maximum intensity that fall in the way of parallel rays traced from the viewpoint to the plane of projection.

6.3.1.7 Voxel

A volume data set is composed of volume elements called voxels. The voxels are the smallest units within the image about which we have distinct information in the form of a measured intensity.

6.3.1.8 Time point

A time point is a single 3D image containing one or many channels. The term is used regardless of what data is actually stored in the channels. In particular, the channels could contain data taken at different points in time with a changing object.

6.3.1.9 Threshold

A threshold in Imaris is a gray value, which acts as a limit. All gray values above (or below) are assigned a particular functionality.

7 REFERENCES

Akhmanova A, Steinmetz MO (2010) Microtubule +TIPs at a glance. Journal of Cell Science **123:** 3415-3419

Alberts B (2008) Molecular biology of the cell, Ed 5th. Garland Science, New York

Anesti V, Scorrano L (2006) The relationship between mitochondrial shape and function and the cytoskeleton. Biochim Biophys Acta **1757:** 692-699

Arimura S, Tsutsumi N (2006) Dynamic Mitochondria, their Fission and Fusion in Higher Plants

Tobacco BY-2 Cells: From Cellular Dynamics to Omics. *In* T Nagata, K Matsuoka, D Inzé, eds, Vol 58. Springer Berlin Heidelberg, pp 225-240

Barsoum MJ, Yuan H, Gerencser AA, Liot G, Kushnareva Y, Graber S, Kovacs I, Lee WD, Waggoner J, Cui J, White AD, Bossy B, Martinou JC, Youle RJ, Lipton SA, Ellisman MH, Perkins GA, Bossy-Wetzel E (2006) Nitric oxide-induced mitochondrial fission is regulated by dynamin-related GTPases in neurons. EMBO J **25:** 3900-3911

Beers EP, Jones AM, Dickerman AW (2004) The S8 serine, C1A cysteine and A1 aspartic protease families in Arabidopsis. Phytochemistry **65:** 43-58

Benard G, Karbowski M (2009) Mitochondrial fusion and division: Regulation and role in cell viability. Semin Cell Dev Biol **20:** 365-374

Bereiter-Hahn J, Voth M (1994) Dynamics of mitochondria in living cells: shape changes, dislocations, fusion, and fission of mitochondria. Microsc Res Tech **27:** 198-219

Besson-Bard Al, Pugin A, Wendehenne D (2008) New Insights into Nitric Oxide Signaling in Plants. Annual Review of Plant Biology **59:** 21-39

Binarová P, Cenklová V, Procházková J, Doskocilová A, Volc J, Vrlík M, Bögre L (2006) γ-Tubulin Is Essential for Acentrosomal Microtubule Nucleation and Coordination of Late Mitotic Events in Arabidopsis. The Plant Cell Online **18:** 1199-1212

Binet MN, Humbert C, Lecourieux D, Vantard M, Pugin A (2001) Disruption of microtubular cytoskeleton induced by cryptogein, an elicitor of hypersensitive response in tobacco cells. Plant Physiol **125:** 564-572

Bisgrove SR, Lee Y-RJ, Liu B, Peters NT, Kropf DL (2008) The Microtubule Plus-End Binding Protein EB1 Functions in Root Responses to Touch and Gravity Signals in Arabidopsis. The Plant Cell Online **20:** 396-410

Bleazard W, McCaffery JM, King EJ, Bale S, Mozdy A, Tieu Q, Nunnari J, Shaw JM (1999) The dynamin-related GTPase Dnm1 regulates mitochondrial fission in yeast. Nat Cell Biol **1:** 298-304

Boldogh IR, Pon LA (2007) Mitochondria on the move. Trends Cell Biol **17:** 502-510

Bolduc N, Brisson LF (2002) Antisense down regulation of NtBI-1 in tobacco BY-2 cells induces accelerated cell death upon carbon starvation. FEBS Lett **532:** 111-114

Bredesen DE, Mehlen P, Rabizadeh S (2004) Apoptosis and dependence receptors: a molecular basis for cellular addiction. Physiol Rev **84:** 411-430

Brown GC, Borutaite V (2002) Nitric oxide inhibition of mitochondrial respiration and its role in cell death. Free Radical Biology and Medicine **33:** 1440-1450

Budihardjo I, Oliver H, Lutter M, Luo X, Wang X (1999) Biochemical pathways of caspase activation during apoptosis. Annu Rev Cell Dev Biol **15:** 269-290

Chan J, Calder GM, Doonan JH, Lloyd CW (2003) EB1 reveals mobile microtubule nucleation sites in Arabidopsis. Nat Cell Biol **5:** 967-971

Charng Y-y, Liu H-c, Liu N-y, Chi W-t, Wang C-n, Chang S-h, Wang T-t (2007) A Heat-Inducible Transcription Factor, HsfA2, Is Required for Extension of Acquired Thermotolerance in Arabidopsis. Plant Physiology **143:** 251-262

Chen S, Dickman MB (2004) Bcl-2 family members localize to tobacco chloroplasts and inhibit programmed cell death induced by chloroplast-targeted herbicides. Journal of Experimental Botany **55:** 2617-2623

Clark D, Morgan A, Hananeia L, Coulter D, Olds R (2000) Drug metabolism genotypes and their association with adverse drug reactions in selected populations: a pilot study of methodology. Pharmacoepidemiol Drug Saf **9:** 393-400

Clarke AR (2000) Controlling apoptosis: implications for carcinogenesis? Symp Soc Exp Biol **52:** 265-275

Clough SJ, Bent AF (1998) Floral dip: a simplified method for Agrobacterium-mediated transformation of *Arabidopsis thaliana*. Plant J **16:** 735-743

Collings D (2008) Crossed-wires: Interactions, cross-talk and signal exchange between the microtubule and microfilament networks in plants. In Plant Microtubules – Development and Flexibility. *In* P Nick, ed, Vol 11. Springer Berlin / Heidelberg, pp 47-79

Collings DA, Lill AW, Himmelspach R, Wasteneys GO (2006) Hypersensitivity to cytoskeletal antagonists demonstrates microtubule-microfilament cross-talk in the control of root elongation in *Arabidopsis thaliana*. New Phytol **170:** 275-290

Corpas FJ, Barroso JB, Carreras A, Valderrama R, Palma JM, Leon AM, Sandalio LM, del Rio LA (2006) Constitutive arginine-dependent nitric oxide synthase activity in different organs of pea seedlings during plant development. Planta **224:** 246-254

Corpas FJ, Palma JM, Del Río LA, Barroso JB (2009) Evidence supporting the existence of l-arginine-dependent nitric oxide synthase activity in plants. New Phytologist **184:** 9-14

Cvetkovska M, Vanlerberghe GC (2012) Alternative oxidase modulates leaf mitochondrial concentrations of superoxide and nitric oxide. New Phytol **195:** 32-39

De Pinto MC, Paradiso A, Leonetti P, De Gara L (2006) Hydrogen peroxide, nitric oxide and cytosolic ascorbate peroxidase at the crossroad between defence and cell death. The Plant Journal **48:** 784-795

Deeks MJ, Fendrych M, Smertenko A, Bell KS, Oparka K, Cvrčková F, Žárský V, Hussey PJ (2010) The plant formin AtFH4 interacts with both actin and microtubules, and contains a newly identified microtubule-binding domain. Journal of Cell Science **123:** 1209-1215

Doniwa Y, Arimura S-i, Tsutsumi N (2007) Mitochondria use actin filaments as rails for fast translocation in Arabidopsis and tobacco cells. Plant Biotechnology **24:** 441-447

Douce R, Neuburger M (1999) Biochemical dissection of photorespiration. Curr Opin Plant Biol **2:** 214-222

Drew MC, He CJ, Morgan PW (2000) Programmed cell death and aerenchyma formation in roots. Trends Plant Sci **5:** 123-127

Dryková D, Cenklová V, Sulimenko V, Volc J, Dráber P, Binarová P (2003) Plant γ-Tubulin Interacts with αβ-Tubulin Dimers and Forms Membrane-Associated Complexes. The Plant Cell Online **15:** 465-480

Durner J, Wendehenne D, Klessig DF (1998) Defense gene induction in tobacco by nitric oxide, cyclic GMP, and cyclic ADP-ribose. Proc Natl Acad Sci U S A **95:** 10328-10333

Dyall SD, Brown MT, Johnson PJ (2004) Ancient invasions: from endosymbionts to organelles. Science **304:** 253-257

Ehrhardt DW, Shaw SL (2006) Microtubule dynamics and organization in the plant cortical array. Annual Review of Plant Biology **57:** 859-875

Ellett F, Pase L, Hayman JW, Andrianopoulos A, Lieschke GJ (2011) mpeg1 promoter transgenes direct macrophage-lineage expression in zebrafish. Blood **117:** e49-e56

Esteve MA, Carre M, Braguer D (2007) Microtubules in apoptosis induction: are they necessary? Curr Cancer Drug Targets **7:** 713-729

Flores T, Todd CD, Tovar-Mendez A, Dhanoa PK, Correa-Aragunde N, Hoyos ME, Brownfield DM, Mullen RT, Lamattina L, Polacco JC (2008) Arginase-negative mutants of Arabidopsis exhibit increased nitric oxide signaling in root development. Plant Physiol **147:** 1936-1946

Fosket DE, Morejohn LC (1992) Structural and Functional Organization of Tubulin. Annual Review of Plant Physiology and Plant Molecular Biology **43:** 201-240

Frank S, Gaume B, Bergmann-Leitner ES, Leitner WW, Robert EG, Catez F, Smith CL, Youle RJ (2001) The Role of Dynamin-Related Protein 1, a Mediator of Mitochondrial Fission, in Apoptosis. Developmental cell **1:** 515-525

Franklin-Tong VE, Gourlay CW (2008) A role for actin in regulating apoptosis/programmed cell death: evidence spanning yeast, plants and animals. Biochem J **413:** 389-404

Frederick RL, Shaw JM (2007) Moving Mitochondria: Establishing Distribution of an Essential Organelle. Traffic **8:** 1668-1675

Frey TG, Mannella CA (2000) The internal structure of mitochondria. Trends Biochem Sci **25:** 319-324

Furuse K, Takemoto D, Doke N, Kawakita K (1999) Involvement of actin filament association in hypersensitive reactions in potato cells. Physiological and Molecular Plant Pathology **54:** 51-61

Gadjev I, Stone JM, Gechev TS (2008) Chapter 3: Programmed Cell Death in Plants: New Insights into Redox Regulation and the Role of Hydrogen Peroxide. *In* WJ Kwang, ed, International Review of Cell and Molecular Biology, Vol Volume 270. Academic Press, pp 87-144

Gao C, Xing D, Li L, Zhang L (2008) Implication of reactive oxygen species and mitochondrial dysfunction in the early stages of plant programmed cell death induced by ultraviolet-C overexposure. Planta **227:** 755-767

Garcia-Perez C, Roy SS, Naghdi S, Lin X, Davies E, Hajnóczky G (2012) Bid-induced mitochondrial membrane permeabilization waves propagated by local reactive oxygen species (ROS) signaling. Proceedings of the National Academy of Sciences **109:** 4497-4502

Gas E, Flores-Perez U, Sauret-Gueto S, Rodriguez-Concepcion M (2009) Hunting for plant nitric oxide synthase provides new evidence of a central role for plastids in nitric oxide metabolism. Plant Cell **21:** 18-23

Gechev T, Gadjev I, Van Breusegem F, Inze D, Dukiandjiev S, Toneva V, Minkov I (2002) Hydrogen peroxide protects tobacco from oxidative stress by inducing a set of antioxidant enzymes. Cell Mol Life Sci **59:** 708-714

Gechev TS, Van Breusegem F, Stone JM, Denev I, Laloi C (2006) Reactive oxygen species as signals that modulate plant stress responses and programmed cell death. Bioessays **28:** 1091-1101

Gibbon BC, Kovar DR, Staiger CJ (1999) Latrunculin B has different effects on pollen germination and tube growth. Plant Cell **11:** 2349-2363
Gourlay CW, Ayscough KR (2005) The actin cytoskeleton: a key regulator of apoptosis and ageing? Nat Rev Mol Cell Biol **6:** 583-589
Gourlay CW, Carpp LN, Timpson P, Winder SJ, Ayscough KR (2004) A role for the actin cytoskeleton in cell death and aging in yeast. J Cell Biol **164:** 803-809
Grierson C, Schiefelbein J (2002) Root Hairs. The Arabidopsis Book**:** e0060
Guo F-Q, Crawford NM (2005) Arabidopsis Nitric Oxide Synthase1 Is Targeted to Mitochondria and Protects against Oxidative Damage and Dark-Induced Senescence. The Plant Cell Online **17:** 3436-3450
Guo F-Q, Okamoto M, Crawford NM (2003) Identification of a Plant Nitric Oxide Synthase Gene Involved in Hormonal Signaling. Science **302:** 100-103
Hanahan D (1983) Studies on transformation of Escherichia coli with plasmids. J Mol Biol **166:** 557-580
Harper JF, Breton G, Harmon A (2004) Decoding Ca(2+) signals through plant protein kinases. Annual Review of Plant Biology **55:** 263-288
Hashimoto T (2011) Microtubule cytoskeleton determines plant shape. Seikagaku **83:** 374-378
He R, Drury GE, Rotari VI, Gordon A, Willer M, Farzaneh T, Woltering EJ, Gallois P (2008) Metacaspase-8 Modulates Programmed Cell Death Induced by Ultraviolet Light and H2O2 in Arabidopsis. Journal of Biological Chemistry **283:** 774-783
Heggeness MH, Simon M, Singer SJ (1978) Association of mitochondria with microtubules in cultured cells. Proceedings of the National Academy of Sciences **75:** 3863-3866
Henriquez FL, McBride J, Campbell SJ, Ramos T, Ingram PR, Roberts F, Tinney S, Roberts CW (2009) Acanthamoeba alternative oxidase genes: identification, characterisation and potential as antimicrobial targets. Int J Parasitol **39:** 1417-1424
Hermann GJ, Shaw JM (1998) Mitochondrial dynamics in yeast. Annu Rev Cell Dev Biol **14:** 265-303
Hugdahl JD, Morejohn LC (1993) Rapid and Reversible High-Affinity Binding of the Dinitroaniline Herbicide Oryzalin to Tubulin from Zea mays L. Plant Physiol **102:** 725-740
Jacobson MD, Burne JF, King MP, Miyashita T, Reed JC, Raff MC (1993) Bcl-2 blocks apoptosis in cells lacking mitochondrial DNA. Nature **361:** 365-369
Jones A (2000) Does the plant mitochondrion integrate cellular stress and regulate programmed cell death? Trends Plant Sci **5:** 225-230
Jones AME, Thomas V, Bennett MH, Mansfield J, Grant M (2006) Modifications to the Arabidopsis Defense Proteome Occur Prior to Significant Transcriptional Change in Response to Inoculation with Pseudomonas syringae. Plant Physiology **142:** 1603-1620
Jouhet J, Gray JC (2009) Is chloroplast import of photosynthesis proteins facilitated by an actin-TOC-TIC-VIPP1 complex? Plant Signal Behav **4:** 986-988
Karbowski M (2010) Mitochondria on guard: role of mitochondrial fusion and fission in the regulation of apoptosis. Adv Exp Med Biol **687:** 131-142
Karbowski M, Youle RJ (2003) Dynamics of mitochondrial morphology in healthy cells and during apoptosis. Cell Death and Differentiation **10:** 870-880
Kelekar A, Thompson CB (1998) Bcl-2-family proteins: the role of the BH3 domain in apoptosis. Trends Cell Biol **8:** 324-330

Kerr JF (2002) History of the events leading to the formulation of the apoptosis concept. Toxicology **181-182:** 471-474
Kerr JF, Wyllie AH, Currie AR (1972) Apoptosis: a basic biological phenomenon with wide-ranging implications in tissue kinetics. Br J Cancer **26:** 239-257
Ketelaar T, Anthony RG, Hussey PJ (2004) Green fluorescent protein-mTalin causes defects in actin organization and cell expansion in Arabidopsis and inhibits actin depolymerizing factor's actin depolymerizing activity in vitro. Plant Physiol **136:** 3990-3998
Kobayashi H, Fukuda H, Shibaoka H (1988) Interrelation between the spatial disposition of actin filaments and microtubules during the differentiation of tracheary elements in cultured Zinnia cells. Protoplasma **143:** 29-37
Kohler RH, Zipfel WR, Webb WW, Hanson MR (1997) The green fluorescent protein as a marker to visualize plant mitochondria in vivo. Plant J **11:** 613-621
Korthout HA, Berecki G, Bruin W, van Duijn B, Wang M (2000) The presence and subcellular localization of caspase 3-like proteinases in plant cells. FEBS Lett **475:** 139-144
Kost B, Spielhofer P, Chua NH (1998) A GFP-mouse talin fusion protein labels plant actin filaments in vivo and visualizes the actin cytoskeleton in growing pollen tubes. Plant J **16:** 393-401
Kroemer G, Galluzzi L, Brenner C (2007) Mitochondrial Membrane Permeabilization in Cell Death. Physiological Reviews **87:** 99-163
Kroemer G, Zamzami N, Susin SA (1997) Mitochondrial control of apoptosis. Immunol Today **18:** 44-51
Lam E (2004) Controlled cell death, plant survival and development. Nat Rev Mol Cell Biol **5:** 305-315
Lam E, del Pozo O (2000) Caspase-like protease involvement in the control of plant cell death. Plant Mol Biol **44:** 417-428
Lam E, Kato N, Lawton M (2001) Programmed cell death, mitochondria and the plant hypersensitive response. Nature **411:** 848-853
Lewis MR, Lewis WH (1914) Mitochondria in Tissue Culture. Science **39:** 330-333
Liesa M, Palacin M, Zorzano A (2009) Mitochondrial dynamics in mammalian health and disease. Physiol Rev **89:** 799-845
Liu K, Luan S (1998) Voltage-dependent K+ channels as targets of osmosensing in guard cells. Plant Cell **10:** 1957-1970
Lockshin RA, Williams CM (1965) Programmed cell death: I. Cytology of the degeneration of the intersegmental muscles of the Pernyi silkmoth. J Insect Physiol **11:** 123-133
Logan DC (2006) The mitochondrial compartment. J Exp Bot **57:** 1225-1243
Logan DC (2006) Plant mitochondrial dynamics. Biochim Biophys Acta **1763:** 430-441
Logan DC (2008) Having a swell time--mitochondrial morphology and plant cell death programmes. J Microsc **231:** 215-224
Logan DC (2010) The dynamic plant chondriome. Seminars in Cell & Developmental Biology **21:** 550-557
Logan DC, Leaver CJ (2000) Mitochondria • targeted GFP highlights the heterogeneity of mitochondrial shape, size and movement within living plant cells. Journal of Experimental Botany **51:** 865-871
Logan DC, Scott I, Tobin AK (2003) The genetic control of plant mitochondrial morphology and dynamics. Plant J **36:** 500-509

Lord CE, Gunawardena AH (2011) Environmentally induced programmed cell death in leaf protoplasts of Aponogeton madagascariensis. Planta **233:** 407-421
Lord CE, Gunawardena AH (2012) Programmed cell death in C. elegans, mammals and plants. Eur J Cell Biol
Lord CE, Wertman JN, Lane S, Gunawardena AH (2011) Do mitochondria play a role in remodelling lace plant leaves during programmed cell death? BMC Plant Biol **11:** 102
Mackenzie S, McIntosh L (1999) Higher plant mitochondria. Plant Cell **11:** 571-586
Marc J, Granger CL, Brincat J, Fisher DD, Kao T, McCubbin AG, Cyr RJ (1998) A GFP-MAP4 reporter gene for visualizing cortical microtubule rearrangements in living epidermal cells. Plant Cell **10:** 1927-1940
Mathur J, Chua NH (2000) Microtubule stabilization leads to growth reorientation in Arabidopsis trichomes. Plant Cell **12:** 465-477
Mathur J, Mathur N, Kernebeck B, Srinivas BP, Hulskamp M (2003) A novel localization pattern for an EB1-like protein links microtubule dynamics to endomembrane organization. Curr Biol **13:** 1991-1997
McCabe PF, Leaver CJ (2000) Programmed cell death in cell cultures. Plant Molecular Biology **44:** 359-368
McCabe PF, Pennell RI (1996) Apoptosis in plant cells *in vitro*. *In* TG Cotter, SJ Martin, eds, Techniques In Apoptosis: A User's Guide. Portland Press, London, pp 301-326
McConnell SJ, Stewart LC, Talin A, Yaffe MP (1990) Temperature-sensitive yeast mutants defective in mitochondrial inheritance. J Cell Biol **111:** 967-976
Modolo LV, Augusto O, Almeida IMG, Magalhaes JR, Salgado I (2005) Nitrite as the major source of nitric oxide production by *Arabidopsis thaliana* in response to Pseudomonas syringae. FEBS Letters **579:** 3814-3820
Moisoi N, Erent M, Whyte S, Martin S, Bayley PM (2002) Calmodulin-containing substructures of the centrosomal matrix released by microtubule perturbation. J Cell Sci **115:** 2367-2379
Møller IM (2001) Plant mitochondria and oxidative stress: Electron transport, NADPH turnover and metabolism of reactive oxygen species. Annu Rev Plant Physiol Plant Mol Biol **52:** 561-591
Mollinedo F, Gajate C (2003) Microtubules, microtubule-interfering agents and apoptosis. Apoptosis **8:** 413-450
Morrissette NS, Mitra A, Sept D, Sibley LD (2004) Dinitroanilines bind alpha-tubulin to disrupt microtubules. Mol Biol Cell **15:** 1960-1968
Palade GE (1953) An electron microscope study of the mitochondrial structure. J Histochem Cytochem **1:** 188-211
Pennell RI, Lamb C (1997) Programmed Cell Death in Plants. Plant Cell **9:** 1157-1168
Petronilli V, Penzo D, Scorrano L, Bernardi P, Di Lisa F (2001) The mitochondrial permeability transition, release of cytochrome c and cell death. Correlation with the duration of pore openings in situ. J Biol Chem **276:** 12030-12034
Pical C, Fredlund KM, Petit PX, Sommarin M, Moller IM (1993) The outer membrane of plant mitochondria contains a calcium-dependent protein kinase and multiple phosphoproteins. FEBS Lett **336:** 347-351
Picault N, Hodges M, Palmieri L, Palmieri F (2004) The growing family of mitochondrial carriers in Arabidopsis. Trends Plant Sci **9:** 138-146

Planchet E, Jagadis Gupta K, Sonoda M, Kaiser WM (2005) Nitric oxide emission from tobacco leaves and cell suspensions: rate limiting factors and evidence for the involvement of mitochondrial electron transport. The Plant Journal **41:** 732-743

Pollard TD, Cooper JA (2009) Actin, a Central Player in Cell Shape and Movement. Science **326:** 1208-1212

Posey SC, Bierer BE (1999) Actin Stabilization by Jasplakinolide Enhances Apoptosis Induced by Cytokine Deprivation. J. Biol. Chem. **274:** 4259-4265

Reape TJ, McCabe PF (2008) Apoptotic-like programmed cell death in plants. New Phytol **180:** 13-26

Reape TJ, Molony EM, McCabe PF (2008) Programmed cell death in plants: distinguishing between different modes. J Exp Bot **59:** 435-444

Reape TJ, Molony EM, McCabe PF (2008) Programmed cell death in plants: distinguishing between different modes. Journal of Experimental Botany **59:** 435-444

Richberg MH, Aviv DH, Dangl JL (1998) Dead cells do tell tales. Curr Opin Plant Biol **1:** 480-485

Richter C, Gogvadze V, Laffranchi R, Schlapbach R, Schweizer M, Suter M, Walter P, Yaffee M (1995) Oxidants in mitochondria: from physiology to diseases. Biochim Biophys Acta **1271:** 67-74

Rintoul GL, Bennett VJ, Papaconstandinou NA, Reynolds IJ (2006) Nitric oxide inhibits mitochondrial movement in forebrain neurons associated with disruption of mitochondrial membrane potential. J Neurochem **97:** 800-806

Robson CA, Vanlerberghe GC (2002) Transgenic plant cells lacking mitochondrial alternative oxidase have increased susceptibility to mitochondria-dependent and -independent pathways of programmed cell death. Plant Physiol **129:** 1908-1920

Šamaj J, Baluška F, Voigt B, Schlicht M, Volkmann D, Menzel D (2004) Endocytosis, Actin Cytoskeleton, and Signaling. Plant Physiology **135:** 1150-1161

Sambrook J, Russell DW (2001) Molecular Cloning: A Laboratory Manual. Cold Spring Harbor Laboratory Press

Sampathkumar A, Lindeboom JJ, Debolt S, Gutierrez R, Ehrhardt DW, Ketelaar T, Persson S (2011) Live Cell Imaging Reveals Structural Associations between the Actin and Microtubule Cytoskeleton in Arabidopsis. The Plant Cell Online **23:** 2302-2313

Sanchez P, de Torres Zabala M, Grant M (2000) AtBI-1, a plant homologue of Bax inhibitor-1, suppresses Bax-induced cell death in yeast and is rapidly upregulated during wounding and pathogen challenge. Plant J **21:** 393-399

Saviani EE, Orsi CH, Oliveira JFP, Pinto-Maglio ClAF, Salgado I (2002) Participation of the mitochondrial permeability transition pore in nitric oxide-induced plant cell death. FEBS Letters **510:** 136-140

Schaap IAT, Carrasco C, de Pablo PJ, MacKintosh FC, Schmidt CF (2006) Elastic Response, Buckling, and Instability of Microtubules under Radial Indentation. Biophysical Journal **91:** 1521-1531

Scheffler IE (2007) History. John Wiley & Sons, Inc.

Schramm F, Ganguli A, Kiehlmann E, Englich G, Walch D, von Koskull-Döring P (2006) The heat stress transcription factor HsfA2 serves as a regulatory amplifier of a subset of genes in the heat stress response in Arabidopsis. Plant Molecular Biology **60:** 759-772

Scott I, Logan DC (2007) Mitochondrial Dynamics: The Control of Mitochondrial Shape, Size, Number, Motility, and Cellular Inheritance. John Wiley & Sons, Inc.

Scott I, Logan DC (2008) Mitochondrial morphology transition is an early indicator of subsequent cell death in Arabidopsis. New Phytol **177:** 90-9101

Scott I, Logan DC (2010) Mitochondrial Dynamics. In Plant Mitochondria. *In* F Kempken, ed, Vol 1. Springer New York, pp 31-63

Sesaki H, Jensen RE (1999) Division versus fusion: Dnm1p and Fzo1p antagonistically regulate mitochondrial shape. J Cell Biol **147:** 699-706

Shaw JM, Nunnari J (2002) Mitochondrial dynamics and division in budding yeast. Trends Cell Biol **12:** 178-184

Sheahan MB, Rose RJ, McCurdy DW (2004) Organelle inheritance in plant cell division: the actin cytoskeleton is required for unbiased inheritance of chloroplasts, mitochondria and endoplasmic reticulum in dividing protoplasts. The Plant Journal **37:** 379-390

Shi HT, Li RJ, Cai W, Liu W, Wang CL, Lu YT (2012) Increasing nitric oxide content in *Arabidopsis thaliana* by expressing rat neuronal nitric oxide synthase resulted in enhanced stress tolerance. Plant Cell Physiol **53:** 344-357

Sjostrand FS (1953) Electron Microscopy of Mitochondria and Cytoplasmic Double Membranes: Ultra-Structure of Rod-shaped Mitochondria. Nature **171:** 30-31

Smertenko A, Franklin-Tong VE (2011) Organisation and regulation of the cytoskeleton in plant programmed cell death. Cell Death Differ **18:** 1263-1270

Sorger PK, Dobles M, Tournebize R, Hyman AA (1997) Coupling cell division and cell death to microtubule dynamics. Curr Opin Cell Biol **9:** 807-814

Staiger CJ (2000) Signaling to the Actin Cytoskeleton in Plants. Annu Rev Plant Physiol Plant Mol Biol **51:** 257-288

Staiger CJ, Sheahan MB, Khurana P, Wang X, McCurdy DW, Blanchoin L (2009) Actin filament dynamics are dominated by rapid growth and severing activity in the Arabidopsis cortical array. J Cell Biol **184:** 269-280

Strasser A, O'Connor L, Dixit VM (2000) Apoptosis signaling. Annu Rev Biochem **69:** 217-245

Sweetlove LJ, Foyer CH (2004) Roles for reactive oxygen species and antioxidants in plant mitochondria *In* DA Day, AH Millar, J Whelan, eds, Plant mitochondria: from genome to function. Kluwer Academic, Dordrecht ; London, pp xvi, CP-1 - CP-8, 325 p.

Swidzinski JA, Sweetlove LJ, Leaver CJ (2002) A custom microarray analysis of gene expression during programmed cell death in *Arabidopsis thaliana*. Plant J **30:** 431-446

Takasugi M, Yagi S, Hirabayashi K, Shiota K (2010) DNA methylation status of nuclear-encoded mitochondrial genes underlies the tissue-dependent mitochondrial functions. BMC Genomics **11:** 481

Thomas C, Tholl S, Moes D, Dieterle M, Papuga J, Moreau F, Steinmetz A (2009) Actin bundling in plants. Cell Motil Cytoskeleton **66:** 940-957

Thomas SG, Huang S, Li S, Staiger CJ, Franklin-Tong VE (2006) Actin depolymerization is sufficient to induce programmed cell death in self-incompatible pollen. J Cell Biol **174:** 221-229

Thyberg J, Moskalewski S (1999) Role of Microtubules in the Organization of the Golgi Complex. Experimental Cell Research **246:** 263-279

Tominaga M, Yokota E, Vidali L, Sonobe S, Hepler PK, Shimmen T (2000) The role of plant villin in the organization of the actin cytoskeleton, cytoplasmic streaming and the architecture of the transvacuolar strand in root hair cells of Hydrocharis. Planta **210:** 836-843

Toyota M, Furuichi T, Tatsumi H, Sokabe M (2008) Cytoplasmic Calcium Increases in Response to Changes in the Gravity Vector in Hypocotyls and Petioles of Arabidopsis Seedlings. Plant Physiology **146:** 505-514

Ueda K, Matsuyama T (2000) Rearrangement of cortical microtubules from transverse to oblique or longitudinal in living cells of transgenic *Arabidopsis thaliana*. Protoplasma **213:** 28-38

Vacca RA, Valenti D, Bobba A, Merafina RS, Passarella S, Marra E (2006) Cytochrome c Is Released in a Reactive Oxygen Species-Dependent Manner and Is Degraded via Caspase-Like Proteases in Tobacco Bright-Yellow 2 Cells en Route to Heat Shock-Induced Cell Death. Plant Physiology **141:** 208-219

Vacca RA, Valenti D, Bobba A, Merafina RS, Passarella S, Marra E (2006) Cytochrome c is released in a reactive oxygen species-dependent manner and is degraded via caspase-like proteases in tobacco Bright-Yellow 2 cells en route to heat shock-induced cell death. Plant Physiol **141:** 208-219

Van Damme D, Van Poucke K, Boutant E, Ritzenthaler C, Inze D, Geelen D (2004) In vivo dynamics and differential microtubule-binding activities of MAP65 proteins. Plant Physiol **136:** 3956-3967

Van Doorn WG (2011) Classes of programmed cell death in plants, compared to those in animals. J Exp Bot **62:** 4749-4761

Van Doorn WG, Woltering EJ (2005) Many ways to exit? Cell death categories in plants. Trends Plant Sci **10:** 117-122

Van Gestel K, Kohler RH, Verbelen JP (2002) Plant mitochondria move on F-actin, but their positioning in the cortical cytoplasm depends on both F-actin and microtubules. J Exp Bot **53:** 659-667

Vannini C, Marsoni M, Cantara C, De Pinto MC, Locato V, De Gara L, Bracale M (2012) The soluble proteome of tobacco Bright Yellow-2 cells undergoing H2O2-induced programmed cell death. Journal of Experimental Botany **63:** 3137-3155

Vercammen D, Declercq W, Vandenabeele P, Van Breusegem F (2007) Are metacaspases caspases? The Journal of Cell Biology **179:** 375-380

Vos JW, Dogterom M, Emons AMC (2004) Microtubules become more dynamic but not shorter during preprophase band formation: A possible "search-and-capture" mechanism for microtubule translocation. Cell Motility and the Cytoskeleton **57:** 246-258

Vranova E, Atichartpongkul S, Villarroel R, Van Montagu M, Inze D, Van Camp W (2002) Comprehensive analysis of gene expression in Nicotiana tabacum leaves acclimated to oxidative stress. Proc Natl Acad Sci U S A **99:** 10870-10875

Watanabe N, Lam E (2011) Arabidopsis metacaspase 2d is a positive mediator of cell death induced during biotic and abiotic stresses. The Plant Journal **66:** 969-982

Westermann B, Neupert W (2000) Mitochondria-targeted green fluorescent proteins: convenient tools for the study of organelle biogenesis in *Saccharomyces cerevisiae*. Yeast **16:** 1421-1427

Wightman R, Turner S (2010) Trafficking of the Plant Cellulose Synthase Complex. Plant Physiology **153:** 427-432

Yaffe MP (1999) Dynamic mitochondria. Nat Cell Biol **1:** E149-E150

Yaffe MP, Harata D, Verde F, Eddison M, Toda T, Nurse P (1996) Microtubules mediate mitochondrial distribution in fission yeast. Proceedings of the National Academy of Sciences **93:** 11664-11668

Yoneda A, Akatsuka M, Kumagai F, Hasezawa S (2004) Disruption of actin microfilaments causes cortical microtubule disorganization and extra-phragmoplast formation at M/G1 interface in synchronized tobacco cells. Plant Cell Physiol **45:** 761-769

Yoshinaga K, Arimura S, Niwa Y, Tsutsumi N, Uchimiya H, Kawai-Yamada M (2005) Mitochondrial behaviour in the early stages of ROS stress leading to cell death in *Arabidopsis thaliana*. Ann Bot **96:** 337-342

Young RE, Bisgrove SR (2011) Microtubule Plus End-Tracking Proteins and Their Activities in Plants:The Plant Cytoskeleton. *In* B Liu, ed, Vol 2. Springer New York, pp 95-117

Zago E, Morsa S, Dat JF, Alard P, Ferrarini A, Inze D, Delledonne M, Van Breusegem F (2006) Nitric oxide- and hydrogen peroxide-responsive gene regulation during cell death induction in tobacco. Plant Physiol **141:** 404-411

Zanelli SA, Trimmer PA, Solenski NJ (2006) Nitric oxide impairs mitochondrial movement in cortical neurons during hypoxia. J Neurochem **97:** 724-736

Zhang L, Li Y, Xing D, Gao C (2009) Characterization of mitochondrial dynamics and subcellular localization of ROS reveal that HsfA2 alleviates oxidative damage caused by heat stress in Arabidopsis. J Exp Bot **60:** 2073-2091

Zhang L, Xing D (2008) Methyl jasmonate induces production of reactive oxygen species and alterations in mitochondrial dynamics that precede photosynthetic dysfunction and subsequent cell death. Plant Cell Physiol **49:** 1092-1111

Zheng M, Beck M, Müller J, Chen T, Wang X, Wang F, Wang Q, Wang Y, Baluška F, Logan DC, Šamaj J, Lin J (2009) Actin Turnover Is Required for Myosin-Dependent Mitochondrial Movements in *Arabidopsis* Root Hairs. PLoS One **4:** e5961

Zheng M, Wang Q, Teng Y, Wang X, Wang F, Chen T, Šamaj J, Lin J, Logan D (2010) The speed of mitochondrial movement is regulated by the cytoskeleton and myosin in *Picea wilsonii* pollen tubes. Planta **231:** 779-791

Zottini M, Formentin E, Scattolin M, Carimi F, Lo Schiavo F, Terzi M (2002) Nitric oxide affects plant mitochondrial functionality in vivo. FEBS Letters **515:** 75-78